A Stand-alone Parabolic Dish Solar Cooker for African Conditions

by

Omotoyosi Onalapo Craig

Thesis presented in fulfilment of the requirements for the degree of Master of Engineering (Mechanical) in the Faculty of Engineering at Stellenbosch University

Supervisor: Robert Thomas Dobson

December 2015

Declaration

By submitting this thesis electronically, I declare that the entirety of the work contained therein is my own, original work, that I am the sole author thereof (save to the extent explicitly otherwise stated), that reproduction and publication thereof by Stellenbosch University will not infringe any third party rights and that I have not previously in its entirety or in part submitted it for obtaining any qualification.

Date: 23 November 2015

Abstract

The reduction in the availability and the ever-increasing prices of fossil fuels, as well as the expensive and insufficient electricity supply, are some of the reasons explaining why the public awareness of the use of alternative cooking methods has increased in recent years. In most rural areas of Africa, the use of wood is even more preferred for cooking than either fossil fuel or electricity, and this has led to deforestation in many areas. However, the time spent on wood collection by women, who often walk kilometres under scorching hot, sunny conditions, can be utilised better in more productive activities. Most of those lacking access to convenient cooking methods live in places with good solar resources and where solar cookers would thrive if developed.

The study presented in this report considered a prototype solar cooking system that is relatively cheap and that can be modified to meet these challenges faced in African communities. A parabolic solar cooker, which uses a parabolic dish as concentrator, was designed and developed. The concentrator used was a television satellite dish of 2 m in diameter, in which the reflecting area was covered with reflective aluminium strips. The dish concentrates radiation from the sun onto a conical cavity receiver placed at its focal point. The system uses heat transfer fluid as its working fluid and a cuboid- shaped storage tank insulated with ceramic wool to enhance the sensible heat storage technique used. A specially modified automotive pump was used to circulate the heat transfer fluid throughout the system, while a cooking head in the form of a flat spiral copper tube put onto the storage tank was used as the cooking section. The cost of manufacturing the system was approximately R9 000, without considering the cost of the tracking system. However, this amount is expected to decrease if the system is mass produced.

The solar cooker was tested under winter conditions in South Africa, and each cooking test was done according to international standard procedures for testing solar cooker performance. A utilisation efficiency of 47 % was achieved, the exergy efficiency was 0.05 %, while the average characteristic boiling time was around 13.32 min/kg. The solar cooker can be used indoors, thus eliminating the need for its user to stay in the sun. The reflecting dish was mounted on an automated dual tracking system stand, which eliminated the need for regular adjustment by the user. The cooking section of the system can be modified to be used for other high temperature-based development activities in African communities, such as, among other things, industrial baking.

Keywords: Parabolic solar cooker, conical cavity receiver, utilisation efficiency, characteristic boiling time, modifications for African communities

Opsomming

Die verlaging in die beskikbaarheid en ewig-stygende pryse van fossielbrandstowwe, sowel as duur en onvoldoende elektrisiteitsvoorsiening, is net van die redes hoekom openbare bewustheid van die gebruik van alternatiewe kookmetodes die afgelope paar jaar toegeneem het. In die meeste landelike gebiede in Afrika word die gebruik van hout bo fossielbrandstof en elektrisiteit verkies. Dit lei in baie gebiede tot ontbossing. Die tyd wat deur vrouens spandeer word om hout op te tel, soms etlike kilometers ver onder die skroeiende son, kan op meer produktiewe maniere benut word. Die meeste mense wat nie toegang het tot konvensionele kookmetodes nie, bly in areas met goeie sonblootstelling en waar sonkrag-kooktoestelle sal floreer indien dit daar ontwikkel word.

Hierdie studie oorweeg ŉ prototipe kooktoestel wat aangepas kan word om die uitdagings in Afrika-gemeenskappe te oorkom. ŉ Paraboliese son-kooktoestel wat ŉ paraboliese skottel as konsentrator gebruik, is ontwerp en ontwikkel. Die konsentrator wat gebruik is, is ŉ televisie-satellietskottel, 2 m in deursnee, waarvan die weerkaatsende area met weerkaatsende aluminiumstroke bedek is. Die skottel konsentreer uitstraling van die son na ŉ ontvanger in die vorm van ŉ koniese holte wat by die fokuspunt geplaas is. Die stelsel gebruik warmteoordrag vloeistof as sy werksvloeistof en ŉ kubusvormige bergingstenk wat met keramiekwol (*ceramic wool*) geïsoleer is om sodoende die hitte-bergingstegniek wat gebruik word, ten volle te benut. ŉ Spesiaal gewysigde pomp is gebruik om die warmteoordrag vloeistof deur die stelsel te sirkuleer, terwyl ŉ kookkop in die vorm van ŉ plat spiraal koperpyp op die bergingstenk as kookvlak gebruik is. Die vervaardigingskoste hiervan was ongeveer R9 000, hoewel hierdie bedrag moontlik sou verminder indien dit op ŉ groot skaal geproduseer word.

Die son-kooktoestel is tydens die winter in Suid-Afrika getoets en elke kooktoets is volgens internasionale standaardprosedures vir die toets van son-kooktoestelle se werkverrigting uitgevoer. Benuttingsdoeltreffendheid van 47 % is gemeet, die exergie-doeltreffendheid was 0.05 %, en die gemiddelde kenmerkende kooktyd was ongeveer 13.32 min/kg. Die son-kooktoestel kan ook binnenshuis gebruik word, wat beteken dat die gebruiker nie in die son hoef te staan nie. Die weerkaatsende skottel is op ŉ geoutomatiseerde dubbelbaan spoorstelsel wat die son volg, gemonteer, wat beteken dat die gebruiker nie self die skottel hoef te roteer nie. Die kookvlak van die stelsel kan vir ander hoë temperatuur-gebaseerde ontwikkelingsaktiwiteite in Afrika-gemeenskappe aangepas word , soos byvoorbeeld ŉ industriële bakkery.

Trefwoorde: Paraboliese son-kooktoestel, koniese holte ontvanger, benuttingsdoeltreffendheid, kenmerkende kooktyd, aanpassings vir Afrika-gemeenskappe

Dedications

To my darling father, Ademuyiwa Akanni (Baba C) Craig,

and

my angel mother, Atinuke Titilayo (Mama C) Craig

Acknowledgements

To God be the glory. I would like to express my appreciation of my study leader, Mr Robert Dobson, for his guidance and input during the course of this research and also for his financial support for the manufacturing of parts and the purchasing of the equipment used. Mr Dobson is a good man, as he believed in me and gave me a bursary, which reduced my stress and tension outside of the research scope.

I would also like to thank Dr Jaap Hoffman, for believing in me and extending an offer to me to further my studies at Stellenbosch University (SU), and also Prof. Ben Sebitosi, for his input and suggestions on the testing and experimental procedures. Further appreciation goes to the Centre for Renewable and Sustainable Energy (CRSES) at Stellenbosch University, for their counterpart financial support for this study; Solar Thermal Energy Research Group (STERG), for providing the platform; and my office colleagues, for providing a conducive research environment –John Taulo (Malawian), Maria Yvonne Uwera (Rwandese) and, most especially, Gerhardus Prinsloo (South African) and Brian SSebabi (Ugandan) for their informative ideas and not forgetting my support striker in soccer and my right hand man, Jones Musango (Kenyan) for his support.

I acknowledge and appreciate my mentor, Olabode Oyeneye, and my elder brother Deji, who is also my best friend, as he has always been my guardian angel and motivation. Thanks also go to the technologists and technicians in the mechanical engineering workshop at SU. My gratitude also goes to Deola Ogunleye, for his help in setting up the electrical systems for this experiment. I would also like to say thank you for the moral and academic support of my friends, Samson Masebinu, Temitope Oladele and Tobi Fadiji, as well as the pastors and workers of the Redeemed Christian Church of God, Desire of Nations Stellenbosch and Chapel of Reconciliation, Abeokuta, Nigeria. To my dearest, Miss Thobeka Mhlongwe (#AnikeGold), for her moral and emotional support, and also for helping out during the solar cooking experiments and the proof reading, I say thank you.

I cannot but acknowledge my siblings, who denied themselves the comfort of this world for me to have come this far; my sisters and their husbands, Temitope and Olaolu Fakeye, Omolara and Wale Solatan, and my brothers Akindeji and Oluwadamilare (Silversat), as well as my adopted brother Olajide Oguntayo, and not forgetting my cousin Folusho (Flexy), among others. May your generations never be stranded, in Jesus' name, Amen.

Table of Contents

Nomenclature

A	Cross sectional-area, m
A_a	Aperture area, m^2
d	Diameter, m
c	Depth of parabola, m
$E_{optical}$	Rate of optical radiation
g	Acceleration due to gravity, m/s^2
Gr	Grashof number
H	Height of cavity conical section, m; convective heat transfer coefficient, W/m^2K
hfg	Specific enthalpy change of evaporation
$\dot{m}$	Mass flow rate, kg/s
N	Number of days
Nu	Nusset number
p	Parabolic radius, m
P	Pressure, N/m^2
Pr	Prandtl number
Re	Reynolds number
t	Time, s
T	Temperature, ℃
t_c	Characteristic boiling time, min/kg
$U_{fd,i}$	Internal energy of the food item to be cooked
V	Volume, m^3
W	Weight, N; width, m
x	Insulation thickness, m

Greek Symbols

γ	Azimuth, un-shading factor
ρ	Density, kg/m^3; reflectivity
η	Efficiency
α	Elevation angle, thermal diffusivity, m^2/s
ε	Emissivity, effectiveness
Ψ	Exergy
ω	Hour angle, degrees
ψ	Rim angle
φ	Tilt angle, radian
σ	Tracking errors

Superscript

B	Boiling
t	Time

Subscripts

a	Air, aperture
amb	Ambient
b	Bottom part of cooking pot
cav	Cavity
cov	Cover
conv	Convection
corr	Correct
eff	Effective
ev	Evaporator
fd	Food
g	Air between the food and the cover
h	Hot
i	Inner, initial, internal energy
inner	Inner wall of the receiver
ins	Insulation
l	Liquid
lo	Loss
m	Log mean
meas	Measured
o	Oil
p	Pot
par	Parabola
r	Radiation
rad	Radiation
rec	Receiver
s	Side, solar, south

sat	Saturation
t	Top of pot, thickness
u	Utilisation, useful
v	Vapour
w	Water, wall
x	Characteristic dimension of cavity (m)

Abbreviations and Acronyms

BSRN	Baseline Surface Radiation Network
CAD	Computer-aided design
CSP	Concentrated solar power
DC	Direct current, A
DEA	Department of Environmental Affairs
DNI	Direct normal irradiance
EOT	Equation of time
ESKOM	Electricity Supply Commission, South Africa
GHI	Global horizontal irradiation
IFAD	International Fund for Agricultural Development
LC	Longitude correction
LCT	Local time
LH	Length of helix, m
NREL	National Renewable Energy Laboratory
ODE	Ordinary differential equation
PCM	Phase-change material
PV	Photovoltaic
PWM	Pulse width modulation
RSA	Republic of South Africa
SU	Stellenbosch University
UN	United Nations
UO	University of Ottawa
UUT	Unit under test
WFP	World Food Programme

List of Tables

List of Figures

1 Introduction

Over 40% of Africa's population lives in rural areas. Most of them depend on peasant farming, often eat from hand to mouth, and/or live in extreme poverty (Rogers et al., 2012). However, efforts to tackle these problems are being made continuously by world welfare organisations such as the United Nations (UN), World Food Programme (WFP) and the International Fund for Agricultural Development (IFAD). These organisations have offered two solutions, namely food security and global equality (Misselhorn, 2005), and despite all the efforts they have made over the years, the problem seems far from being solved. In recent years, aid to Africa has been greatly reduced compared to its levels in the 1970s and 1980s (Grundy, 1995). Thus, there is an urgent need for Africans to improve the development of existing solutions to the aforementioned challenges, in line with the Yoruba[1] adage, *Oníkálùkù lómo ibi tí bàtà ti n tà'un lésè*.[2]

In South Africa, for example, only 34 % of the households had access to electricity in 1994, and, by 2012, the percentage has reached 89 % (Department of Environmental Affairs, 2012). Despite this progress, a new concept now trends in the country: "load shedding". The term load shedding refers to when an electricity regulating agency interrupts its supply to some areas to favour other areas for a specific time in order to balance its electricity demands, which surpass its supply (Eskom, 2014). In 2012, the South African Department of Environmental Affairs (DEA) stated that, despite the use of wood and paraffin as sources of heat for cooking, electricity was used the most, as shown in Figure 1-1. Cooking with electricity consumes an appreciable amount of the overall energy produced in the country. A follow-up survey by the DEA showed that the residential sector was the third highest consumer of energy after the transport and the industrial sectors, as shown in Figure 1-2. This means that, if some of the home-cooking or heating systems would use alternative sources of energy, such as the one proffered in this report, the term "load shedding" will soon be forgotten.

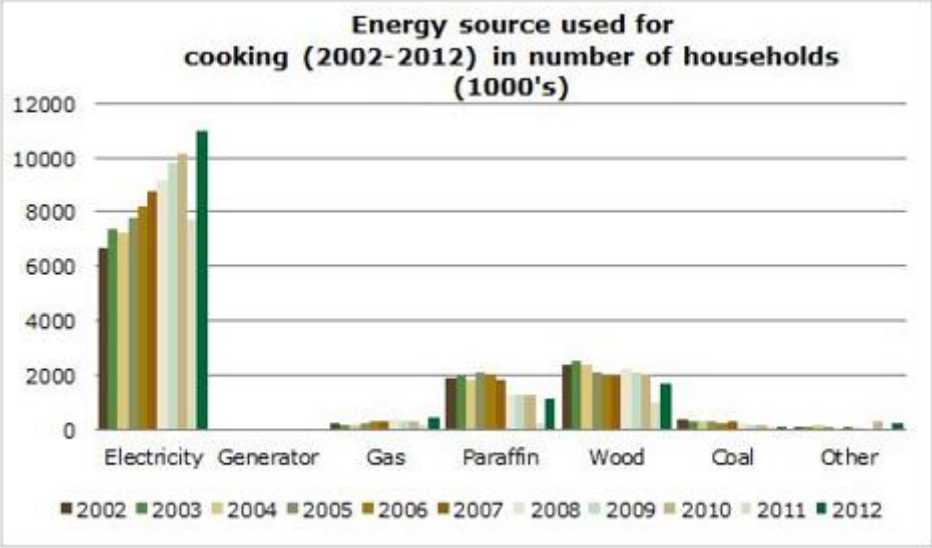

Figure 1-1: Sources of energy for cooking (Department of Environmental Affairs, 2012)

[1] Yoruba is a language that is widely spoken in West Africa.
[2] Only he who wears a shoe knows where it hurts most.

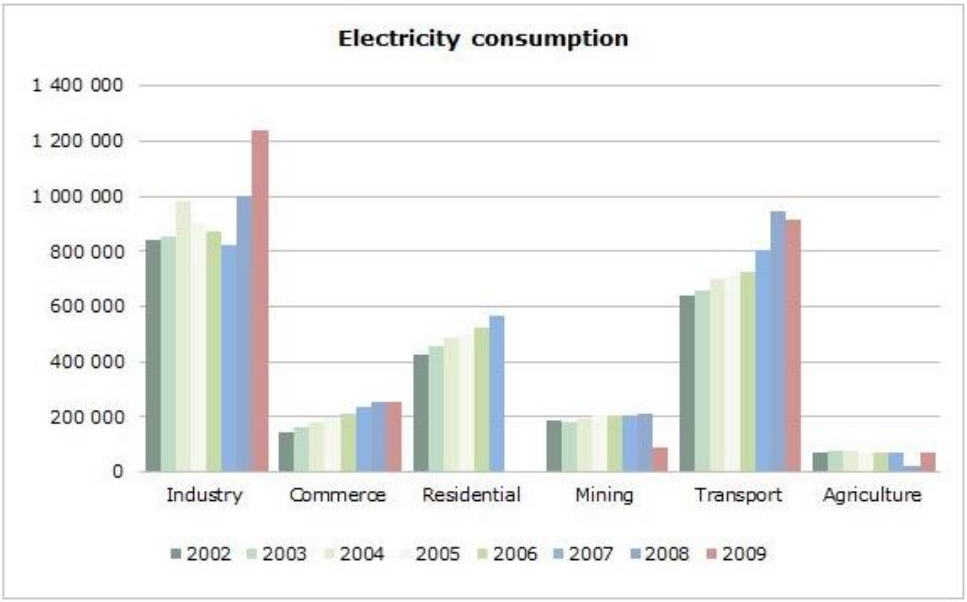

Figure 1-2: Ways in which electricity is consumed in South Africa (Department of Environmental Affairs, 2012)

The sun is one of the gifts of nature. Its ability to solve most of Africa's challenges, some of which have been stated above, is unquestionable. The sun is the ultimate source of energy and its availability allows for various ways to utilise its free energy. One of the major ways in which the energy from the sun (often called solar energy) has been utilised is through solar cooking technology (Ahmad, 2001), which is available in different types – from the relatively cheap using low levels of technology, to big, expensive ones that can be used in industrial heating systems or cooking for hundreds of people (Otte, 2013). A solar cooking system makes use of the energy from the sun to heat or cook food and even to boil or pasteurise water (Solar-Cooker-International, 2001). Different types of solar cookers have been developed around the world and can be categorised broadly into three different types, as shown in Figure 1-3 below.

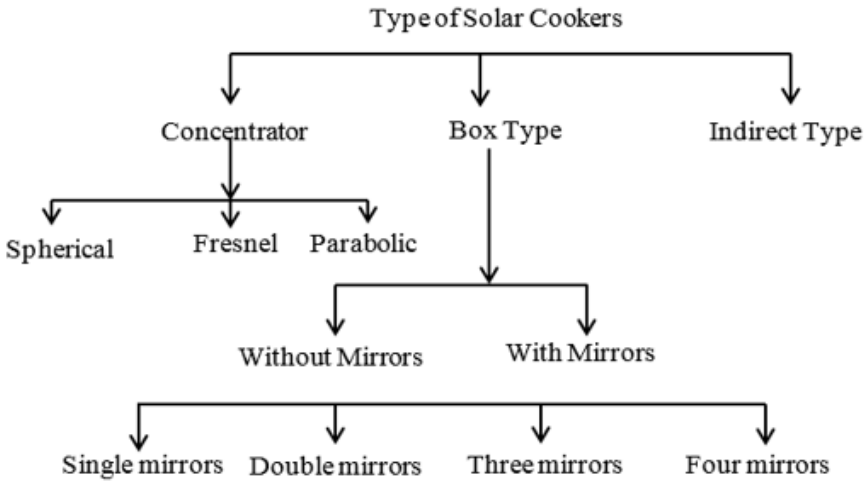

Figure 1-3: Classification of solar cookers

The concentrator types in Figure 1-3 above reflect the sun's rays onto the cooking section and are divided into three types, namely spherical, Fresnel and parabolic. The box types retain the heat in a box-shaped cooking system, while the indirect solar cookers transfer the captured heat to a secondary cooker. Details of these are provided in Chapter two of this report. According to Wentzel and Pouris (2007), solar cookers have long been presented as a realistic solution to the world's problem of deforestation as a result of the use of wood for fuel, as well as other environmental problems associated with the demand of wood fuel for cooking.

1.1 Background

Concentrating solar power (CSP) is a technology employed to convert solar thermal energy into either electrical power or heat energy (NUFUNetwork, 2013). There are many forms in which CSP can be used as a heat source, as shown under the concentrators in Figure 1-3; however, the parabolic concentrators have been proven over the years to be the most efficient in terms of heat generation (Reddy & Ranjan, 2003). They are also considered the fastest in terms of the time it takes to make food when used as a solar cooker (Panwar et al., 2012). Solar cookers, especially the parabolic types, have been identified as a potential solution to some of the challenges facing developing communities, such as overdependence on an insufficient electricity supply that causes load shedding, food insecurity, unemployment, rural-urban migration and other social issues (Bryceson, 1996;Von Braun, 2010). Despite this potential, parabolic cookers still face many challenges, some of which are low utilisation efficiencies, complexity in design and low social acceptance. There is, therefore, a need to increase the efficiencies of these types of cookers and eliminate the major challenges facing their ability to compete with other types of convectional cookers.

1.2 Aim

The aim of this study was to develop a stand-alone solar cooking system that can be used in rural communities to reduce hunger, dependence on wood fuel, expensive fossil fuels and other energy sources, and to alleviate poverty.

1.3 Specific Objectives

The study in this report was carried out with the following objectives:

- To develop a parabolic solar cooker that tracks the sun in two axes and can cook when there is no sun or at night
- To develop a more efficient heat-generating system that can be modified for rural industrialisation
- To analyse and compare the performance of the solar cooker with the existing ones

1.4 Problem Statement and Motivation

Solar cooking is a realistic solution to the challenges associated with the use of wood and electricity as means of generating heat needed for cooking. More than two billion people worldwide use wood either as a source of fuel to cook or as a source of heat (Wentzel & Pouris, 2007). This scenario is not so different in Africa. For example, South Africa's domestic usage of wood for fuel is estimated at 840 000 m^3 per annum (Christie & Gandar,

1994). Further, Diabaté et al. (2004) claim that a quarter of wood fuel users often face the challenge of fuel shortages (in terms of wood and electricity), yet they live in climatic areas that are ideal for the use of solar cookers. In the quest to obtain the wood used for cooking, many women walk several miles and are often exposed to danger, and the continuous reliance on wood as a source of energy has led to deforestation and rural-urban migration in many areas of Africa (Barrios et al., 2006; Diabaté et al., 2004; IFAD, 2009).

The use of solar cookers is often limited due to the fact that the sun is not available 24 hours a day. As a result, solar cookers are often either not functional or fully effective on cloudy days or when there is no sunshine. The development of solar cookers with thermal energy storage has been identified as a breakthrough in the challenges and limitations faced by solar cookers. Yettou et al. (2014) identified problems facing the social acceptability of solar cookers, including complexity in design, longer cooking time, unregulated temperatures, sun tracking, solar cooker sizing, low efficiencies and exposure to sun by the users, which leads to sunburn. All these problems hinder the ease with which solar cookers can compete favourably with other means of cooking. However, these issues are being attended to by on-going research around the world. The need to develop a solar cooker with suitable simple thermal storage, reduced heat loss, solar tracking, accurate sizing and cooking charts, and to eliminate exposure to sun by the users, along with less monitoring and higher efficiency, is of utmost importance. This project is part of a bigger project at Stellenbosch University aimed at developing a system that can stand alone in heat and electricity generation, and that can be used for rural development. The aspect of solar cooking is presented in this report.

1.5 Project Description

The project presented in this report is a small, stand-alone, solar-powered, active parabolic cooking system. These terms are described below:

Small: A heat-generating system with a peak temperature of lower than 220 ℃

Active: A pump is used to circulate the heat-transfer fluid through the whole system.

Stand-alone: It is entirely self-contained and can serve as a means of cooking for a small rural community, thereby reducing the cost of food preparation.

Parabolic cooking system: A two-axis, solar tracking 2 m parabolic dish-shaped reflecting concentrator.

In this study, the radiation from the sun was used to generate the high temperatures needed for home or industrial use. These rays were concentrated onto a cavity receiver using a reflective parabolic dish of 2 m in diameter. The heat from the reflected rays were absorbed by the receiver and then transported through a heat-transfer medium to the storage tank, where it was stored for use. The inclusion of heat storage was needed for the system to be usable when there is no sunshine and at night. Also, the storage tank had to perform the dual function of saving the heat and cooking, for which a maximum temperature of about 220 ℃ was desired. The individual parts of the system setup had to be manufactured first before the final assembly was done at the experimental site. The whole setup was mounted on a dual axis tracker stand. Several experiments and experimental cooking attempts were performed on the system to check the effectiveness of the cooker and to validate its operations.

All experimental analyses in this report are in line with the international standard for testing solar cookers and reporting their performance. The possible usage of the system was identified and is presented in this report.

1.6 Thesis Layout

There are seven chapters in this report. The first chapter is a short overview of the work that was done. The chapter introduced and highlighted the need for the development of solar technology. Chapter two presents the literature survey done for the work, including on the history of solar cookers and existing technologies. It further presents the advantages and disadvantages of such technologies. In Chapter three, the analysis of solar angles, resources and the tracking system are discussed. The chapter also analyses the modified tracker that was used for the setup, and the result of its comparison with standard solar resource instruments. The theoretical calculations, models and heat transfer analysis for the system are presented in Chapter four, while the experimental setup, innovation and improvisation decisions, and what the whole system looks like in reality constitute the fifth chapter. In Chapter six, the various experiments performed (both cooking and non-cooking) with the manufactured system, as well as the different solar cooker performance tests and evaluation analyses (with results displayed graphically), are presented. Furthermore, the experimental goals and procedures for each experiment are stated and the necessary analysis and discussions are presented in the chapter. In addition to the conclusions and recommendations, the final chapter of this report presents a table comparing the efficiency and characteristics of the current research with the existing technologies. Several ways in which the solar cooker in this report can be used are also presented. Each chapter of this report ends with a section summarising the work presented in the chapter.

1.7 Chapter Summary

This chapter highlighted the challenges of using wood fuel for cooking in Africa, it also showed that the use of alternative cooking techniques like solar cookers can reduce over dependence on electricity and with this need to develop an indigenous technology as a means to reduce overdependence on the insufficient energy available, the option to use parabolic solar cookers was introduced. The objective of the study – to develop a more efficient parabolic solar cooker that can be used as an alternative cooker and heat-generating system – was pointed out. The next chapter discusses the literature review on solar cooking system technologies.

2 Literature Review

Many people choose to cook with the sun because it is presented in literature as simple, safe and more convenient. Its convenience is such that, actually, it is the most appropriate way to cook food without using fuel or even heating up the kitchen (Craig & Dobson, 2015). Cuce & Cuce (2013) observed that solar cookers are more of a blessing than just a cooking system to those who walk several kilometres under the scotch of the sun to gather fire wood. Cochetel (2012) showed that the risks of sun burn, snake bite, stress or sometimes insufficient fund to purchase the gas or fuel needed for cooking can be avoided by using solar cookers. The solar cooking concept can also be extended to water heating, which can be used to achieve water pasteurisation (Helal *et al*., 2011; Kousksou *et al*., 2011). This can provide safe drinking water and, in the long run, prevent many water-borne diseases (Yogo & Ishikawa, 2000). There is a wide range of reasons to improve the efficiencies of solar cookers as well as their social acceptance (Knudson, 2004; Lecuona *et al*., 2013; Yettou *et al.*, 2014). The sections in this chapter discuss the history, types as well as the advantages and disadvantages of existing solar cookers to serve as background to developing a better one.

2.1 Historical Background

Much of the research on solar cooking in the literature highlights that the ancient Greeks, Romans and Chinese had all performed experiments using angular curved mirrors positioned the sun, causing objects to sublimate. In the 16th century, some used it for military purposes. Years later, the Dutch, French and English started the considerable use of greenhouses, which were heated when solar heat passed through the glass and would warm up the inside of the house. The English and Dutch were able to raise a lot of tropical plants in this manner. By the year 1767, Swiss scientist Horace de Saussure developed a solar cooker using the greenhouse effect, where several glass boxes were set inside one another and placed on a darkened surface (Halacy & Halacy, 1992; Otte, 2013; Panwar et al., 2012; Wentzel & Pouris, 2007).

Radabaugh (2011) states that, in the 1950s, many certified engineers decided to study different aspects of solar cooker designs. On submission of the reports, it was realised from their case studies that solar cookers were easy to design and manufacture. They also cooked thoroughly (well-done meals) and nutritiously (Panwar et al., 2012). Most of the time, the solar-cooked food passed olfactory tests and retained the traditionally desired taste of the food (Radabaugh, 2011). Also in the 1950s, Maria Telkes developed the box type of solar cooker with support from the Massachusetts Institute of Technology. This was an insulated box on which most of the present designs are based. The top part of this cooker was covered with glass and had four reflectors, which angled the direct irradiation from the sun into the box (Telkes, 1959; Wentzel & Pouris, 2007). After this breakthrough, international bodies like the UN pioneered studies on how to take solar cooking to countries where fuel is scarce; this unfortunately has not yielded the desired result (Biermann et al., 1999; Cuce & Cuce, 2013; Radabaugh, 2011). Despite the setback on the part of the world bodies, cooking with solar power in China had become widespread and, in 1973, the first solar cooking convention was held in the country, which was then the home of solar cooking (Radabaugh, 2011). More recently, in 1992, the Chinese reported the use of over 100 000 solar box cookers (Solar-Cooker-International, 2001).

2.2 Classification of Solar Cookers

According to Cuce and Cuce (2013), there are a number of ways in which solar cookers can be classified, and countless styles of solar cookers are available in the world today due to the on-going developments in solar cooker design and its increasing societal acceptance. In this report we adopt the three types of solar cooker classification undertaken by Muthusivagami et al. (2010) namely, (i) the box types, (ii) the concentrating types and (iii) the indirect types. These types of solar cookers are discussed in the next sections.

2.2.1 Box types

The box-type solar cooker is the most common type of solar cooker and often the easiest to make. It cooks at an averagely high heat, from 70 ℃ to 140 ℃, and multiple pots can be accommodated on it (Biermann et al., 1999). Presently, there are hundreds of thousands of box solar cookers in India alone (NUFUNetwork, 2013). In Figure 2-1 below, Muthusivagami et al. (2010) show the different ways in which the box type of the solar cooker has been designed.

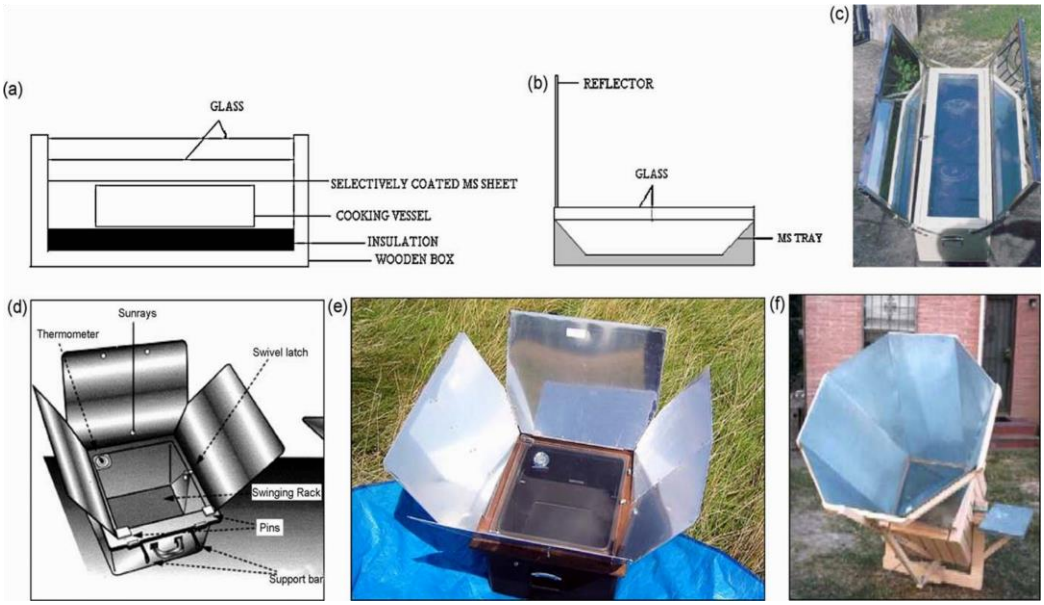

Figure 2-1: Box-type solar cookers (Muthusivagami et al., 2010)

The box cooker shown in Figure 2-1a has no reflector and was designed by Nicholas-de-Saussure. It has a glass pane cover and a wooden box insulated as shown. This box cooker can be said to be the father of all box solar cookers, because most of the present designs are based on it. In Figure 2-1b, a single reflector was added to the design shown in Figure 2-1a. The addition of this reflector was to increase the efficiency of the first box type. Figure 2-1c is a box solar cooker with double reflectors, while three reflectors are used in Figure 2-1d. These three reflectors require different reflectors to be set at specific angles to ensure they are all reflecting into the box, with the space between each reflector having a triangular shape. Halacy and Halacy (1992) developed the box in Figure 2-1e to check whether an increase in the number of reflectors leads to an increase in efficiency. They found that the time it took to cook with the four reflectors was not reduced by 25 % compared to the time it took using a single reflector. They also stated that the major

challenges of these solar cookers included the duration of cooking (i.e. cooking took long), the need for several supports and regular efforts required to twist and move the reflectors to face the sun. Telkes (1959) earlier made a box solar cooker with eight angular reflectors and achieved a temperature of 225℃, as shown in Figure 2-1f, although it looks as if Telkes combined box and concentrating cookers. As a result, these types of cookers are often classified as panel cookers.

In conclusion, box solar cookers can keep food warm for a long time and they can act as an insulator box for the food, as seen in Figure 2-2, which provides a standard schematic diagram for box solar cookers. The box-type solar cookers are stable, simple to design and require less monitoring or inspection time. Despite these advantages, cooking with a box solar cooker takes very long due to the low temperature it usually attains. Even when used with booster mirrors and a low concentration, these cookers only achieve temperatures up to 100 ℃. In the case of varying cloud cover, most food in the boxes is left half done and often wasted because it cannot be recooked using other, conventional cooking methods.

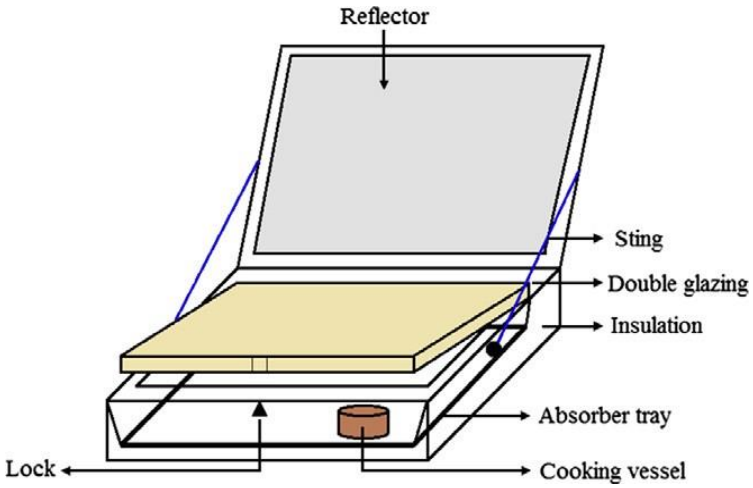

Figure 2-2: Components of a box solar cooker (Cuce & Cuce, 2013)

2.2.2 Concentrating cookers

Curve or concentrating cookers are solar cookers in which the cooking pot is often placed at the focus of the concentrating device (Schwarzer & Vieira da Silva, 2008). They cook fast at high temperatures, but require frequent adjustment and supervision for safe operation. They are especially useful for outdoor and large-scale institutional cooking (Lecuona et al., 2013). When these types of cookers have either a single or double sun-tracking system attached to them, have a concentration ratio of up to 50, and the temperature in the cooking section often rises to 300 ℃ in a short time and these temperatures are often stable (Muthusivagami et al., 2010). There are several types of concentrating cookers, some of which have several joined mirrors, some which use Fresnel lenses, and others which use parabolic-shaped concentrators to reach the desired high temperature. As shown in Figure 2-3, some of these cookers concentrate the reflected light under the cooking section and others concentrate the reflected light on the top of the solar cookers.

The first two pictures in Figure 2-3 show the method of concentrating light onto the top of the pot. Figure 2-3a, which is easy to use, shows a panel cooker that needs a covered pot

for optimal performance. This can be improved when the cooking pot is black or another dark colour (Cuce & Cuce, 2013). Panel cookers make meals for an average of four to five persons in few hours of sunshine, preserve the food's nutritional value and are simple to build (Muthusivagami et al., 2010). Figure 2-3b is a funnel solar cooker that is easy to make and for which less material is required. It is often not balanced but can be supported with stones or rested on a plank.

In Figure 2-3c, light rays are concentrated to the bottom of the pot, and this is often called a spherical reflector. It has been in existence since 1961. The cooking pot can be held in position by a tripod or any stand that places it in the focus of the spherical cooker. Figure 2-3d shows a parabolic reflector, which is known for having the sharpest and broadest focus of all concentrating solar cookers (Muthusivagami et al., 2010). It is very efficient in terms of heat generation, but sensitive to the slightest changes in sun position. For this reason it requires constant solar tracking (Pih & Kalogirou, 1997). The limitation to this type of cooker is that the parabolas are always made with specific design parameters and often are not easy to construct at home or with available materials. The type of cooker shown in Figure 2-3e is gaining acceptance, as it can be made by placing aluminium polyester on some rings and arranging it in circular discs to form Fresnel concentrators.

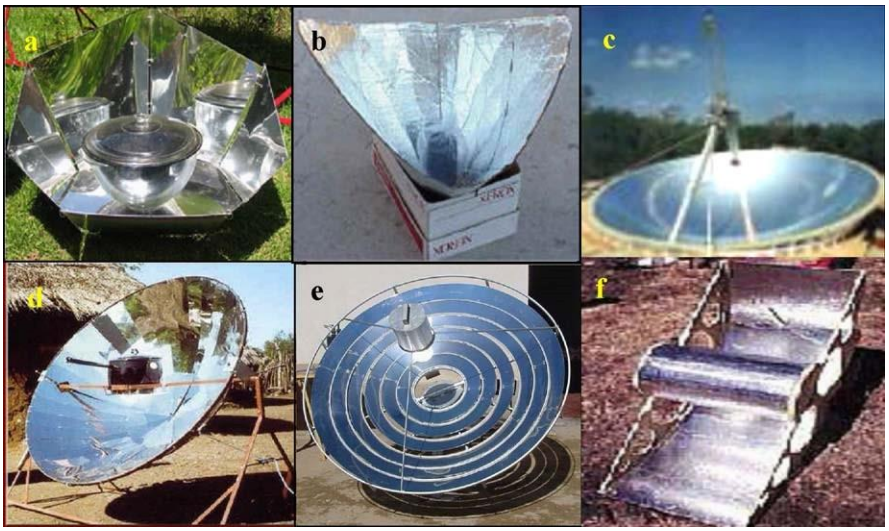

Figure 2-3: Parabolic type solar cooker (Muthusivagami et al., 2010)

Muthusivagami et al. (2010) refers to the cooker in Figure 2-3f as a cylindrical-parabolic concentrator, where the sun's rays are concentrated on an insulated cylindrical box where cooking pots can be placed. Although mostly used for water heating, it is also used to cook food.

Several experimental and numerical analyses have been done on the performance of parabolic cookers, and an analysis based on thermodynamic laws by Öztürk (2004), who studied a low-cost parabolic cooker at a location in Adana, Southern Turkey (latitude and longitude 37 °N and 35 °E respectively), showed an energy output of between 20.9 W and 78.1 W and also that the calculated energy efficiency was between 2.8 % and 15.7 %. Shukla (2009) found that the energy efficiency of box-type solar cookers was in the range of 3.05 % to 35.2 %, while that of parabolic solar cookers was in the range of 2.8 % to 15.7 %. Several forms of parabolic cookers have been made over the years, for example the umbrella type, which can be collapsed into a small volume, was designed by Arenas (2007)

and attained an average of 175 W power output and 27 % energy efficiency (see Figure 2-4).

Figure 2-4: Schematic collapsible solar cooker design (Arenas, 2007)

An increase in the efficiency of the parabolic solar cookers was seen when a solar tracking system was added (Al-Soud et al., 2010), with water reaching 96 ℃ at a maximum ambient temperature at 36 ℃ and more. The addition of a storage medium either sensible or phase change materials also contributed to the efficiencies of the cookers, making them useful when there is no sunshine (Agyenim et al., 2010). Despite the low energy efficiencies and low power, the parabolic solar cookers attain the desired cooking heat faster and more reliably than other types (Cuce & Cuce, 2013) and there is an obvious need to improve on these findings and increase the overall energy output and efficiencies.

2.2.3 Indirect solar cookers

In indirect solar cooking there is no direct contact of the reflected or concentrated rays of sun with the cooking; rather the heat generated is transferred to the cooking section with a heat-transfer medium. These types of solar cookers were developed to be available commercially. Some manufacturers have made use of the concentrating types of solar collectors because of the high heat generated, while others have used evacuator tubes because of their efficiency. The picture in Figure 2-5a shows an outdoor cooker with heat storage used by a primary school in the northern part of Chile, which was developed by Schwarzer and Vieira da Silva in 2008. It is made up of flat plate collectors. The heat-transfer medium is a vegetable oil like groundnut or sunflower oil; the cooker also has two separate fixed pots inside it. This solar cooker is known for faster cooking and has the ability to accommodate a large-sized pot. The side with the flat plate can be placed outside a building, while the cooking section is inside. The fact that the two pots are fixed makes it difficult to clean the cooking section, which reduces the required hygienic standard. Another major disadvantage of this system is that it is not always reliable in the absence of direct sunshine or on a cloudy day, considering that the cycle will be reversed.

Figure 2-5b shows a tube collector developed by Balzar as reported by Muthusivagami et al. (2010). The heat-transfer medium is a set of heat pipes, which transfer heat from vacuum tube collectors to the cooking section. This type of cooking is on the high side because it

does not require solar tracking and also eliminates the user's exposure to the sun, as the oven side could be inside the house while the collector is outside.

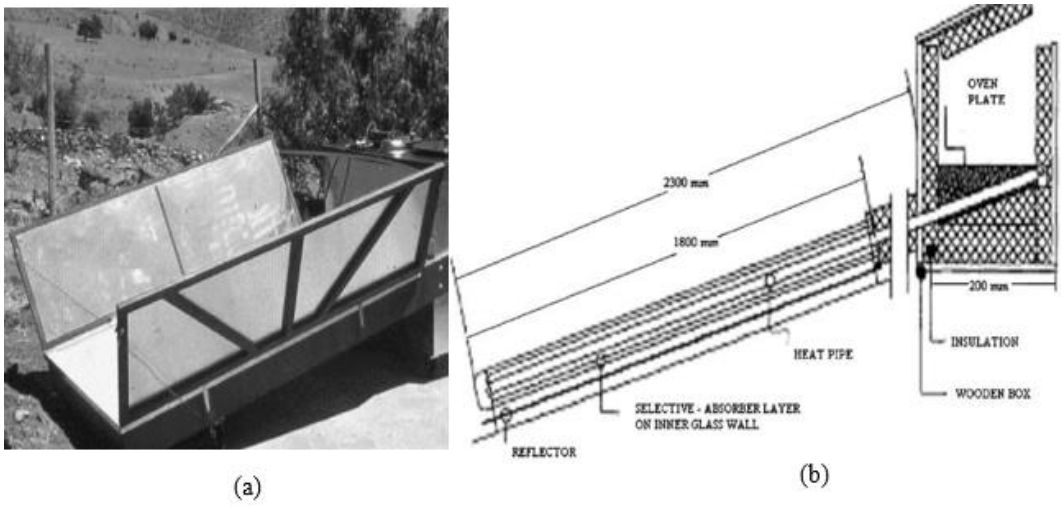

Figure 2-5: Indirect solar cookers: flat plate in Chile (Schwarzer & Vieira da Silva, 2008),(a); Evacuated tube (Muthusivagami et al., 2010), (b)

Muthusivagami et al. (2010) claimed that this type of cooker generates heat at a higher temperature than the flat plate collector in Figure 2.5a – up to 120 ℃. Kumar and Reddy (2007) used the mechanisms of flat plates to invent a solar pressure cooker that has an evacuator tube connected to a pressure cooker with the aid of highly effective heat exchangers.

As shown in Figure 2-6, the idea of heat pipes introduced in the previous paragraph was used by Esen (2004) to check the efficiencies of different refrigerants. It was proved that faster cooking can be achieved using different refrigerants and long heat pipes when compared to concentrating cookers or box cookers.

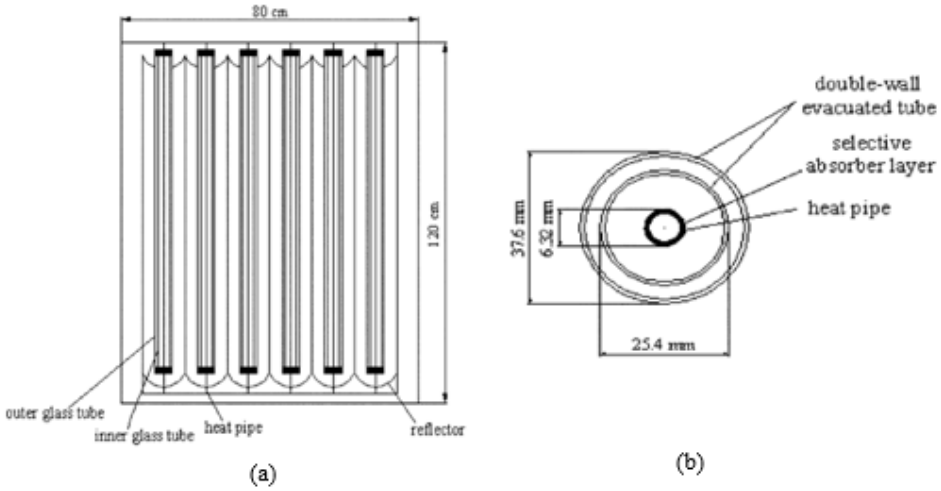

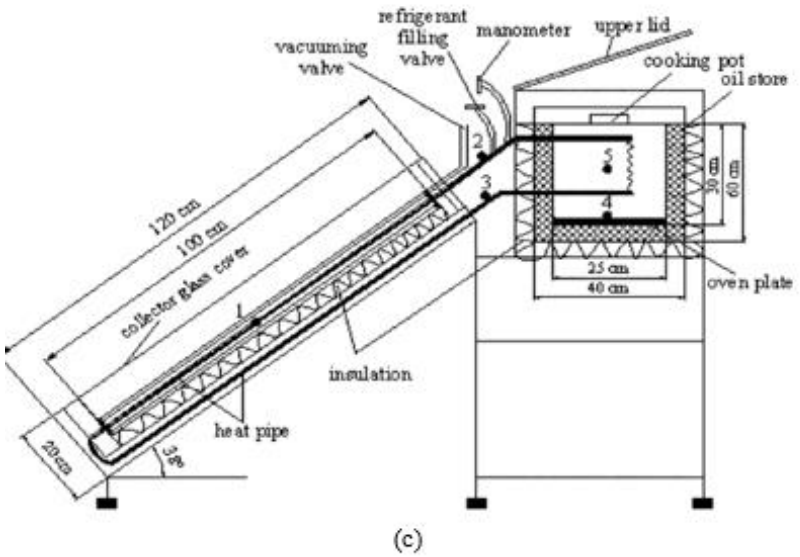

Figure 2-6: Front view of heat pipe (a); sectional view of the heat pipe (b); overall setup (c) (Esen, 2004)

The system in Figure 2-6 consists of three sections: the cooking area, the collector and the heat pipes. The collector side consists of a parabolic concentrating chrome–nickel reflector with 0.96 m^2 collector aperture area. The exposed side of the heat pipe was painted black and each of the heat pipes was made to form coils to 1 m in order to increase the heat transfer area of the pipes. The various conditions under which these experiments were carried out and the average results of water boiling are presented in Figure 2-6. Figure 2-6a and b show the solar radiation as a function of the ambient temperatures for the two different days considered. It was reported that these experiments were carried out under clear sky conditions, with an average ambient temperature of between 21 ℃ and 36 ℃. The water-heating experiments were performed and the results are shown in Figure 2-7 c and d. The different temperature readings from the setup according to the numbering are also shown.

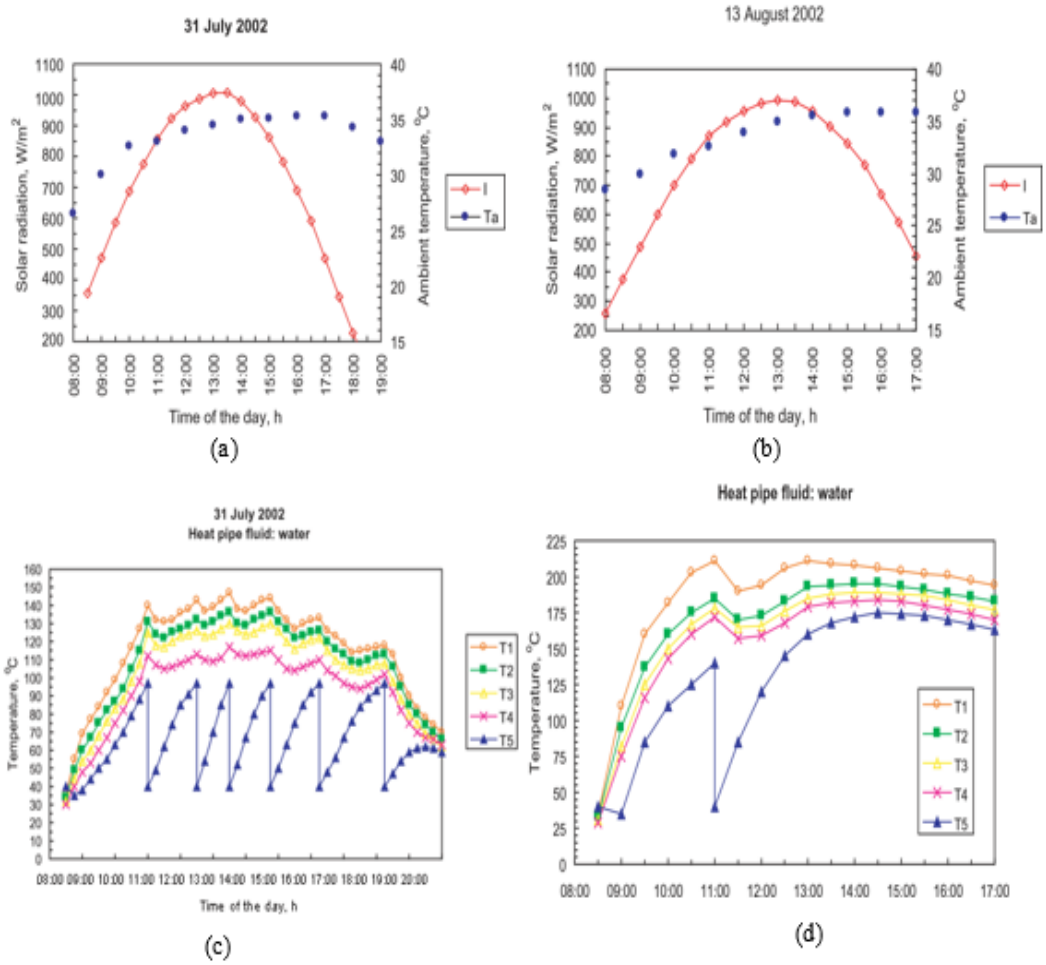

Figure 2-7: Experimental result of cooking with refrigerants: solar radiation a and b; water heating, b and c (Esen, 2004)

The temperature from the water experiment was taken between 40 ℃ and 97 ℃ and whenever the water reached boiling, it was poured out and new cold water was poured in, as seen in the Figure. This can be noticed in the sharp drop in the graph in Figure 2-7c.

Table 2-1 below compares the results of cooking various foods with this system for each of the refrigerants, namely Freon 22, Freon 134a, and Freon 407C.

Table 2-1: Result of cooking with heat pipe and different refrigerants (Esen, 2004)

	R-134a	R-407C	R-22
Test date	8 August 2002	19 August 2002	27 July 2002
Daily total solar radiation incident on tilted collector surface (kWh)	6.65	6.41	6.86
Daily average ambient temperature (℃)	26.5	25.4	26.4
Food and quantity of cooked item (g)	Time taken for cooking item (min)		
250 g rice in 400 g water	63	50	55
250 g macaroni in 400 g water	58	44	48
250 g chicken in 300 g water	60	45	50
Omelette (3 eggs)	40	29	33
Tea (4 cups)	36	27	32

The efficiencies of this type of cooker would not depend only on the climatic conditions, but also on the thermo-physical properties of the refrigerants as well as the design parameters. Compared to other types of cookers, the heat pipe with refrigerants is faster and more effective; it also reduces exposure to the sun and requires less monitoring. Despite all these, it is highly disadvantageous, as Esen (2004) reported that it is very expensive and requires a lot of expertise because it is complex to set up. The system also needs to be preheated often. This technology cannot compete with existing cooking options that are also effective, cheaper and easier to set up.

2.3 Existing Commercial Indirect Steam Cookers

The idea of cooking with the sun has gone beyond just setting up an alternative cooking system for the third world. It has become a realistic heat-generating system for industrial energy breakthroughs in many countries. Different types of commercial solar cookers are currently available, but in the scope of this thesis we considered only the two largest parabolic solar cooker setups. They are indirect solar cooker types and use steam as the heat-transfer fluid.

Figure 2-8a shows such a cooker on a commercial scale –at Taleti, near Mount Abu**,** Rajasthan, India at a height of 1 219 m above sea level. It generates up to 650 ℃, has 84 parabolic dishes in arrays, and cooks an average of 20 000 meals per day or 38 500 when solar irradiation is at its maximum. It is the largest solar cooker set up globally (Basantani, 2008). The set up in Figure 2-8b is the second largest steam-based solar cooking system in the world. It has 106 parabolic concentrators connected in array and mounted at an elevation on a rooftop. The system cooks up to 30 000 meals at maximum insolation (Muthusivagami et al. 2010). The difference in the output of the two systems is due to the altitude of the sites.

The potential of solar cookers to be a large source of energy when used on large scale as seen in Figures 2-8 a and b above shows that when combined with storage facilities, solar cookers can be used as heat source to many industries and can also serve as means of rural industrialisation to develop some heat based firms in the rural areas.

(a) (b)

Figure 2-8: Commercial indirect solar cookers: parabolic concentrators, (a) (Basantani, 2008); parabolic concentrators at Tirumala, (b) (Muthusivagami et al., 2010)

2.4 Solar Cooking Storage

In all the solar cookers considered in the previous sections, their social acceptance and ability to compete favourably with other convectional cooking methods are the same. Most people in Africa, for example, eat in the evening (Higgins, 2013) and communal cooking is done when the sun is down, therefore the acceptance of solar cookers depends on the ability to cook at night. An easy way to overcome this problem is to develop thermal energy storage and incorporate it into the solar cooking system. Several ways have been developed over the years. However, in the scope of this research, only the two most developed and popular types, namely sensible heat storage and latent heat storage, are discussed.

2.4.1 Sensible heat storage

Sensible heat storage is a simple method of storage in which the temperature of a solid or liquid is raised. Various mediums have been tested. For example, Figure 2-9 below shows a double layer 22 SWG aluminium sheet used to make a box and the space between the sheets filled with 5 kg of used engine oil (Nahar, 2003)

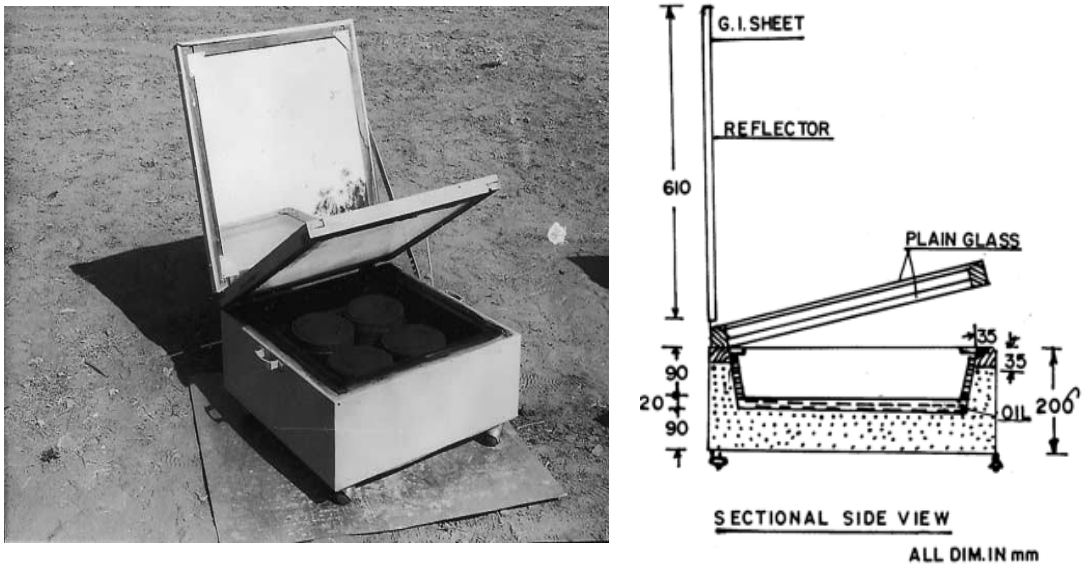

Figure 2-9: Box solar cooker with oil storage (Nahar, 2003)

Nahar obtained an improved efficiency compared to when cooking using a box solar cooker without storage. This is seen in one of his experimental results (see Figure 2-10 below) where 250 g of water was added to the system at 13:00 hours. The results and insolation values of this experiment are also presented. The efficiency of the system with the storage system is 27.5% compared to 14 % of the solar box cookers without storage (Nahar, 2003).

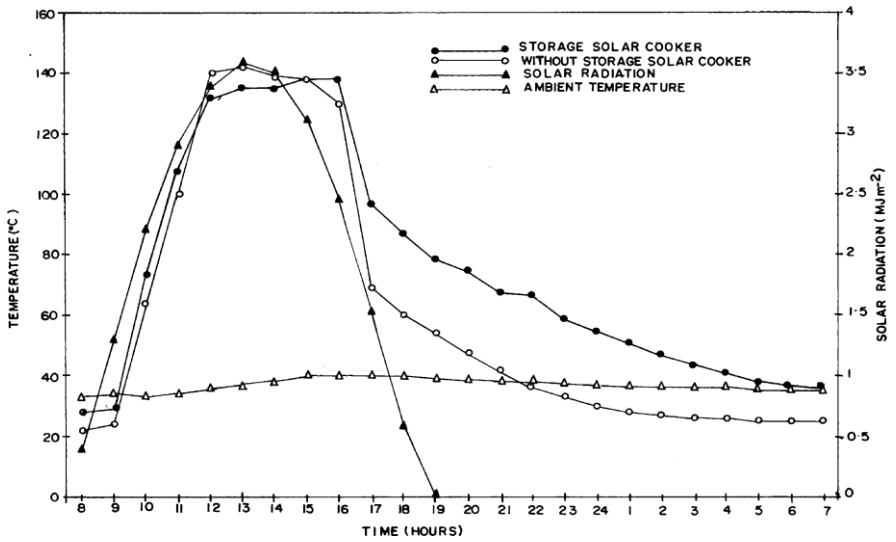

Figure 2-10: Results of experimental comparison of box cookers with and without storage (Nahar, 2003)

Other examples of sensible heat material used in the literature include sand (Ramadan, 1988), which was able to get an efficiency of 28.4 %, with 0.8 kg of water reaching boiling in three hours with an average insolation of 800 W/m^2. Also, Schwarzer and Vieira da Silva (2003) used vegetable oil for an institutional cooker in Chile, as mentioned in Section 2.2.3. This system uses a collector aperture area of 2 m^2 and 50 litres of vegetable oil and

was able to achieve a maximum temperature of 235 ℃ with an ambient temperature of 25 ℃ and global solar irradiation of 900 W/m^2 average.

2.4.2 Latent heat storage

The energy released by a particular material during a constant temperature process is often referred to as the latent heat, and this energy can be used when the material changes phase from one form to another. Phase-change material (PCM) is often compact, with a stable temperature and a high storage density. Various materials have been used in this method. Sharma et al. (2000) used acetamide, which has a latent heat of fusion of up to 263 kJ/kg and a melting point of 82 ℃, as a phase-change material for solar cooking. They had two cylinders in the cooking section and filled the space between them with the acetamide. They proved that they could cook two sets of food if the space in-between the two cylinders was filled with 2 kg of acetamide before 15:30 in the winter. The shortfall of this system is that it cannot cook at night because the melting point of the PCM is too low. Sharma et al. (2000) suggested that a PCM with melting point of around 105 to 100 ℃ would cook when it was dark and that there is a need for a detailed analysis of appropriate melting points and quantities of PCM, as well as the minimum solar radiation needed. The resulting temperature of the solar cooker with PCM and the reference cooker used are presented in Figure 2-11.

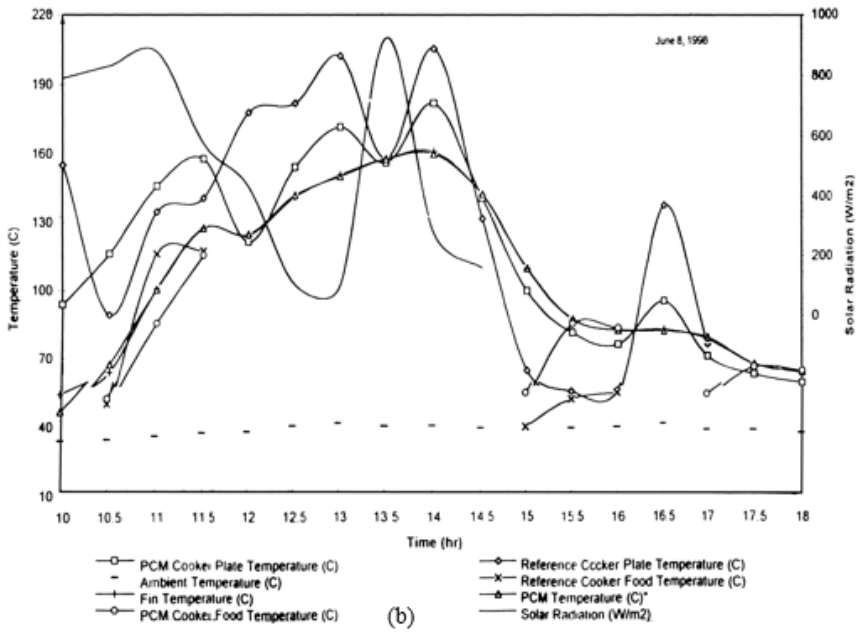

Figure 2-11: Solar cooking with latent heat; graphical result of the experiment (Sharma et al., 2000)

An improved PCM-based solar cooker was developed by Sharma et al. (2005), using an evacuator tube as the collector. The system is active, as it has a pump and a closed loop, as seen in Figure 2-12. The heat-transferring fluid in the system is water and it is pumped throughout the entire system. Stainless steel high-temperature pipe was used for the heat

exchangers. The PCM used was erythritol, which has a melting point of 118 ℃ and a latent heat of fusion of close to 340 kJ/kg.

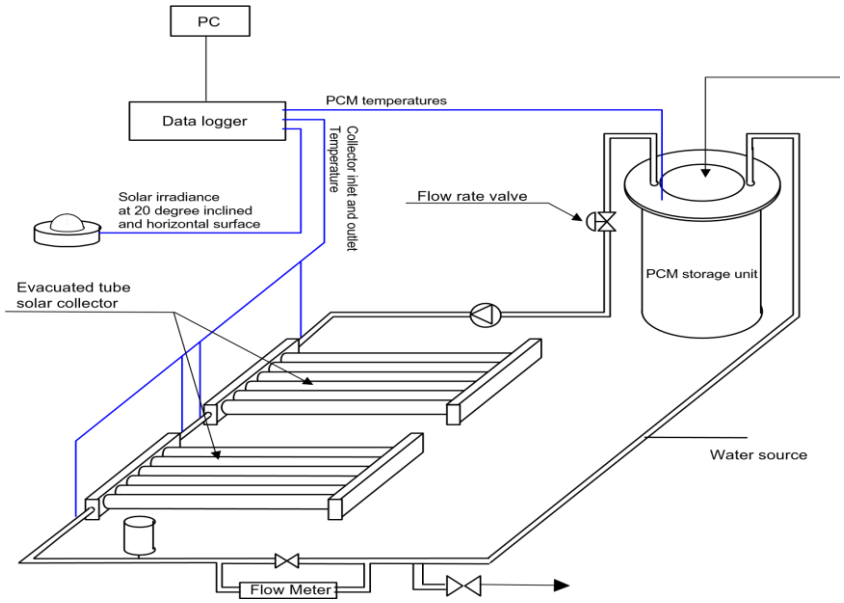

Figure 2-12: Indirect solar cooking latent heat (Sharma et al., 2005)

The fraction ratio of solar insolation to the stored heat in the PCM was very low, but it is a technology for the future. Also, the PCM did not melt in winter, which makes the storage system only usable in the summer, because a stored temperature of up to 75 ℃ overnight was achieved in this period.

The available cookers with thermal storage have been presented as being better in performance than the ones without storage, but, despite this, solar cookers still face some acceptance challenges in Africa. This will be discussed in Section 2.5 below.

2.5 Challenges of Solar Cooking in Africa

Solar cooking was presented earlier in this report as a realistic solution to the problem of poverty and hunger in the world, and particularly in Africa, by supplementing the insufficient energy supply for home and industrial cooking. Wentzel and Pouris (2007) observed that the use of solar cookers in South Africa, for example, although not yet as popular as expected, had brought some savings associated with their use. In their experiment, the GTZ/DME solar cooker field test in South Africa, fuel savings, monetary savings, time savings and poverty reduction were highlighted as some of the benefits of using solar cookers. The reasons for purchasing solar cookers found in their experiment are presented in Table 2-2 below

Table 2-2: Reasons for solar cooker acquisition (Wentzel & Pouris, 2007)

Reason	Entries
Savings	44
Convenience	29
Others	13

Table 2-2 above does not show the specific type of savings that motivate the purchase of solar cookers, either in terms of time, money spent on other cooking or energy generated. Wentzel and Pouris (2007) observed, however, that people in South Africa are motivated by energy to savings efficiencies. Therefore, if an inexpensive, effective system is designed, it will gain market confidence with time.

Solar cookers still face some challenges in their commercialisation in Africa. This is due to the fact that it is a new technology, and a person with insufficient income (as are most people in Africa) may not be willing to take an investment risk. Despite various campaigns in the media and by different bodies, the use of solar cookers is still very low in Africa. Despite the sunshine available and the campaigns for commercialisation, investors continue to lack confidence in these systems (Biermann et al., 1999). Wentzel and Pouris (2007) show in their GTZ/DME solar cooker field test in South Africa that the average use rate of solar cookers in South Africa can be improved, and this situation does not differ in other African nations.

2.6 Sunshine in South Africa

The experiment presented in this report was done in South Africa. Therefore, there is a need to know if the project is realistic in terms of solar resources. Figure 2-13a below shows the intensity of direct normal irradiance (DNI) in Africa, while Figure 2-13b shows the abundance of sunshine in Africa expressed in colour impressions from green and yellow to deep red. The colours indicate the regions with the least supply of DNI to those with the highest possible DNI respectively. The African continent as a whole receives 365 days of sunshine in a year, with the northern and southern regions having some of the best DNI locations on earth. This means that developing a system that can maximise the available sunshine in Africa will be a profitable venture. The solar resources available in South Africa mean that it has good potential to lead the world market in solar renewable energy. In South Africa alone, as seen in Figure 2-13b, most of the areas get more than 2 500 hours of sunshine in a year and an average daily solar insolation of between 4.5 and 6.5 $kWhr/m^2$ (NREL GIS, 2015). This makes the country a good location to develop the idea proposed in this report

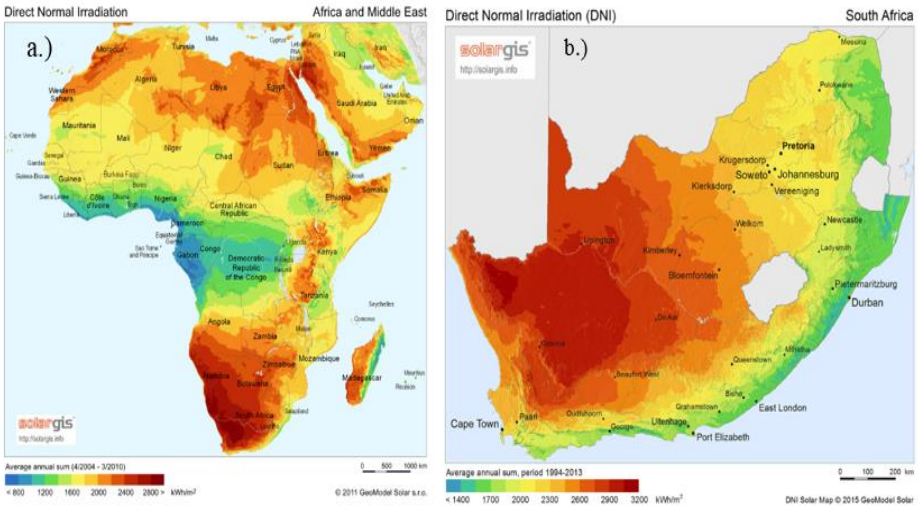

Figure 2-13: DNI map: Africa (a); South Africa (b) (Solar-GIS, 2011)

The department of energy in South Africa claims that the average daily solar radiation received in the country is more than double the amount received in the United Kingdom and Europe in general, and far more than the daily radiation received in the United States of America, as shown in Figure 2-14.

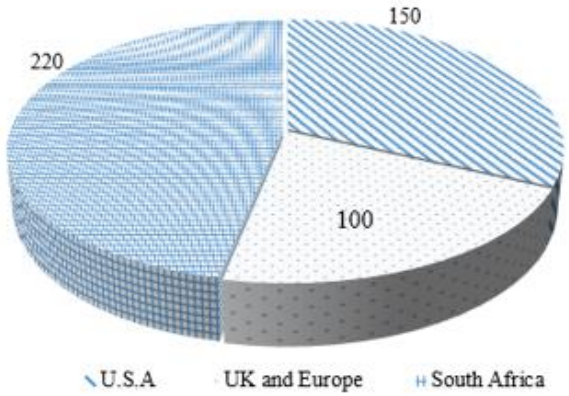

Figure 2-14: Average annual 24-hour global solar radiation

2.7 Chapter Summary

A comprehensive and historic overview of solar cooking was discussed in this chapter, along with its timeline. It was noted that there is no conventional way of classifying solar cookers, but the classifications of Muthusivagami et al. (2010) were in this chapter. The various types of solar cookers were discussed, together with their necessary output and improvements. More emphasis was placed on the experimental and numerical analyses done on the parabolic cookers, as this is related to the setup discussed in this report. The largest existing commercial types of solar cooking installations that use the same parabolic reflector technique (although steam powered) as the one used in this report were been

shown, and the two most popular forms of solar storage, with their advantages and disadvantages, were discussed. The last two sections discussed the challenges of solar cooking in Africa, which is in contrast with the amount of sunshine in South Africa, where these experiments were carried out.

In Chapter three, the discussion will focus on solar angles, resource mapping and tracking, and how the necessary data and measurements were obtained for this particular experiment.

3 Solar Radiation, Angles and Tracking

The sun is the ultimate source of energy and its usefulness households cannot be overemphasised. The irradiation from the sun is a natural resource that can be harnessed to lead a breakthrough in any community that maximises it (Craig & Dobson, 2015). Africa is blessed with good solar energy resources, as already identified in Section 2.6 of Chapter two. To achieve the primary objectives of this research, as stated in Section 1.2, it is of the utmost importance to understand the solar resources available in the location where the setup was arranged. This chapter discusses the available solar resources, the sun-tracking mechanism and the necessary calculations to achieve a successful capturing of the sun's energy to get maximum the usage efficiency of the system.

When a solar system is to be considered for long-term use or commercialisation, the solar resources and data needed for its design should not be based only on the predictive meteorological data, but also on a statistical combination of the solar radiation measured over the years for that same location or a similar place with the same climatic conditions. Often, the hourly diffuse radiation of the sun and the beam solar radiation are available for many areas (Kalogirou, 2009). This radiation data is available in minutes and hours for each day; either of these can be summed to obtain yearly average data.

Two types of radiation sources are often considered in solar process modelling, namely solar or short-wave radiation, and long-wave radiation. While the former is the radiation whose primary source is the sun and has either direct (beam) or diffuse rays of the sun, the latter is long-wave radiation that represents the radiation that is not directly from the sun, but from a solar receiver/collector or its surrounding matter that has a temperature either in parity to the ambient temperature or close to it (Duffie & Beckman, 2013). These terms, which largely will be used in this document, are illustrated in Figure 3-1 below

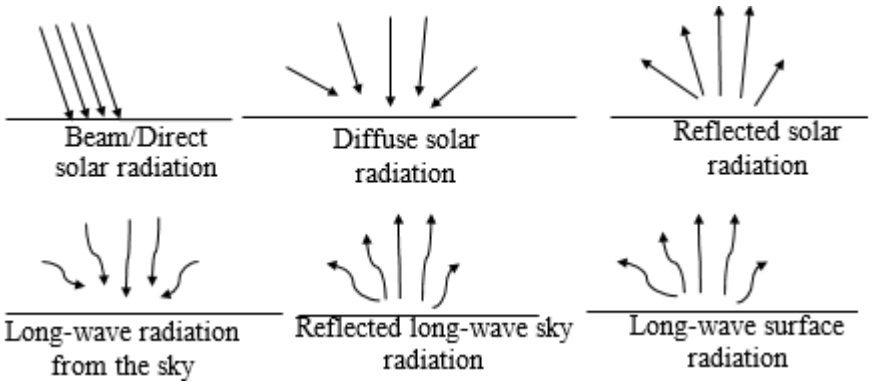

Figure 3-1: Solar energy fluxes showing short/solar and long-wave radiation

The types of solar radiation established in the paragraph above are of the utmost importance to this study, because it is reflected radiation that is needed for the desired solar applications. The theoretical calculations for this radiation will be dealt with in Chapter three of this report. The direct and diffuse radiation of the sun must be known in order to aid the appropriate siting of a solar project and to use for predicting the amount of solar resources that will be available for the system to be set up. Two important instruments are used to measure these solar resources. These are the pyrheliometer, which measures direct

solar radiation, and the pyranometer, which measures global horizontal irradiation (GHI). The latter , (GHI)is the addition of the beam and the diffuse at normal incidence (Espinar et al., 2009; Zawilska & Brooks, 2011).

For this study, the pyrheliometer and pyranometer used are located on the solar roof of the engineering faculty at Stellenbosch University (SU), at a latitude of 33 ° 55 ’S and a longitude of 18 ° 51 ' E, with an elevation of 119 m above sea level. The instrument is a SOLYS 2 sun tracker by Kipp & Zonen (2011), the property of the Solar Thermal Energy Research Group (STERG) in the department of mechanical engineering at SU. It is a fully automatic sun tracker with integrated GPS that allows it to automatically download the time and location data of its site once installed, therefore eliminating the need for software or a computer during the setup. The GPS receiver of SOLYS 2 keeps track of the time and thus prevents the setup from suffering from internal clock drift. The system is used mostly for tracking the sun for either meteorological or solar energy uses, is easy to install and operate, and has a Baseline Surface Radiation Network (BSRN) (Kipp & Zonen, 2011). The system can make use of either alternating (AC) or direct current (DC) at 24 V, and its working temperature range is between -20 °C and 50 °C when working on DC; this can be extended to -40 °C in AC conditions. The system is rugged and its housing is made from cast aluminium material.

The SOLYS 2 system used in this study is shown in Figure 3-2. The arrows show an enlarged view of the pyranometer and pyrheliometer, which were both fastened to the same support stand, making up a complete assembly.

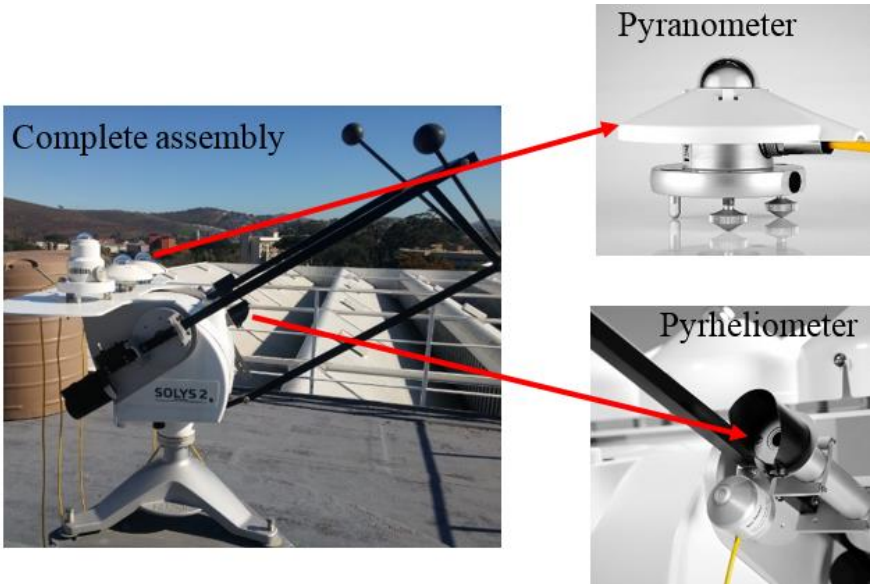

Figure 3-2: SOLYS 2 Sun Tracker on site at SU

The data from this system was then downloaded through the weather station at Stellenbosch University. It is worthy to note here that direct rays, otherwise known as direct normal irradiation (DNI) are of more importance to this study, as the concentrating solar power (CSP) system was considered. The reflected rays are functions of the DNI falling on the solar energy collection platform. Also, it should be noted that these instruments were used just to compare the data from the experiment, as it had its own tracking mechanism, as shown in Section 3.3.

3.1 Solar Radiation and the Sun's Path

Solar irradiance is instantaneous; it is the rate at which a solar receiver receives optical radiation from the sun as a function of its own aperture area (Gueymard, 2012). Solar irradiation, on the other hand, has the same definition but is measured over a longer time, from a day up to yearly data. The harnessing of solar radiation is often easier when the sun path is known. This sun path is defined as the regular change in the position of the sun that occurs either hourly or seasonally. It determines the position of the sun in the sky and is a major factor that dictates the availability of solar radiation. The sun path for the location used for the experiment – the rooftop of the heat transfer laboratory at the department of mechanical engineering, SU, was determined by writing the necessary scripts into the sun-path design software of the University of Oregon (UO) Solar Radiation Monitoring Laboratory (2007). The results from running the scripts are diagrammatically displayed below, where Figure 3-3 shows the sun path for December to June and Figure 3-4 shows the sun's path for June to December.

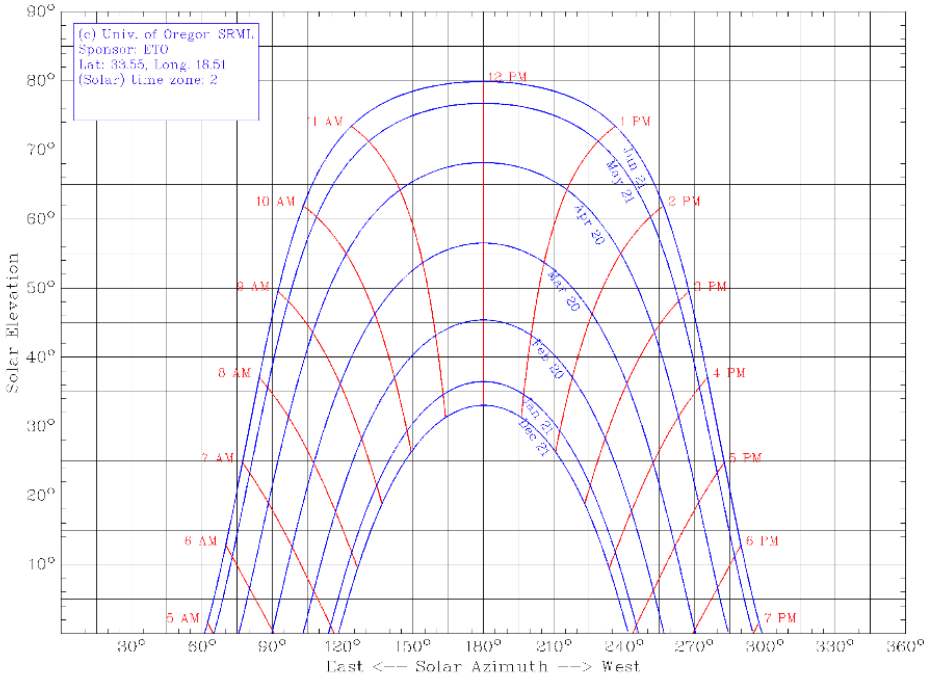

Figure 3-3: Solar azimuth angles for December through June

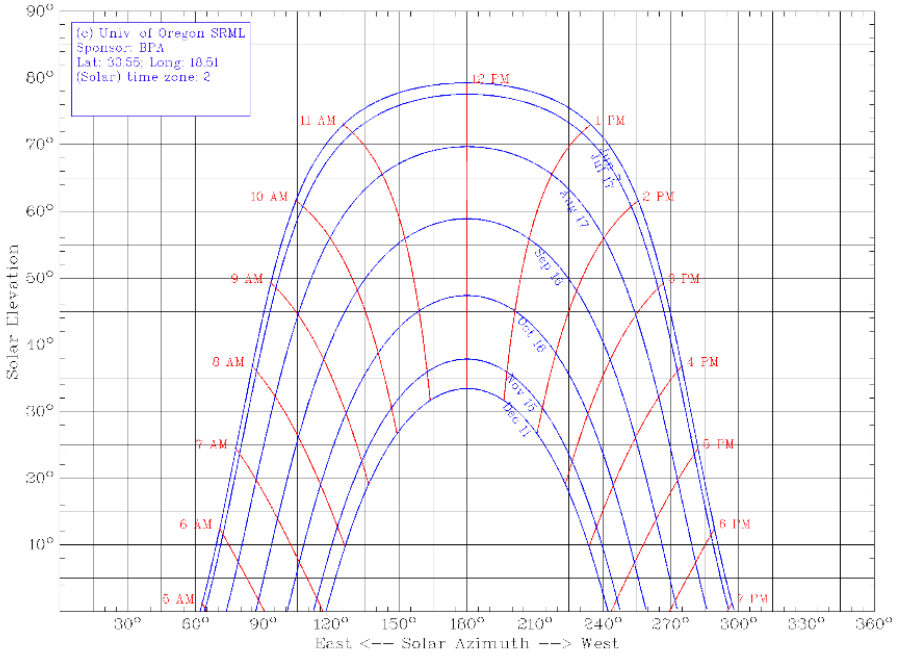

Figure 3-4: Solar azimuth angles for June through December

The angle that the solar collector must face in order to receive the maximum exposure to solar radiation is also displayed in Figures 3-3 and 3-4. Another result generated from running the scripts on UO Solar Radiation Monitoring Laboratory software is displayed in Figure 3-5, where the sun path, in red, is plotted as a function of the solar hour, which is shown in blue as a basis for our locational resource mapping.

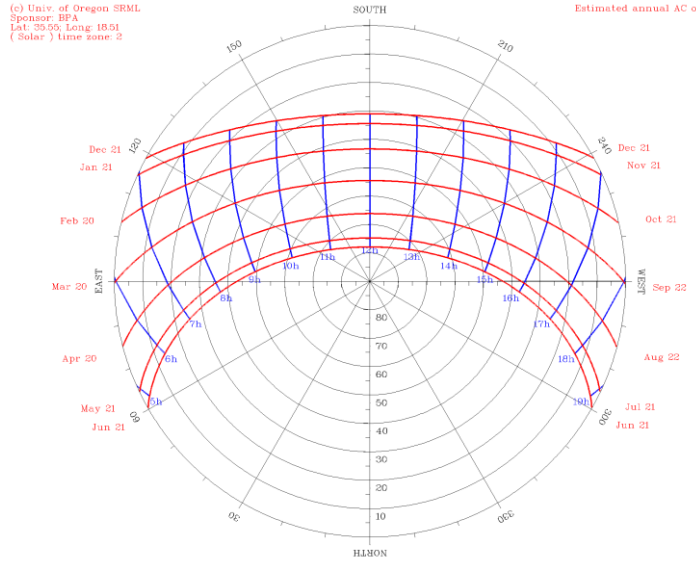

Figure 3-5: Yearly Sun Path for Stellenbosch University

In summary, the needed solar radiation and how to measure it have been identified in this section, and the sun's path throughout the year has been modelled and the angle for maximum solar resources collection has been shown. The next section presents the

theoretical method used to calculate the solar angles for effective mapping; and forms the basis for the design of the tracking system, which will be discussed in Section 3.3 of this chapter.

3.2 Angles of the Sun

In an effort to determine the altitude and azimuth angle needed for accurate positioning of the solar collector to be used in the tracking system with respect to the identified path of the sun, and to generate the necessary data for the theoretical analysis for this experiment, various equations and angles of the sun were defined, as shown in Figure 3-6.

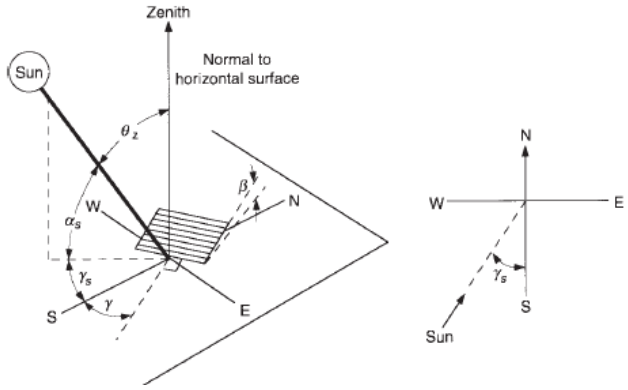

Figure 3-6: Angles of the sun relative to horizontal surface (Duffie & Beckman, 2013)

In Figure 3-6, N, E, W and S represents north, east, west and south respectively, while other parameters are defined below, in sections 3.2.1 to 3.2.5.

3.2.1 Equation of the time (EOT)

The equations of time (EOT) refers to the difference between the true solar time and the mean solar time, and can be determined using the equation presented by Stine and Geyer (2001):

$$EOT = 0.2587cos(x) - 7.416sin(x) - 3.648cos(2x) - 9.228sin(2x)\ \ (mins) \quad (3.1)$$

The "x'' term in the equation of time is in degrees and it also defined as

$$x = \frac{360(N-1)}{365.242} \quad (3.2)$$

where N is the number of days calculated from January, as shown in Table 3-1.

Table 3-1: Calculation for day of the month

Month	N for ith day of the month
January	i
February	31 + i
March	59 + i
April	90 + i
May	120 + i
June	151 + i
July	181 + i
August	212 + i
September	243 + i
October	273 + i
November	304 + i
December	334 + i

3.2.2 Solar time and hour angle (ω)

For easy analysis of the earth's rotation about its axis, the hour angle ω is defined to show a specific position on earth (Yao et al., 2014). It increases at 15 degrees per hour and it is zero; at solar noon it can measure east and west of the meridian; it is negative in the morning and negative in the afternoon (Duffie & Beckman, 2013). Solar time t_s, however is often not equal to the normal day time and it varies for different places on planet earth, as it is a function of the longitude of the location. This is necessary as it is used to predict the sun's ray direction at any point on earth. The expression below relates hour angle to solar time in degrees.

$$\omega = 15(t_s - 12) \tag{3.3}$$

To convert the solar time to local time in hours, the general solar time-local time conversion equation can be used

$$LCT = t_s - EOT + LC + D \tag{3.4}$$

Stine and Geyer (2001) state that the parameter D is given a value of 1 when daylight saving is in use and zero otherwise, and the equation of the time is measured in hours and represented by EOT in Equation 3.4. The factor for longitude correction is represented by LC and is defined as:

$$LC = \frac{(local\ longitude) - (longitude\ of\ standard\ time\ zone\ meridean)}{15} \tag{3.5}$$

In Equation 3.4, the solar time can be calculated by making t_s the subject of the formula and putting in the values.

3.2.3 Declination angle (δ)

The declination angle is the angular distance of the sun to the north or south with reference to the equator. It can be determined using the equation offered by Pih and Kalogirou (1997):

$$\delta = sin^{-1}(0.3975cos\,[0.98563(N-173)]) \tag{3.6}$$

where N is the day number defined in Table 3-1.

3.2.4 Zenith angle (θ_z) and altitude angle ($\propto$)

The solar zenith angle θ_z, seen in Figure 3-6, is the angle between the sun's rays and the vertical, and the altitude angle (α) is the angle between the sun's rays and the horizontal; both are expressed as seen in Equations 3.7 and 3.8 below:

$$\propto = sin^{-1}[sin(\delta)sin(\emptyset) + cos(\delta)cos(\omega)cos(\emptyset)] \tag{3.7}$$

$$\theta_z = 90^{\circ} - \alpha \tag{3.8}$$

3.2.5 Solar azimuth angle

The solar azimuth angle is the sun's rays measured in a horizontal plane in the direction due north, while to the east it is negative and to the west it is positive.

$$\gamma_s = sin^{-1}\left(\frac{cos(\delta)sin(\omega)}{cos(\alpha)}\right) \tag{3.9}$$

On the other hand, γ is the surface azimuth angle defined as the deviation of the projection on the horizontal plane in Figure 3-16 from the surface of the local meridian, $-180^{\circ} \leq \gamma \leq 180^{\circ}$ (Duffie & Beckman, 2013). It is calculated as a function of the latitude angle and the declination angle, as

$$cos\,\gamma = \left(\frac{sin(\alpha)\,sin(\emptyset) - sin(\alpha)}{cos(\alpha)\,cos(\emptyset)}\right) \tag{3.10}$$

The latitude angle $\emptyset$ was given a negative value, since this experimental setup was located in the southern hemisphere.

3.3 Solar Tracking System

It is now generally accepted by researchers that solar cookers with tracking systems are more efficient than stationary ones (Al-Soud et al., 2010). In this section, a tracking system that is easy to use and user friendly is introduced. The aim here was to develop a tracking system that can support the desired solar cooking system. A two-axis tracking system was selected, as it automatically reduces the regular inspection and unnecessary exposure to the sun when the system is in operation. To achieve this, a modification of Prinsloo's (2014) Siemens solar tracking system test facility was done using the model (Roth et al., 2005) shown in Figure 3-7.

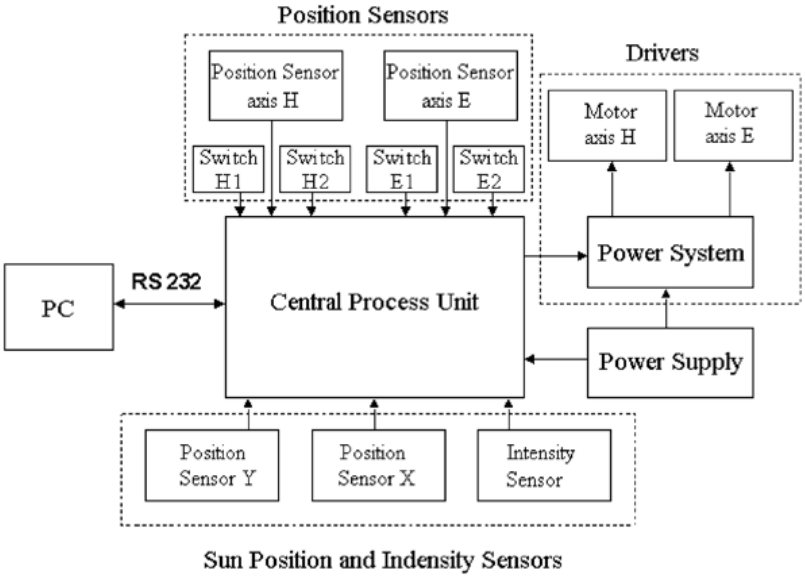

Figure 3-7: Tracking system and control (Roth et al., 2005)

The tracker was designed to be dual axis; it uses the altitude (α) and azimuth(γ) tracking and both axes of the drive have potentiometer attached to them. This system was modified using four switches, two switches for each axis and two of the switches are always closed, this is used to determine the minimum and the maximum position of the sun as well as the limit of rotation. The two tracking axes in terms of their motion are represented by A and E in our case as compared to H and E in Figure3-7. Figure 3-8 shows the definition of these two axes A and E in their minimum positions when $A = 0°$ and $E = 0$ .These notations (A1, A2, E1 and E2) represent the switches that define the minimum and maximum positions of the axes as shown in the Figure 3-8 below.

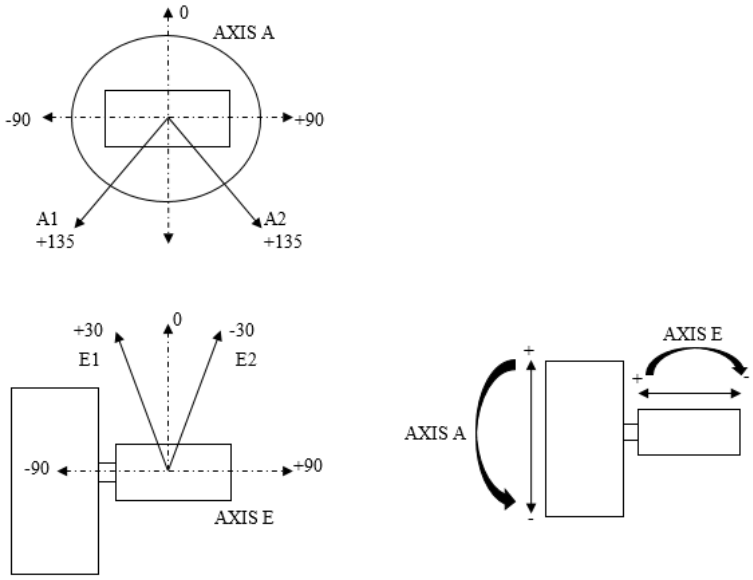

Figure 3-8: Minimum and maximum positions of the A and E motion axes

When the setup traces the sun in an East-West direction, the tracking angle ρ becomes a function of the solar angle and is defined as

$$tan\,\rho = \frac{sin(A)}{tan\,\alpha} \tag{3.11}$$

When it is tracking the sun from the North, the tracking angle becomes

$$tan\,\rho = \frac{-cos(A)}{tan\,\alpha} \tag{3.12}$$

The combined incidence, angle θ_i, can be written in terms of the cosine values of the aperture area A and the solar angle α:

$$cos\,\theta_i = \sqrt{1 - cos^2(\alpha)\,cos^2(A)} \tag{3.13}$$

The tracking axis developed for the tracking angle ρ is shown in Figure 3-9.

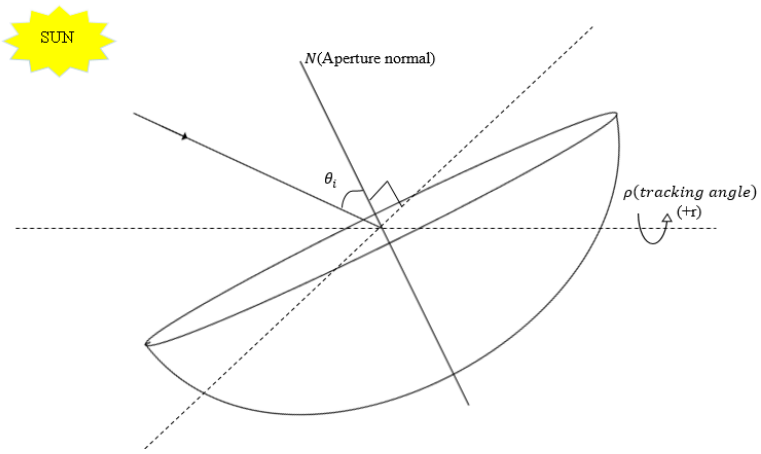

Figure 3-9: Tracking angles

A dual-element actuator drive was used to achieve the desired rotation in the two axes when the solar tracking operation was on. The two DC motors (H and E) in Figure 3-7 receive their electric signal as a 24 V pulse-width modulation (PWM), which is sent from the power line communication (Prinsloo, 2014). The accuracy and efficiency of the tracking system were analysed by placing the photo sensor on the pole mounted on the tracker stand, as will be discussed in the experimental setup in Chapter four. The system was then connected to a data logger. It started with the motors rotating according to the azimuth and altitude of the sun, and the solar irradiance on the photo sensors was recorded. The results of the solar tracking were compared to the data from the SOLYS 2 standard values, which were downloaded from the SU weather station, and the results are shown in the graphs below.

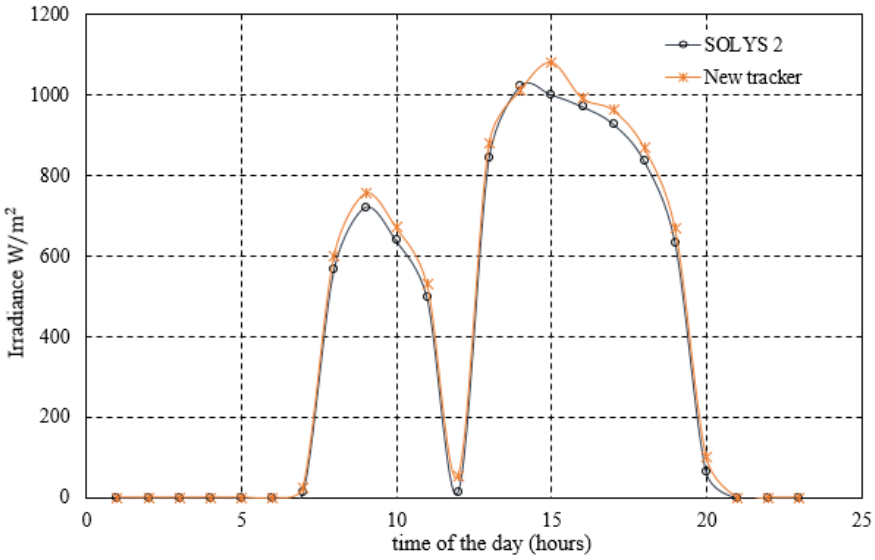

Figure 3-10: Irradiance comparison of SOLYS2 and the manufactured tracker on 14 February 2015, based on hourly data collection

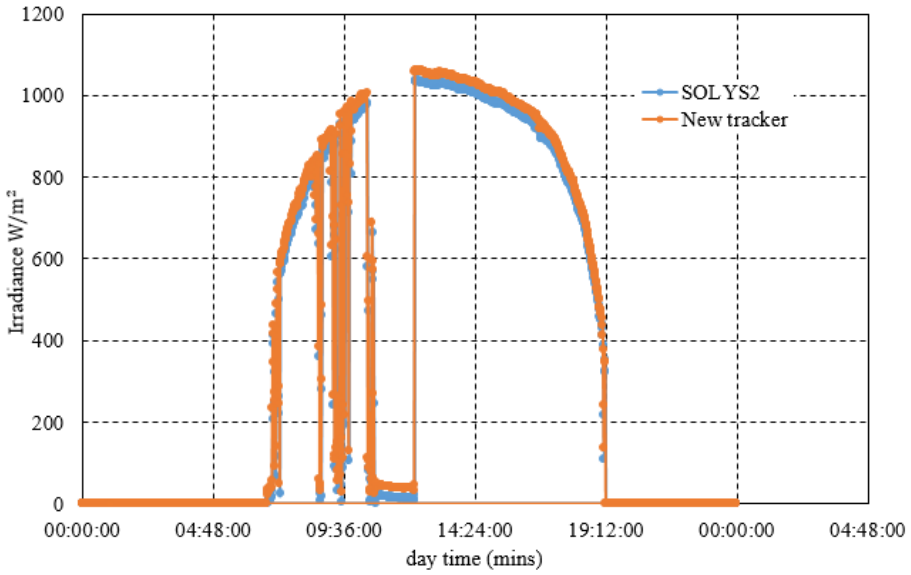

Figure 3-11: Irradiance comparison of SOLYS2 and the newly made tracker on 14 February 2015, based on per minute data collection

Figures 3-10 and 3-11 show that there is closeness in the solar resource mapping of the two tracking systems, although a few deviations occurred, and these were analysed on the combo error graph shown in Figure 3-12.

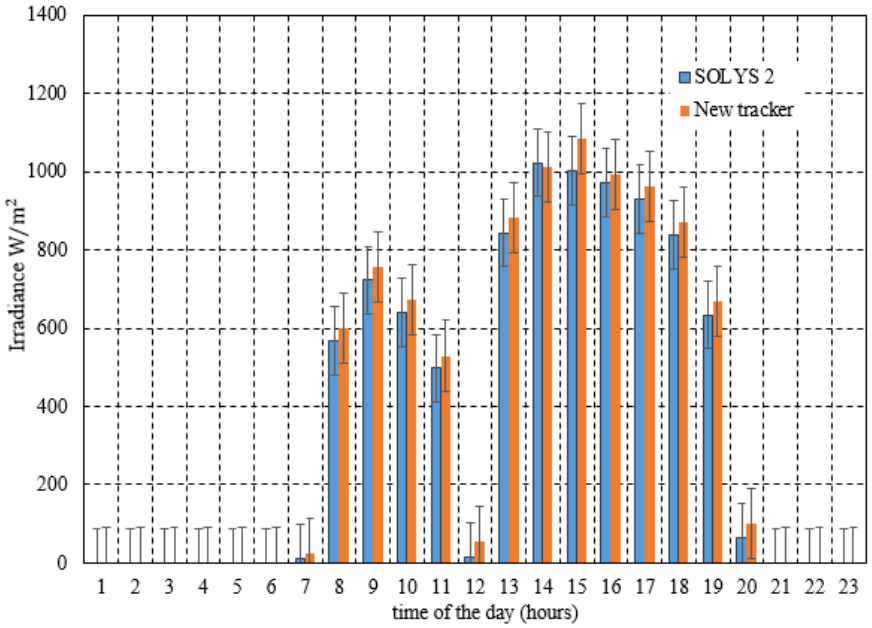

Figure 3-12: Combo chart with errors bar of irradiance – comparison of SOLYS2 and the newly made tracker on 14 February 2015, based on hourly data collection

The average overall deviation in the two sets of compared data for 14 February 2015 was 4.6 %. These losses, however, were accounted for in the design of the solar receiver, as will be shown in the next chapter, while the setup will be dealt with later in this report.

3.4 Chapter Summary

In this chapter, the path of the sun for the location of the experiment was determined; the step by step method to calculate the angles of the sun needed for right tracking and orientation of the solar collector were also calculated. The technique with which the system tracks the sun in the two directions has also been identified. The solar resources reading from the newly improved tracker's reading was compared to the one measured by a standard SOLYS2 and the charts with error bars was presented, the deviation was seen to be average around 0.046.

Having understood how to harness the power of the sun, Chapter four will provide the detailed calculations and optimisation of the collector, the receiver, the storage and the necessary heat transfer and modelling analysis, which were used to size this parabolic cooking system.

4 Theories of Solar Energy Processes

The effectiveness of any engineering design is embedded in the correctness of the choice of its theoretical calculations. This chapter discusses the theoretical background and design models adopted for the experimental setup in this report in order to achieve effective solar cooking. For easy analysis, the solar cooking system that was developed is divided into three subsystems, namely solar energy collection, cooking and thermal energy storage. These subsystems are discussed in this chapter.

4.1 Solar Energy Collection

Harnessing enough solar energy for a desired system and reducing the likely losses in the selected system are the two major issues that drive the modelling of any solar heat process and application (Duffie & Beckman, 2013). In order to address these issues, this subsection discusses the type of solar collector used, how the collector reflects the rays of the sun, the type of receiver adopted, how the reflected energy was collected in terms of heat energy in the receiver, as well as the heat transfer analysis involved in each section. In these calculations, it first was necessary to understand how solar energy collection is achieved and what type of collector must be used to achieve the aim of having a heat output of around 200 to 220 ℃ in the cooking section.

According to Al-Soud et al. (2010), a solar collector is a device that is used to convert direct radiation from the sun to electricity and/or heat. CSP has been identified as the best way to generate heat energy from the sun (Kalogirou, 2009). Against the background of sections 2.2.2 and 2.3 of Chapter two, the parabolic dish type was selected for this study. The principle of operation of this type of system is that the parabolic dish faces the sun and then reflects the rays of the sun to a solar receiver.

Before discussing the details of the parts responsible for solar energy collection, the background overall equations are presented for guidance in the energy balance. In a separate heat transfer analysis for concentrating systems, Shuai et al. (2008) and Reddy and Sendhil Kumar (2009) showed that, in order to carry out a credible energy balance in thermal solar energy-collecting systems, it is often better to single out the collector and receiver and then balance the energy in and out of them. The overall energy balance in this subsection therefore can be written in terms of the rate of useful energy $(\dot{Q}_u)$, the rate of optical radiation that is incident on the receiver from the dish $(E_{optical})$, and the rate at which there are thermal energy losses in the receiver $(\dot{Q}_{loss})$, expressed by Stine and Geyer (2001) as

$$\dot{Q}_u = E_{optical} - \dot{Q}_{loss} \tag{4.1}$$

The setup under consideration in this report is an indirect system that involves a heat-transfer fluid; therefore, the useful heat energy $(\dot{Q}_u)$ can be expressed in terms of the heat that is added to the oil while it travels through the receiver, as

$$\dot{Q}_u = m\, c_p\, (T_{out} - T_{in}) \tag{4.2}$$

Now that the governing equations are known, the various parts of the solar energy collection subsystem will be presented in the following sections

4.1.1 Dish theory: parabolic dish geometry

The parabolic dish was selected as a concentrator in this study because it has the potential to meet both the medium and high temperature needs of humans and has been identified to be most efficient in terms of heat generation (Prakash et al., 2009). When the sun shines on this concentrator, it reflects the rays of the sun to a receiver that is placed at its focus point. The parabola occurs when the locus of a point has the ability to realign itself such that its distance from a stationary point and a fixed line is always the same (Stine & Geyer, 2001). This is shown explicitly in Figure 4-1 below, where the Directix represents the fixed line, the stationary point is the focus represented by F, and the axis of the parabola is the imaginary line drawn passing through the point F and at a right angles to the Directix. The vertex (V) of the parabola is the point at which the axis of the parabola passes through the parabola, and it is also a point that is located at the midpoint between the focus (F) and the Directix of a parabola.

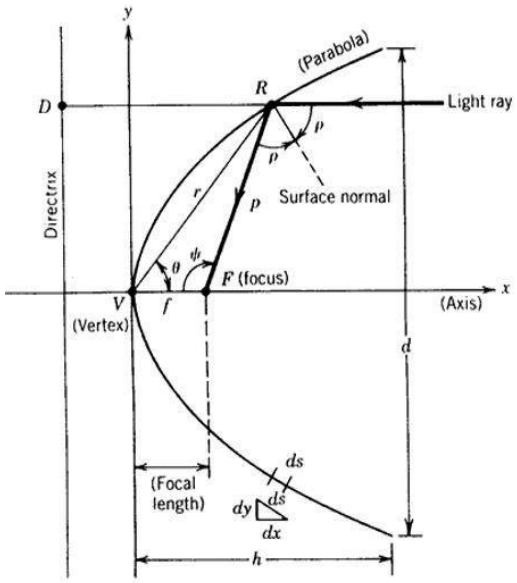

Figure 4-1: Geometry of a parabola (Stine & Geyer, 2001)

Taking the origin as vertex V in Figure 4-1, and the x- axis as the horizontal axis along the parabola, the equation of parabola can be expressed as

$$y^2 = 4\,f\;x \tag{4.3}$$

In Equation 4.3, f is the focal length (the distance VF, which is from the vertex to the focus). However, Stine and Geyer (2001) have illustrated that, for optical calculations, when the point of origin is shifted to the focal point (F), with the vertex on the left-hand side of the origin, Equation 4.3 would become:

$$y^2 = 4\,f\,(f + x) \tag{4.4}$$

The parabolic radius (p) is the distance from the focus to the curve, and ψ is the angle measured from line VF. With the origin still at F, these parameters can be related by an equation (illustrated by Stine & Geyer 2001) as

$$p = \frac{2\,f}{1 + cos\,\psi} \tag{4.5}$$

All the rays from the sun reach the earth in parallel form (Pih & Kalogirou, 1997); therefore, all incident rays on the parabolic dish axis are reflected back to the focal point F, as shown by the thick line in the figure; the reflected angle is the same as the incident angle in accordance with Snell's law, which states that the angle of incidence and reflected angle are equal. From Figure 4-1 above, it can be observed that an expression can be developed as

$$\psi = 2\rho \tag{4.6}$$

All parabolic equations derived thus far are imaginary, as they work for parabolas with infinitely continuous curve lengths, but they are useful because they form the basis on which the size of different parabola can be determined, depending on where the curve is truncated, as shown in Figure 4-2, where all parabolas in it have the same point focus and aperture diameter, but different rim angles. The point or extent of truncation of a parabola is often defined in terms of rim angle ψ, or of the ratio of focal length to aperture diameter (f/d)

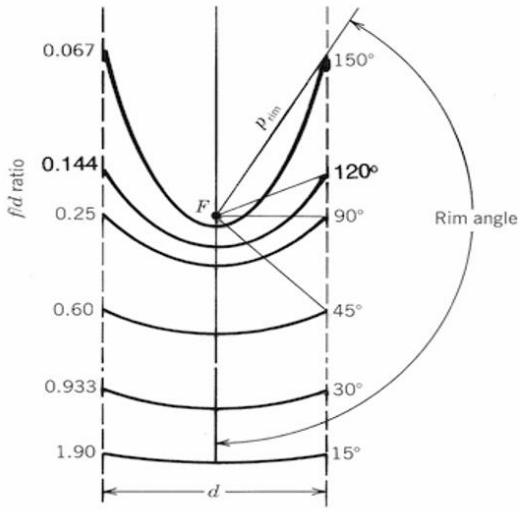

Figure 4-2: Parabolas with the same aperture radius and common focus but varied rim angles

From Figure 4-2 it can be seen that the smaller the rim angle, the further the focal point moves away from the parabolic curves. Also, the parabolas with the higher rim angles are less flat, deeper and have their focal point closer to their parabolic curves. From Figures 4-1 and 4-2, another parameter, h_{par} (which is the height of the curve), can be defined as the maximum or farthest distance from (V) that the vertex is to a straight line drawn across the circular aperture part of a parabola, as shown explicitly in Figure 4-2. The relationship between the height of the curve, h_{par}, and the diameter of the aperture (d) and the focal length (f) can be then stated as

$$f = \frac{d^2}{16\,h_{par}} \tag{4.7}$$

The focal point of the dish is of the utmost importance, as it is the place through which all the reflected rays pass and it is also the point where the most thermally effective reflected shape of the sun is formed. In this setup, the $h_{par,curve}$ and d can be measured directly from the parabolic dish and, from this, the numerical analysis of the parabola can be determined by using Equations 4.4 to 4.7, which relate the focal length to the geometric shape of a parabola on a Cartesian plane. In this study, the results of the geometric analysis using these sets of equation are shown in Figure 4-3

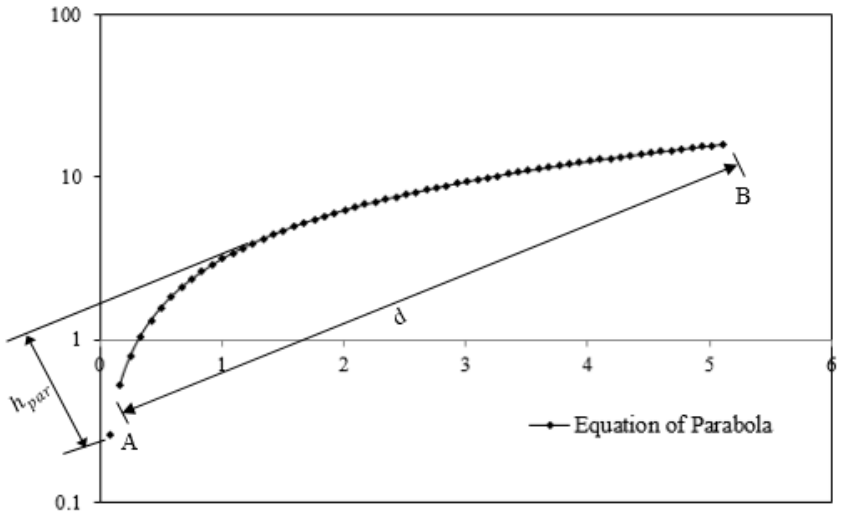

Figure 4-3: Logarithm parabola profile from equations

The line AB in Figure 4-3 represents the diameter of the aperture collector area and it corresponds to the actual aperture diameter. With the dish diameter known and the aperture area of the reflecting side calculated, we can further define the rim angles as

$$tan\,\psi = \frac{1}{\left({}^{d}/_{8\,h}\right) - \left(\frac{2\,h}{d}\right)} \tag{4.8}$$

The arc length (s) in metres can be derived by integrating Equation 4.8 and then set the limits between x = h and y = d/2. These was given in simple form by Stine and Geyer (2001):

$$s = \left\{\frac{d}{2}\sqrt{\left(\frac{4\,h}{d}\right)^{2} + 1}\right\} + 2\,f\,\mathrm{In}\left\{\frac{4\,h}{d} + \sqrt{\left(\frac{4\,h}{d}\right)^{2} + 1}\right\} \tag{4.9}$$

4.1.2 Dish optics and ray tracing

In the previous section, the primary properties of the dish were calculated. In this section, the optics of the dish and how to position it for maximum reflection output will be presented. To analyse the optics of parabolic concentrators, the plane of curvature needs to be defined for easy analysis, and the plane shown in Figure 4-4 below shows a two-dimensional plane that cuts a parabolic axis perpendicularly. In parabolic troughs, the plane extend to the axis of the concentrator, but in the case of a parabolic dish the plane of curvature can be rotated to form the dish geometry

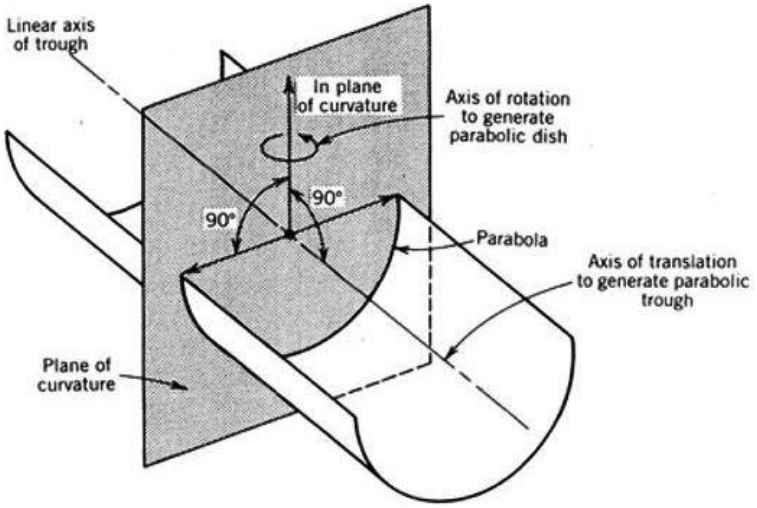

Figure 4-4: Plane of Curvature of parabolic concentrators (Stine & Geyer, 2001)

The optical analysis, which concerns how the dish reflects the incident rays for this setup, was performed using ray trace diagrams, as shown in Figure 4-5. The offset was taken to be zero in Figure 4-5a, with the incident rays normal to the receiver aperture. In Figure 4-5b, an offset value of one degree was set in order to compare the accuracy of the focal point of parabolic dishes when the rays are parallel and when they are not.

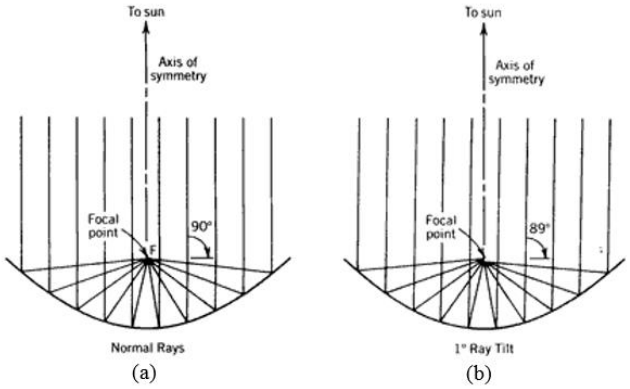

Figure 4-5: Optics of parabolic reflectors Parallel rays to the symmetry axis (a), Parallel rays offset by 1 degree (b)

From Figure 4-5a above it is clear that the rays reflected by a parabolic dish when they are parallel to the axis of symmetry always converge at the focal point F, while it can also be noticed that the parabolic dish is not symmetrical to rotation, and any tilt or shift of the incident rays of the sun from the normal of the parabolic dish leads to a resultant dispersion, and no sharp image is formed on the focal point, as shown in Figure 4-5b. From these diagrams we therefore can ascertain that, for a parabolic dish to be effective, it must track the sun accurately in order to ensure that the incident rays of the sun always are parallel to the normal axis.

4.1.3 Reflection of energy to the receiver

Now that the way in which a dish reflects energy is known, the next thing to know is how to reflect such energy to the receiver. It can be assumed that all parallel sun's rays are normal to the collector (dish) aperture area, and this makes it easy to develop an equation in terms of the rim angles. The angular errors of the sun's ray as relating to the aperture surface of the dish (slope errors) can then be computed. The way in which the reflected rays of the sun are spread from the concentrator are dependent on its tracking and slope accuracies. These analyses of the reflection of rays of the sun can be used to further determine the optimum size of the receiver that must be manufactured so as to capture enough reflected rays. The step-by-step analysis to achieve these goals is presented in the logic chart in Figure 4-6 below. It should be noted that the equation for rim angle was defined earlier in Equation 4.8

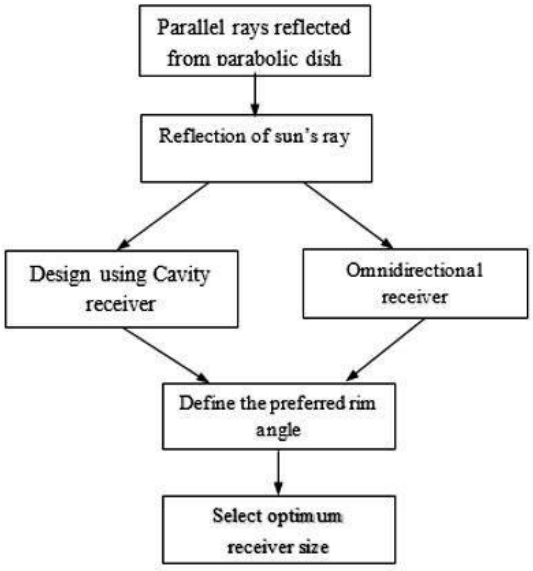

Figure 4-6: Optical analysis of parabolic concentrator

4.1.4 Error calculations and actual parabolic reflection

The reflection method of the dish was displayed in Section 4.1.2, where the need for accurate knowledge of its focus and correct positional tracking were shown. In this section, the errors that accompany this positioning and tracking are analysed. When a dish reflects the sun, the reflected sun forms a small spherical disc at the focus, and this is the portion needed to generate the heat energy. The theoretical analysis to determine the actual size of the reflected sun disc is presented here.

Ideally, all parallel rays that hit a parabolic surface at right angles are supposed to be reflected through a single point on the focus, F, but because of the definite angular disc of the sun, which Stine and Geyer (2001) estimated to be approximately 33 minutes of an arc or 9.6 mrad, not all the reflected rays from the parabolic surface pass through the point. However, it has been noticed that, in parabolic reflectors, reflected rays form a small circular image with a width of Δr at the focal point F, with the midpoint lying on the focal plane (Kalogirou, 2009), as shown in Figure 4-7

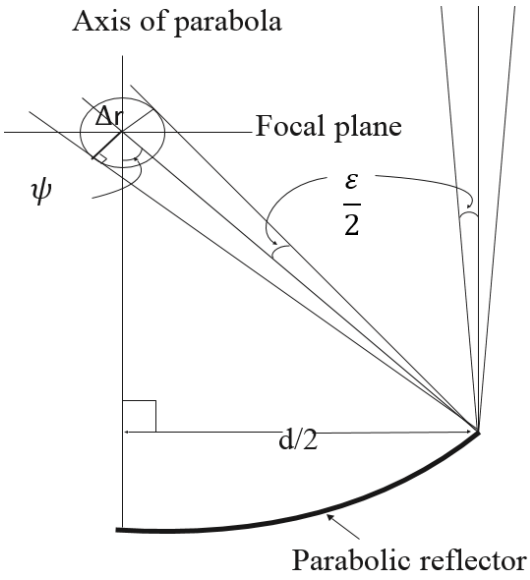

Figure 4-7: Sun disc formed from reflected rays of the dish in the focal point in a parabolic concentrator

The 'ε' in the Figure 4-7 represents angular width of the sun's disc as seen from any point on earth and it is equal to 33 minutes as earlier mentioned, and the 'Δr' is the width of the sphere just large enough to intercept all reflected beam form the parabola. A standard expression for this sphere radius that would be reflected by a parabolic dish in terms of the rim angle ψ was given by Pih & Kalogirou (1997) as

$$\Delta r = \frac{d}{2\ sin\ \psi} \sin\left(\frac{\varepsilon}{2}\right) \tag{4.10}$$

When a parabolic system is to be used in tracking the sun, there is a need to incorporate the effect of errors that will arise as a result of the movement of the dish, as well as the position of the receiver and the width of the reflected sphere formed. This can be achieved by analysing the total effective errors, σ_{total}, on the system, and this kind of solution was presented by Stine and Geyer (2001), who presented two different equations for tracking single and two axes, as shown below.

For a single-axis tracking system, the total effective error is the summation of the errors arising from structure wobble or misalignment or tilt, $\sigma_{\text{structure}}$. The tracking errors σ_{tracking} either lag or lead in the rotation of the drives and the errors that could arrive from the receiver σ_{rec} , which are placed at the focus of the dish, as summarised in Equations 4.11 and 4.12

$$\sigma_{total} = \sigma_{structure} + \sigma_{tracking} + \sigma_{rec} \tag{4.11}$$

$$\sigma_{tracking} = \sum \sigma_{sensor}\,, \sigma_{drive} \tag{4.12}$$

The tracking errors in Equation 4.12 include, on the one hand, the alignment errors and other likely related errors. The total effective error when using a two-axis tracking system, on the other hand, can be calculated by accounting for the two dimensional errors that is involved and then σ_{total} becomes

$$\sigma_{total} = \sqrt{\sigma_{1d}^2 + \sigma_{2d}^2} \tag{4.13}$$

σ_{1d} in Equation 4.13 represent one dimensional errors which are errors that cause beam to spread around the plane of curvature and its component, it is expressed below in Equation 4.14 comprising the slope, sensor, drive and receiver misalignment errors.

$$\sigma_{1d} = \sqrt{\left(2\,\sigma_{slope}\right)^2 + (\sigma_{sensor})^2 + (\sigma_{drive})^2 + (\sigma_{rec})^2} \qquad [mrad] \tag{4.14}$$

The slope error in Equation 4.14 was multiplied by a factor of 2 because when a dish has a slope error, only the direction of the dish changes while the receiver fixed on dish stays in its position. Stine &Geyer (2001) explained this phenomenon using Figure 4-8 below in which Figure 4-8a shows the reflection from the dish in no-slope conditions while Figure 4.8b shows that a slope error of 5° will lead to a 10° deviation in the direction of the reflected beam.

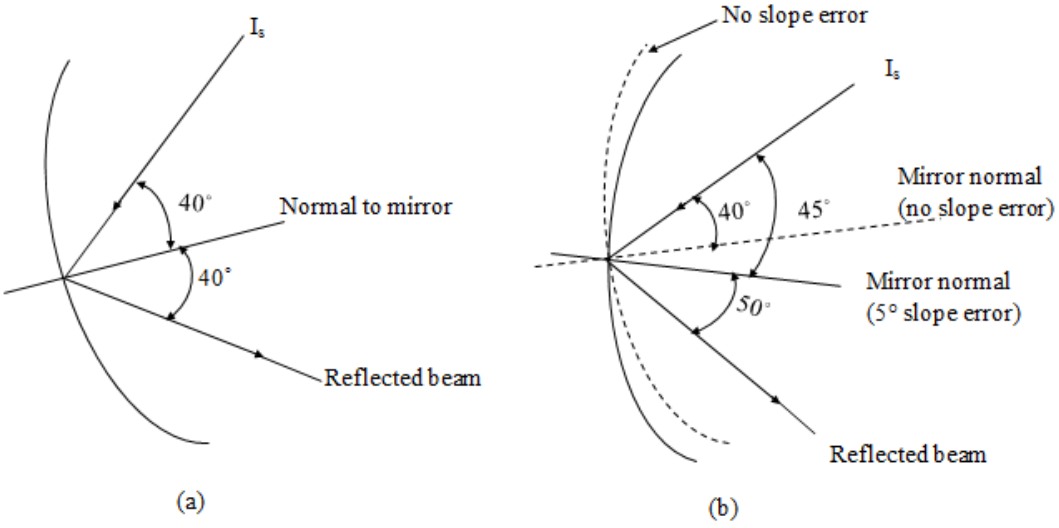

Figure 4-8: Effect of slope error on beam reflection (Stine & Geyer, 2001)

The tracking errors which include the sensor and the drive errors, does not have a factor of 2 multiplying them because the dish turns together with the receiver mounted on it, therefore there is no need to multiply the tracking errors by a factor of 2.

σ_{2d} on the other hand are the errors that are two dimensional. The non-specular reflection and the angular width of the sun earlier discussed are covered in this parameter. These terms are summed up to make Equation 4.15

$$\sigma_{2d} = \frac{\left(\sigma_{sun}^2 + \sigma_{ref}^2\right)^{\frac{1}{2}}}{cos\theta_i} \tag{4.15}$$

Concentrating reflectors experience normal solar incidence angle, thus $\theta_i = 0$ at normal and thus the cosine effect on incidence angle becomes

$$cos\theta_i = 1 \tag{4.16}$$

Equation 4.15 then can be re-written as

$$\sigma_{2d} = \sqrt{\sigma_{sun}^2 + \sigma_{ref}^2} \tag{4.17}$$

All the errors in the collector system can be expressed as indicated using Equations 4.11 to 4.17. However, to incorporate these errors into the equation to determine the optimum size of a reflected image that would be formed by a parabolic dish tracking the sun, the $\frac{\varepsilon}{2}$ in the Equation 4.10 was replaced with multiples of $\frac{\sigma_{total}}{2}$ and the modified equation then becomes:

$$\Delta r = 2\, p \tan\left(n \frac{\sigma_{total}}{2}\right) \tag{4.18}$$

Where n represents the number of deviation considered and p remains the parabolic radius. The percentage of accuracy of reflected ray collection as reflected to the single or multiple standard deviations considered are presented in Table 4-1 below.

Table 4-1: Percentage of flux received within multiples of different Standard deviation (Stine & Geyer, 2001)

Multiple of Standard Deviation	n	% within
± 1	2	68.27
± 2	4	95.45
± 3	6	99.73

Now that the size of the reflected image from the parabolic dish which means the maximum disc image of the sun that will be formed as a function of the rim angle has been determined, this can be used to determine the actual width of the collector aperture entrance size which is large enough to capture the disc. The reflected image formed can be projected to the focal plane where the entrance of the aperture would be placed and ensuring that the beam spread error is minimal, and at this position the receiver entrance/aperture size can be determined using an equation by Stine & Geyer (2001) as

$$W_n = \frac{\Delta r}{\cos \psi} \tag{4.19}$$

Then combining Equation 4.18 and Equation 4.19, the minimum size for the entrance of the receiver would be

$$W_n = \frac{2\, p \tan\left(n \frac{\sigma_{total}}{2}\right)}{cos\ \psi} \tag{4.20}$$

Substituting the desired values of the number of days, n, from January as shown in table 4-1 and other defined parameters into Equation 4.20, the maximum size of the disc of the image that the parabola will form can be determined.

In this section the errors that occur from sun tracking, system set up and the parabolic axis parameters were used to determine the actual and effective width of the reflected sun. The subsequent sections discuss how to effectively capture the whole energy from this reflected sun's disc.

4.1.5 Geometric concentration ratio

Concentration ratio is defined as the geometric ratio of the aperture area of the collector to the entrance surface area of the receiver cavity as shown in Equation 4.21, it is the basis used to measure the intensity of the reflected rays.

$$C = \frac{A_{dish}}{A_{cav,a}} \tag{4.21}$$

Parabolic concentrators are known to produce high heat flux that sometimes exceed the needed value for a particular application (Goldstein *et al.*, 2010) and in order to obtain the desired amount of heat flux from the excess amount generated, the concentration ratio must be reduced and this can be achieved by varying either the aperture are of the receiver or the aperture area of the parabolic collector (Shuai. *et al.*, 2008). In this set-up, a 2 m television dish was used, this dish had been made a parabola already and the sizes could not be altered to achieve the desired flux; therefore, the geometric concentration ratio was done to know the intensity of reflection in order to vary the receiver size to get the desired output. In other designs when the concentrator's design parameters can be altered, either of the receiver size or the concentrator size can be varied.

Much has been said about the width of the sun's disc formed by the reflected beam from the parabolic dish. In the following section an effective method of capture of the energy in form of the solar cavity receiver is introduced.

4.1.6 Receiver design

For improved efficiency of an indirect solar cooker using a parabolic reflector, the use of cavity receivers had been encouraged (Al-Soud et al., 2010; Haridas, 2013; Zawilska & Brooks, 2011). In this system, therefore, an innovative cavity receiver was designed with the aim of maximising the amount of heat flux coming from the dish. Several types of cavity receivers were considered by Kuehn and Goldstein (1976). This was the first effective solar cavity receiver in the form of a horizontal circular design. Other popular types include the plain horizontal annular cavities of Shilston and Probert (1979), the tubular cavity of Kumar and Reddy (2007), as well as other cavity types. When a conical cavity receiver is used with concentrating reflectors, high temperatures and increased heat fluxes are often developed. This is because solar energy is concentrated on the system's working fluid, especially from the reflecting surface or concentrator (Shuai et al., 2008). These aforementioned desired properties of cavity receivers make it the most preferred for the setup under consideration in this study, where a high temperature and long heat retention are required. A closed type of cavity was selected over the open cavity type due to less thermal and optical losses that occur in covered cavity receivers compared to open ones.

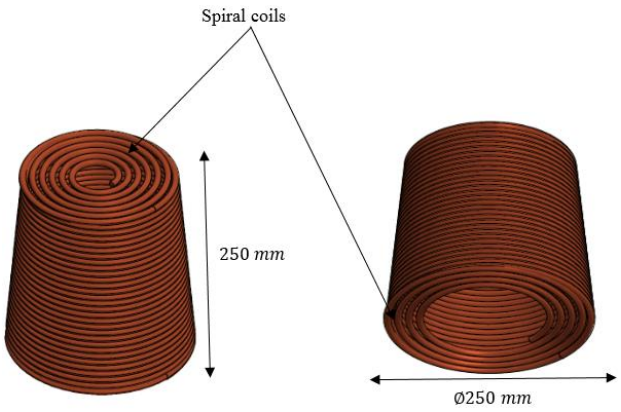

Figure 4-9: CAD drawing of receiver cavity coil

A CAD drawing of the closed cavity type of receiver developed for this setup is shown in Figure 4-8. The material used was a copper tube of diameter of 0.0095 mm and, in order to determine the minimum length of material required to achieve the desired heat output, the conical tube was taken as a heat exchanger and its desired log mean temperature, ΔT_m, which is the expected temperature difference between its hot side and the cold side, was used along with an assumed overall heat transfer coefficient, as shown in Equation 4.22. The area, A, of material needed could thus be determined and the minimum length of copper needed was obtained from the calculated area.

$$Q = U\ A\ \Delta T_m \tag{4.22}$$

In order to maximise the length calculated and reduce heat losses through convection, an innovative cavity receiver was developed. The copper tube was made into different shapes: two spirals and a frustum shape, with the specifications for the frustum shaped shown in Table 4-2 below. One of the spirals was placed at the entrance and the other at the back, with the frustum shape copper tubes in between them.

The formula to calculate the length of a flat spiral helix is straightforward, as shown in Equation 4.23.

$$L = \pi\ N\ \frac{(D + d)}{2} \tag{4.23}$$

To calculate the required length of the frustum-shaped cavity (tapered helix), the equations had to be formulated. This derivation was achieved by assuming that the length L was stretched out in a flat spiral helix. Combining this length with the desired height h for the tapered helix, the equation derived for the new length of tapered helix (LH) is

$$LH = \sqrt{(L^2 + h^2)} \tag{4.24}$$

The process for making the receiver and the optimised cavity receiver are shown in Figure b-l of Appendix H. The design parameters for the cavity receiver walls of the frustum shape are shown in Table 4-2.

Table 4-2: Receiver coil parameters

Coil shape parameter	Value
Pitch	10 mm
Height	290 mm
Tapered angle	5°

4.1.7 Solar energy transfer analysis

With the type of the receiver chosen, the next step is to know how energy is transferred from the dish to the receiver and how some part of this energy is lost. In this section, the heat transfer in the solar energy subsystem is presented as a follow-up to the initial energy balance in Equations 4.1 and 4.2, and the necessary equations for determining the efficiencies of this subsystem are presented.

Convection and radiation losses to the air are the major thermal losses from solar cavity receivers (Melchior et al., 2008; Wu et al., 2010b); the other heat loss is due to conduction through the cover and insulation wall behind the helical tubes. In the determination of these losses, it was assumed that cavity walls were either uniformly heated or that one wall was heated and others were maintained at adiabatic conditions. Another assumption made to reduce the complexity of the heat transfer analysis in the cavity receivers was that the receiver tube and the heat-transfer fluid had the same temperature. Kalogirou (2009) proved that the temperature difference between the walls of the heat exchanger and the heat-transfer fluid in a solar cavity does not necessarily affect the output of the system, since temperature differences between the heat exchanger and the HTF will reach equilibrium when the storage is charged.

Combining the facts in the previous paragraphs, further assumptions made in the heat transfer modelling for the solar energy collection system are listed below:

- Steady state
- Wind direction effect negligible
- The temperature of the tube is the temperature of the HTF
- All the rays entering the cavity are absorbed into the subsystem

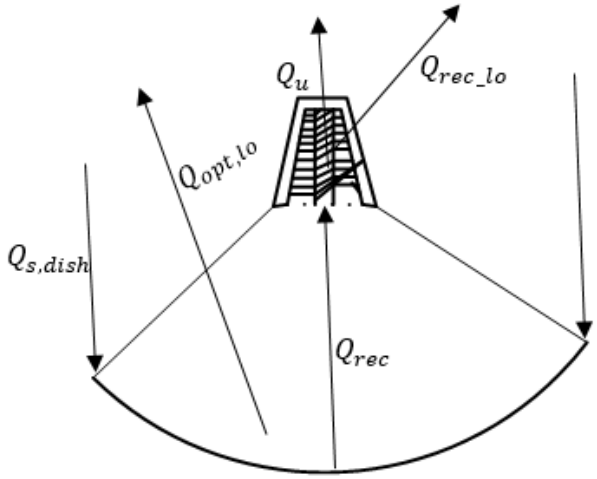

Figure 4-10: Energy balance in solar collector

Figure 4-10 shows the energy movement around the solar collection side. Under the assumptions made here, the amount and rate of the solar radiation flux, $\dot{Q}_{s,dish}$, received by the reflecting parabolic surface is dependent on the aperture area and the direct normal irradiation (DNI), as shown in Equation 4.25.

$$\dot{Q}_{s,dish} = I_s\, A \tag{4.25}$$

The collector (dish) efficiency, η_{dish}, is the ratio of the solar radiation flux, $\dot{Q}_{s,dish}$, falling on the dish to the portion of that flux that is useful, $\dot{Q}_u$, as shown in Equation 4.26.

$$\eta_{dish} = \frac{\dot{Q}_u}{\dot{Q}_{s,dish}} \tag{4.26}$$

The useful heat energy in this collection section, $\dot{Q}_u$, can be determined by the overall difference between the amount of reflected solar energy from the parabolic dish falling on the cavity receiver, $\dot{Q}_{rec}$, and the amount of heat that is lost from the receiver to the surroundings, $\dot{Q}_{rec,loss}$, as shown in Equation 4.27.

$$\dot{Q}_u = \dot{Q}_{rec} - \dot{Q}_{rec,loss} \tag{4.27}$$

The $\dot{Q}_{rec}$ is dependent on the optical efficiency, η_{opt}, of the reflecting surface (Kalogirou, 2009). This optical efficiency of the dish can be used to determine what fraction of the incident energy would be transferred to the receiver and, in this setup, the optical efficiency was taken as the ratio of the total energy reaching the receiver to the initial incident energy that has been received by the aperture area of the reflecting dish, as shown in Equation 4.28.

$$\eta_{opt} = \frac{\dot{Q}_{rec}}{\dot{Q}_{s,dish}} \tag{4.28}$$

The next important thing was to determine the efficiency of the receiver in order to know what amount of energy getting to it would be useful. This receiver efficiency, η_{rec}, was defined by Wu et al. (2010a) as the ratio of the energy usable in the receiver $\dot{Q}_u$ to the total

amount of energy coming in to the receiver from the reflecting dish $\dot{Q}_{rec}$, as shown in Equation 4.29.

$$\eta_{rec} = \frac{\dot{Q}_u}{\dot{Q}_{rec}} \tag{4.29}$$

Combining the above equations (4.24 to 4.28) leads to the development of an expression for the dish efficiency in terms of the optical and receiver efficiency:

$$\eta_{dish} = \frac{\dot{Q}_u}{\dot{Q}_{s,dish}} = \frac{\dot{Q}_{rec}}{\dot{Q}_{s,dish}} * \frac{\dot{Q}_u}{\dot{Q}_{rec}} = \eta_{opt}\,\eta_{rec} \tag{4.30}$$

Equation 4.30 can be arranged to become

$$\eta_{dish} = \eta_{opt} * \frac{\dot{Q}_{rec} - \dot{Q}_{rec,loss}}{\dot{Q}_{rec}} = \eta_{opt}\left(1 - \frac{\dot{Q}_{rec,loss}}{\dot{Q}_{rec}}\right), \tag{4.31}$$

and this can also be expressed as

$$\eta_{dish} = \eta_{opt} - \frac{\dot{Q}_{rec,loss}}{\dot{Q}_{rec}} \tag{4.32}$$

As observed in Equation 4.32, two important variables have been pointed out as the optical efficiency of the dish, η_{opt}, and the receiver losses, $\dot{Q}_{rec,loss}$. The method to determine the values of these two important variables is discussed in the two sections below.

4.1.7.1 Dish optical efficiency

As the name implies, the optical efficiency is highly dependent on the reflecting material or the raw materials from which the reflector is made (Wu et al., 2010a). This is because, according to Kalogirou (2009), any time a reflecting surface receives a beam of thermal radiation, some part of it is reflected from the surface, some fraction is absorbed, and another fraction is transmitted through the body. These properties are reflectivity(ρ), absorptivity (α) and transmissivity (τ), and they add up to one.

$$\rho + \alpha + \tau = 1 \tag{4.33}$$

While the reflected rays from the dish are expected to be absorbed into the receiver cavity, the reflectivity of the reflecting surface, and the absorptivity and transmissivity properties, are dependent on the air space between the dish and the receiver. Wu et al. (2010a) estimated that, in a parabolic CSP system, due to the air space between the dish and the receiver, the combine transmissivity and absorptivity loss in a cavity receiver can be estimated to be from 2 to 4 %. Another important factor to be considered in this setup is spillage of the reflected rays, and this phenomenon in parabolic dish systems was estimated by Wu et al. (2010a) to be between 1 and 3 %, and this value accounts for the reflected rays that miss the receiver or those that are merely reflected to the atmosphere. Shading is also a great factor to be considered in parabolic dish systems, as the cavity is placed at the reflector dish focus point, thus blocking some significant reflective area. This shading loss can be reduced by making the geometric concentration ratio as big as possible (Kribus et al., 2006). The overall equation for the optical loss in terms of the material properties can then be rounded up to be

$$\eta_{opt} = \lambda\, \rho\, \tau\, \alpha\, \gamma \cos(\theta) \tag{4.34}$$

where λ is defined by Wu et al. (2010a) as the factor of un-shading, and γ is the cavity receiver's intercept factor, which is defined as the ratio of energy intercepted by the cavity receiver to the energy that it receives from reflection coming from the parabolic dish. This is the opposite of spillage, and therefore can be taken as 97 to 99 %. The θ in the equation represents the angle of incidence between the dish and the sun's rays. Then $cos(\theta) =$ unity, as already identified in Section 4.1.4 of this chapter. Equation 4.34 then becomes

$$\eta_{opt} = \lambda\, \rho\, \tau\, \alpha\, \gamma \tag{4.35}$$

with the value of the un-shading factor λ taken as 0.99 due to the fact that the geometric concentration ratio of the system was optimised to be as big as possible, and 0.89, the reflectance of the aluminium reflectors substituted as the dish reflectance ρ, the combined optical efficiency of this system based on the analysis in this section, was found to be 0.84 as compared to the 0.85 of Feuermann and Gordon (2001) and Kribus et al. (2006), and the 0.83 of Wu et al. (2010). Now that the optical efficiency has been determined, the determination of the second important factor, the receiver losses, is discussed in the next section.

4.1.7.2 Receiver losses

The term "receiver losses" refers to the summation of all the significant losses involved in the selected cavity receiver of the system setup. Q_{rec_loss} can be determined using the analysis of the loss and energy balance phenomena in the receiver system, as presented in Figure 4-10 below, where the overall energy balance can be written in simple terms of energy conservation, namely that energy coming into the receiver, $\dot{Q}_{total,in}$, is equal to total energy leaving it, $\dot{Q}_{total,out}$, as shown in Equation 4.36.

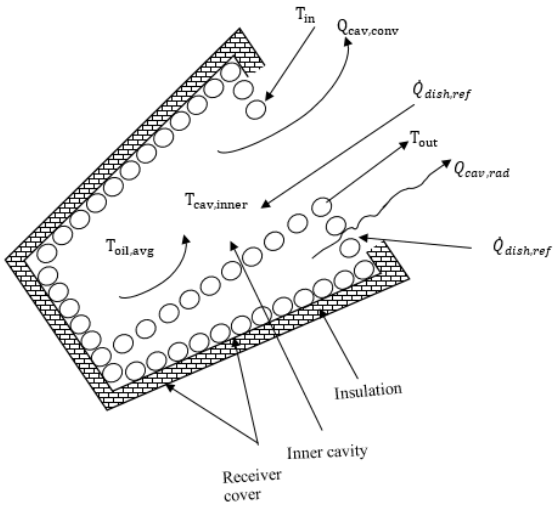

Figure 4-11: Cavity receiver loss diagram

$$\sum \dot{Q}_{total,in} = \sum \dot{Q}_{total,out} \tag{4.36}$$

The expression in Equation 4.36 can be written in terms of each form of energy involved as

$$\dot{Q}_{dish,ref} = \dot{Q}_{conv} + \dot{Q}_{rad} + r\dot{Q}_{dish,ref} \tag{4.37}$$

The r in the equation is define as the overall loss coefficient in the cavity receiver. Also, Equation 4.37 can be written in terms of thermal resistance (R) and temperature as

$$\dot{Q}_{dish,ref} = \frac{T_{cav,inner} - T_{oil,avg}}{R_{conv}} + \frac{T_{cav,inner} - T_{oil,avg}}{R_{rad}} + r\dot{Q}_{dish,ref} \tag{4.38}$$

An easy way to solve these equations is by solving each parameter in Equation 4.37 separately. Starting with the radiative heat loss, $\dot{Q}_{rad,cav}$, which is expected to be small in value because the cavity entrance aperture area $A_{rec,a}$ is small compared to the inner cavity area, $A_{cav,inner}$, then the losses due to radiation can be expressed as

$$\dot{Q}_{rad,cav} = A_{cav,a}\, h_{rad,cav} \left(T_{cav,inner} - T_a\right) \tag{4.39}$$

The radiative heat transfer coefficient for the conical cavity receiver as a function of effective surface emittance ε_{eff} was developed as

$$h_{rad,cav} = \varepsilon_{eff}\, \sigma \left[\frac{T_{cav,inner}^4 - T_a^4}{T_{cav,inner} - T_a}\right] \tag{4.40}$$

This effective surface emittance of cavity receiver ε_{eff}, however, has been presented by Kaushika and Reddy (2000) as

$$\varepsilon_{eff} = \frac{1}{\left[1 + \left(\frac{1}{\varepsilon_{cav,a}} - 1\right) \frac{A_{cav,a}}{A_{cav,inner}}\right]} \tag{4.41}$$

The values from Equation 4.41 can be substituted into Equation 4.39 with the relevant temperatures to get the losses due to radiation in the receiver section.

The next thing to determine was the convective heat losses; in doing this it was necessary to calculate the convective heat transfer coefficient $\left(h_{cav,conv}\right)$. In this study, the receiver used was a frustum-shaped conical cavity receiver with front and back layers of spiral copper tubes that were closely packed, as discussed in Section 4.1.6. This reduced the effect of forced convection to a negligible level in the geometry and made it possible to neglect the influence of wind on the cavity due to a smaller aperture area at the entrance of the receiver. This made it possible to neglect the effect of forced convection. The convective heat transfer coefficient was then expressed in terms of Nusselt number, Nu_x, Grashof number, Gr_x, characteristic length (x) of the cavity and φ as the tilt angle, as shown in the Equations 4.42 to 4.45 below

$$Nu_x = 0.10\, Gr_x^{\frac{1}{3}} \left(\frac{T_{cav,inner}}{T_a}\right)^{0.18} \left(\frac{4.256 A_{cav,a}}{A_{cav,inner}}\right)^{s} h(\varphi) \tag{4.42}$$

where

$$Gr_x = \frac{g\, \beta \left(T_{cav,inner} - T_a\right) x^3}{v^2} \tag{4.43}$$

$$s = 0.56 - 1.01\left(\frac{A_{cav,a}}{A_{cav,inner}}\right)^{\frac{1}{2}} \tag{4.44}$$

An expression for convective heat coefficient as a function of the tilt angle was given by Wu et al., 2010a, as

$$H(\varphi) = 1.1677 - 1.0762sin(\varphi^{0.8324}) \tag{4.45}$$

In this setup, the characteristic length (x) of the conical cavity receiver is the diameter of the cavity. The reference temperatures were taken at film temperature, which in this setup is the average difference in temperature between the ambient air and the wall of the cavity. Thus we can state that the convective heat transfer coefficient is:

$$h_{conv} = \frac{Nu_x\, k}{x} \tag{4.46}$$

The convective heat loss for this solar cavity receiver can then be calculated using Equation 4.47 below.

$$\dot{Q}_{conv,cav} = A_{cav,ins}\, h_{cav,conv}\left(T_{cav,inner} - T_a\right) \tag{4.47}$$

Both the radiative and convective heat losses from the receiver were analysed and determined. The heat loss due to conduction through the walls and the insulator could then be determined using simple Fourier laws:

$$\dot{Q}_{cond,cav} = -k\, A_{cav}\, \nabla T \tag{4.48}$$

Harris and Lenz (1985) presented an approach to analyse conduction in cavity receivers of different shapes, and this has been the basic equation used by most designers of cavity receivers. In the case of zones with concentric boundary circles (cylindrical), Harris and Lenz gave the heat loss from these zones through conduction as

$$\dot{Q}_{cond,cav} = \frac{\pi\, k\, H\left(T_{cav,inner} - T_a\right)}{t}, \tag{4.49}$$

and for zones with non-concentric circles around them (conical or frustum), the equation to determine the conductive heat losses in the receiver as a function of the ambient air temperature and the temperature inside the cavity receiver is shown in Equation 4.50.

$$\dot{Q}_{cond,cav} = \frac{2\,\pi\, k\, H\left(T_{cav,inner} - T_a\right)}{In\left[\frac{(C + 2tH)}{C}\right]} \tag{4.50}$$

where the constant C is defined as

$$C = (R_1 + R_2)[(R_1 + R_2)^2 + H^2]^{\frac{1}{2}} \tag{4.51}$$

From all the calculations in this section, the total heat losses in the receiver could then be determined:

$$\dot{Q}_{rec,loss} = \dot{Q}_{conv,cav} + \dot{Q}_{conv,cav} + \dot{Q}_{rad,cav} \tag{4.52}$$

The useful heat from the receiver, Q_u, therefore is determined using Equation 4.27. This useful heat is sent to the heat storage section using the high-temperature heat hose. The receiver losses are expected to be minimised by the introduction of an insulating material, namely ceramic wool, which will be discussed in detail in Chapter five.

In this section, the efficiencies, energy, heat transfer model and losses between the dish and the receiver were established. The next challenge was to identify the correct governing equations to allow the heat generated to be saved effectively. This is discussed in the next section.

4.2 Storage Section

One of the design objectives of this setup was to store the heat generated to allow cooking when there is no sunshine or at night. Therefore, in this section, the theories guiding how the storage system can be designed will be established. Several methods to save the heat from a CSP system were shown in Chapter two. Due to its simplicity, and the advantages of sensible storage presented in Section 2.4.1, sensible storage was selected for this setup. The theoretical analysis of the heat flux for an insulated tank was done by first determining the insulation thickness (x) needed to achieve the desired storage time. For a storage tank with the thermal diffusivity of the storage material (α) and the desired time that the heat transfer fluid needs to stay heated (t), an expression could be developed, as shown in Equation 4.53:

$$x = 4\sqrt{\alpha t} \tag{4.53}$$

According to Mills and Ganesan (2009), the thermal diffusivity is a thermo-physical property of the material that can be determined from the thermal conductivity k, the density ρ, and the specific heat capacity c, using

$$\alpha = {}^{k}/_{\rho c} \tag{4.54}$$

The overall thermal resistance of any sensible heat thermal storage system can be calculated using the equations illustrated by Mills and Ganesan (2009) for determining overall resistance in a rectangular block in terms of the convective heat transfer coefficient of the heat transfer oil h_o, the thermal conductivity of the insulating material K_{ins}, and the insulation thickness Δx, as:

$$R_{thermal,ins} = \frac{1}{h_o A_{tank}} + \frac{\Delta x}{K_{ins} A_{ins}} \tag{4.55}$$

Incorpea et al. (2007) showed that the overall thermal resistance, $R_{thermal,ins}$, calculated here in Equation 4.55, can be used to work out the heat flux developed in the storage tank when it is insulated, as shown below:

$$\dot{Q}_{thermal,ins} = \frac{T_{tank} - T_{ins}}{R_{thermal,ins}} \tag{4.56}$$

where $\dot{Q}_{thermal,ins}$ is the heat flux developed in the tank that is insulated, the T_{tank} is the average temperature inside the tank, and the T_{ins} is the average temperature of the insulating material. In contrast, if the storage tank was not insulated, the heat flux inside the tank can be calculated using simple heat equations as illustrated by Mills and Ganesan (2009), as

$$\dot{Q}_{thermal,no\_ins} = hA_{tank}(T_{tank} - T_{amb}) \quad (4.57)$$

where $\dot{Q}_{thermal,no\_ins}$, is the heat flux when there is no insulator attached, h is the convective heat transfer coefficient, and the term T_{amb} is the ambient temperature.

For a comparison of the rate at which the heat flux is lost between the insulated and the uninsulated storage system, Equations 4.56 and 4.57 can be solved using numerical integration to determine the variation in temperature with time. Using the relationship between heat flux ($\dot{Q}$) and the mass (m), the specific heat capacity of the heat transfer fluid is c_p and time, as shown in Equation 4.58 below.

$$\dot{Q} = mc_p \frac{\partial T}{\partial t} \quad (4.58)$$

$\frac{\partial \mathrm{T}}{\partial \mathrm{t}} =$ instantaneous change in temperature with respect to time

From the above calculations, the retention capacity of the different types of storage mechanisms could be determined experimentally. The time rate at which the heat was lost could also be determined. This analysis was performed and the necessary charts are shown in Section 5.6 of Chapter five.

The equations provided in this section can be used to determine the thickness of any type of insulating material needed to achieve a particular energy storage for a specific desired storage time. The next section discusses the theoretical bases for how the stored energy can be used for cooking.

4.3 Cooking Section

Making the most use of the heat energy from the sun that has been collected and/or saved to achieve cooking is a major desire for the manufacturers of solar cookers. Different methods of cooking with energy from the sun, as well as different materials, have been described by different researchers, ranging from cooking directly with solar irradiation to indirectly with transferred heat. Another method is to use copper tubes and, most recently, to use heat pipes (Esen, 2004; Khalifa, 1986; Mathioulakis & Belessiotis, 2002). While some of these are still being developed, some are quite simple and others appear complicated.

In selecting an appropriate method to transfer the heat from the storage to the cooking side, three questions were asked: Is it effective? Is it ambiguous? Is it economic? The ultimate desire was to develop an appropriate and low-cost technology for which the materials are readily available. Therefore, a spiral-type copper cook head was made and, in order to achieve an accurate theoretical analysis of this type of solar cooking section, the first assumption made was that a constant heat is supplied to the pot. If the cooking is done in a shaded place or in a place where there is no direct exposure of the cooking pot to the sun, the energy from the storage tank is modelled as the only energy supplied to the cooking plate. However, if the cooking is done outside, an additional direct irradiation from the sun should be added to the energy input as the secondary irradiation falling on the pot (Craig & Dobson, 2015). These simple facts were used to analyse all the work done by the energy supplied to the cooking section, including all the losses. Figure 4-11 shows how the energy transferred to the cooking pot from the spiral cooper head $\dot{Q}_1$ was utilised

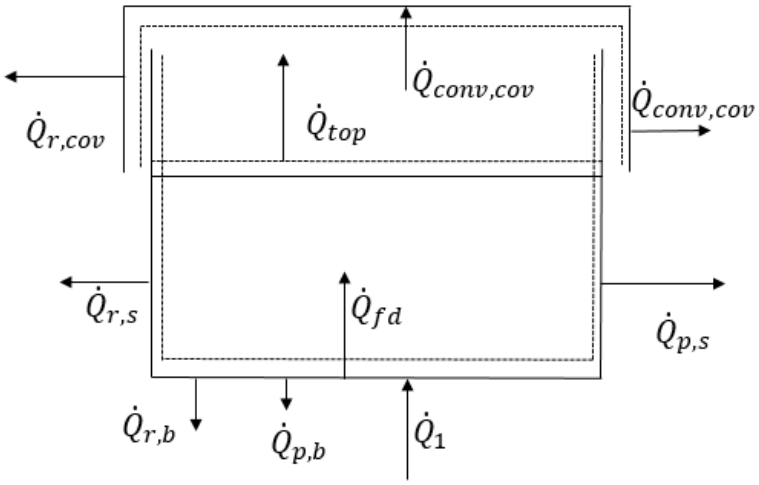

Figure 4-12: Heat transfer in cooking section

The model for the analysis of the solar cooking pot presented by El-Kassaby (1991) and modified by Amer (2003) and Kimambo (2007), who worked backed from the energy supplied to the food to analyse their systems. In this system, however, $\dot{Q}_{fd}$ represents the energy supplied to whatever is being heated up in the pot (food, pancake, water, etc.). The work that this energy performs can be divided into two. First, it has to raise the internal energy of the food, $U_{fd,i}$, and second, it has to overcome the convective losses through the air top of the pot, as $\dot{Q}_{top}$.

$$\dot{Q}_{fd} = \dot{Q}_{top} + U_{fd,i} \tag{4.63}$$

Writing Equation 4.63 explicitly in terms of the instantaneous temperature of the food $\frac{dT_{fd}}{dt}$, the mass of food that is cooked, m_{fd}, the specific heat capacity of the food and the heat transfer coefficient between the inside of the cooking pot and the food being cooked are shown in Equation 4.64.

$$\dot{Q}_{fd} = \dot{Q}_{top} + m_{fd}c_{fd}\frac{dT_{fd}}{dt} = h_{fd}A_{fd}\left(T_{pot} - T_{fd}\right) \tag{4.64}$$

The heat energy from the tank is transferred to the cooking pot through the copper tube cooker head, represented as $\dot{Q}_1$, and this energy is transferred to the food as $\dot{Q}_{fd}$, which is expressed in Equation 4.63 and 4.64 to perform the two functions identified in the previous paragraph. The energy lost through convection from the side walls of the cooking pot is represented as $\dot{Q}_{p,s}$, and that lost from the bottom of the pot to the surroundings is $\dot{Q}_{p,b}$. The radiation from the pot bottom to the and from the sides to the cover is represented by $\dot{Q}_{r,b}$ and $\dot{Q}_{r,s}$ respectively in Figure 4-11. These energies can all be combined in an energy balance equation, presented as

$$\dot{Q}_1 = m_{pot}\, c_{pot}\, \frac{dT_{pot}}{dt} + \dot{Q}_{fd} + \dot{Q}_{p,s} + \dot{Q}_{p,b} + \dot{Q}_{r,s} + \dot{Q}_{r,b} \tag{4.65}$$

where

$$\dot{Q}_{p,s} = h_g\, A_{side}\, (T_{pot} - T_a) \tag{4.66}$$

$$\dot{Q}_{p,b} = h_a\, A_{top}(T_{top} - T_a) \tag{4.67}$$

$$\dot{Q}_{r,b} = \sigma\, \varepsilon_{pot}\, A_{top}\, ({T_{pot}}^4 - {T_a}^4) \tag{4.68}$$

$$\dot{Q}_{r,s} = \sigma\, A_{side}\, ({T_{pot}}^4 - {T_a}^4)(1/\varepsilon_{pot} - 1/\varepsilon_{cover} - 1) \tag{4.69}$$

The air trapped between the tank cover and the inside part of the pot section was also modelled, because it was expected to transfer the heat to and/or get the heat from both the pot and the pot cover. This can be expressed as

$$\dot{Q}_{p,s} + \dot{Q}_{top} + \dot{Q}_{p,s2} = m_a c_a \frac{dT_g}{dt} \tag{4.70}$$

where the newly introduced convection term, $\dot{Q}_{p,s2}$, for the air trapped in the cooking section is defined as follows:

$$\dot{Q}_{p,s2} = h_g A_{cov}(T_{cov} - T_g) \tag{4.71}$$

Two types of cooking can be performed with the experimental setup: the first is cooking under direct sunshine, where the top of the cooking section is left exposed to direct sunshine, and the second is when the top part of the cooking section is covered with insulators (this was used to represent indoor cooking). When cooking was done in sunshine and the top of the cooking section in the storage tank was not covered with insulation, to allow additional direct heating from sunshine, it was necessary to model the exposed cover into the set of defined equations, because the cover of the pot was also expected to receive direct irradiation (DNI) from the sun and to gain heat from the inner part of the pot through convection $\dot{Q}_{p,s2}$. It was also expected to store some heat as latent internal energy, and to lose heat to the atmosphere through radiation ($\dot{Q}_r$) and convection ($\dot{Q}_{cov,conv}$). The energy balance for this expression is given below, where $\dot{Q}_2$ is the secondary DNI falling on the cooking section:

$$\dot{Q}_2 + \dot{Q}_{rs} = \dot{Q}_r + \dot{Q}_{p,s2} + \dot{Q}_{cov,conv} + m_{cov}\, c_{cov} \frac{dT_{cov}}{dt} \tag{4.72}$$

where

$$\dot{Q}_2 = A_{cov} \alpha_{cov}\, I \tag{4.73}$$

$$\dot{Q}_r = \sigma\, \varepsilon_{cov}\, A_{cov}({T_{cov}}^4 - {T_a}^4) \tag{4.74}$$

$$\dot{Q}_{cov,conv} = h_a\, A_{cov}\, ({T_{cov}}^4 - {T_a}^4) \tag{4.75}$$

Rearranging the above equations to form a first-order differential equation that can be solved numerically gives the following sets of equations:

$$\frac{dT_{fd}}{dt} = F_{fd}\, (T_{fd}, T_{pot}, t) \tag{4.76}$$

$$\frac{dT_{pot}}{dt} = F_{pot}\, (T_{fd}, T_{pot}, T_g, T_{cov}, t) \tag{4.77}$$

$$\frac{dT_g}{dt} = F_g\left(T_{fd}, T_{pot}, T_g, T_{cov}, t\right) \tag{4.78}$$

$$\frac{dT_{cov}}{dt} = F_{cov}\left(T_{fd}, T_{pot}, T_{cov}, t\right) \tag{4.79}$$

The above sets of equations can be solved using the fourth-order Runge-Kutta method for numerical solutions of first-order differential equations. The Chapra and Canale (2003) model was used to generate the results. The time was taken in minutes, as T_{fd}, T_{pot}, T_g and T_{cov}, with all temperatures in ℃, and can be used to compare the theoretical and experimental results. However, when the second type of cooking was performed and the top part of the cooking section was covered with insulation, Equation 4.79 was excluded from the analysis because there was no direct exposure of the cover of the top to the DNI, and Equations 4.76 to 4.78 are used with the temperature time derivative independent of T_{cov}.

An alternative way to solve the heat transfer in the cooking section is by using the thermal resistance method. Figure 4-12 shows an alternative method to analyse the heat flow in the cooking section by using the concept of thermal resistance. This resolves heat transfer as the basic electricity equation, $V = IR$, with V the electrical potential in analogy to temperature difference, the current, I, analogical to the rate of heat transfer, and the resistance R relating to thermal resistance, as shown in Figure 4-12 below

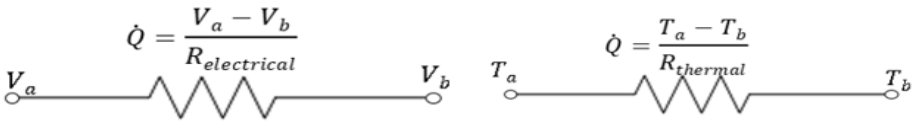

Figure 4-13: Analogical relationship between electrical and thermal resistance

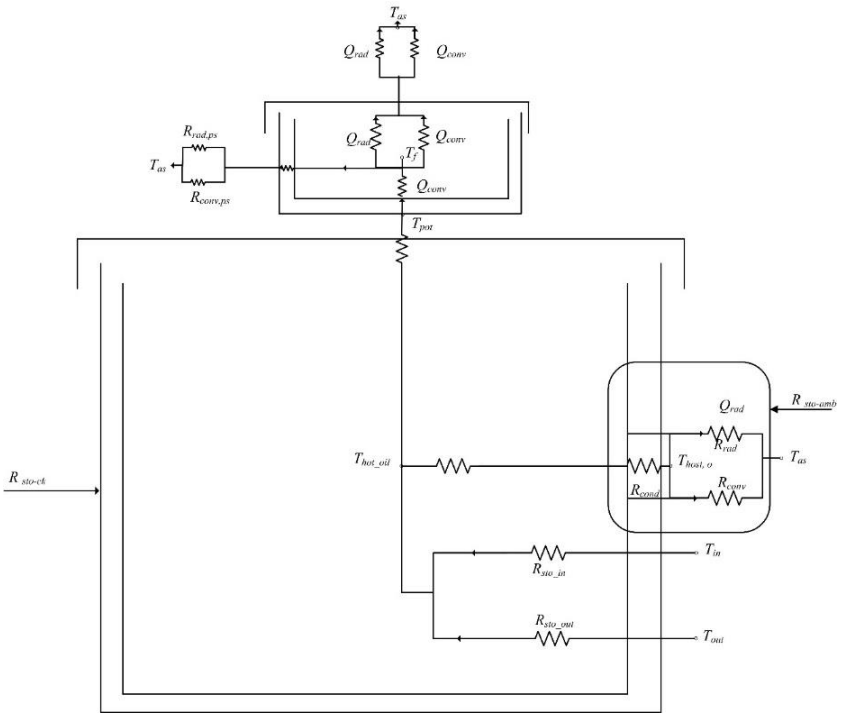

Figure 4-14: Thermal resistance diagram of the cooking section

The analogy in Figure 4-12 can be used to solve the energy equations using the resistances shown in Figure 4-13. The various heat transfer modes with resistance analysis are shown in the sets of equations below:

$$R_{conv} = \frac{1}{hA} \qquad (°C/W) \qquad (4.80)$$

$$R_{cond} = \frac{\Delta x}{kA} \qquad (°C/W) \qquad (4.81)$$

$$R_{rad} = \frac{1}{\varepsilon\sigma A\left(T_a{}^2 + T_b{}^2\right)} \qquad (°C/W) \qquad (4.82)$$

4.4 Solar Cooker Performance Evaluation Theories

Several methods had been identified by Funk (2000) to how the efficiency or the performance of solar cookers can be measured. Some of these methods are cooking power, latent efficiency and heat loss coefficient. The utilisation efficiency, η_u, and the characteristic boiling time, t_c, are the most relevant performance criteria when different cookers are compared under different insolation conditions. The utilisation efficiency is defined in Equation 4.83 in terms of the temperature difference, ΔT, between the initial and the final temperature of the water during the test; the mass of water m, in kg, the time it took the water to reach boiling at temperature Δt , the aperture area of the solar collector, and the available DNI during cooking.

$$\eta_u = \frac{m_{fd}\, c\, \Delta T}{I_s\, A_{ap}\, \Delta t} \tag{4.83}$$

The characteristic boiling time is defined in terms of a reference DNI I_{ref} and the specific boiling time t^b

$$t_c = t^b\, \frac{I_s}{I_{ref}} \tag{4.84}$$

Details of this will be discussed in the water boiling experiment evaluation in Chapter six.

4.5 Chapter Summary

This chapter has highlighted all the necessary theoretical calculations needed for setting up a successful and more efficient parabolic solar cooker, the first part of the chapter highlighted all the necessary optics, errors, as well as reflection mechanism of a two axis parabolic solar system parabolic dish with a cavity receiver that was used. It was also shown that reflected rays from a parabolic dish forms a distinct image (disc) of the sun at its focal length where the beam are reflected instead of just passing through a point. The size of the reflected sun's disc calculated was then used to determine the minimum entrance aperture width for a receiver to be manufactured. The storage and cooking sections thermal analysis were also performed and sets of equation that can be used to theoretically know the temperature at different sections in the system were also developed.

An overall heat transfer analysis of the system was performed in this chapter, two parameters, namely the optical efficiency and the receiver losses were identified to be the most significant contributors to the overall useful efficiency of the system. An equation to determine the thickness of the semi-infinite insulation needed was also derived. The next chapter five discusses the system design and the experimental set up.

5 System Design and Construction

The setup used in this study was an indirect cooking system, as shown in Figure 5-1. It comprised a parabolic dish reflector placed on a tracker stand, a solar cavity receiver placed at the dish's focus, high temperature hoses for heat transfer, a cuboid-shaped storage tank and the cooking section. The storage tank was filled with cold heat-transfer oil. The oil was pumped into the copper tubes packed inside the receiver cavity. The parabolic dish reflected the rays of the sun to a point in its focus. A receiver was placed at this point to absorb the majority of the heat coming from the reflected beam. The heat was then transferred to the copper tubes in the cavity through which the oil was pumped. The copper tube acted as a heat exchanger and the oil was heated as it circulated through the hot receiver copper tube, which was exposed to the heat from the reflected beam. The hot oil was transferred back to the storage tank for charging. The system thus operated in a cycle.

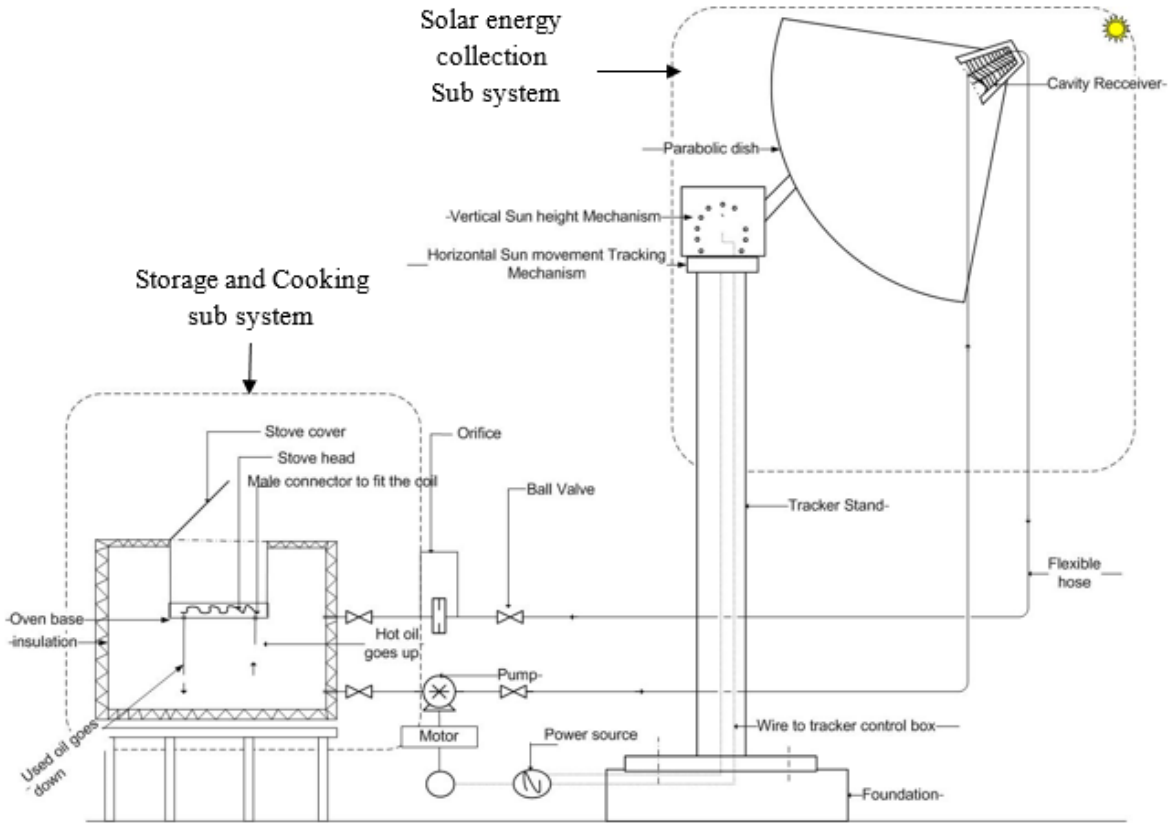

Figure 5-1: The various sections of the experimental setup

The following sections in this chapter discuss the individual parts of the experimental setup.

5.1 Parabolic Dish Reflector

A parabolic dish is often referred to as parabolic dish reflector (PDR). Its schematic reflection technique is shown in Figure 5-2 .

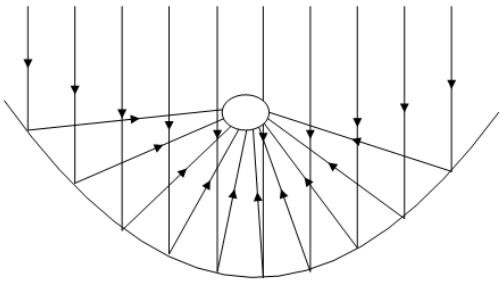

Figure 5-2: Reflection from a parabolic dish

The PDR was selected for this setup due to the following advantages listed by Kalogirou (2009):

- The PDR is the most efficient of all types of solar reflectors, as it is always directed to face the sun
- They are modular reflector/collectors and receivers, because each system can function by itself, or as part of an array of dishes in a larger system
- The concentration ratio of PDRs can be as high as 700 to 2 000, making them very efficient for absorbing thermal energy. This also makes them effective in power-conversion systems.

In Chapter two it was stated that manufacturing a perfect parabola is not easy; therefore, a ready-made, old television satellite dish with a diameter of 2 m was used. The dish was cleaned and painted. The front circular side that served as the reflecting part was covered with aluminium reflector, as shown in Figure 5-3. Strict precautions were taken when laying the strips of aluminium reflector on the dish to prevent air bubbles from being trapped under the foil.

Figure 5-3: The parabolic dish reflector Ø 2.00 m and 0.32 m depth

5.2 Receiver Design

A cavity receiver was selected in this design, as it is known to be the most effective when the collection system is a concentrating type. Conical receivers have been proven by Shuai et al. (2008a) to be more effective in reducing radiation and convection losses. It has more flux generation in the same focal length and concentrator size compared to other types of cavity receivers, as shown in Figure 5-4

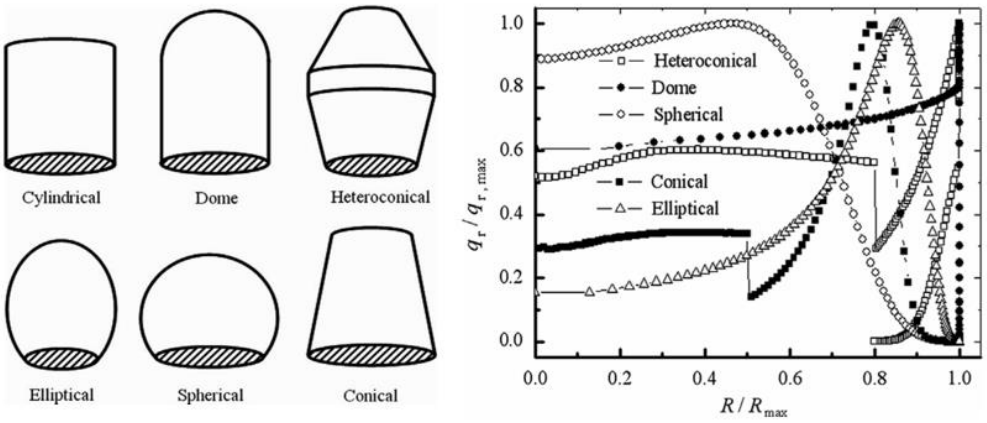

Figure 5-4: Comparison of flux developed by various types of cavity receivers (Shuai et al. 2008a)

The conical cavity type of receiver also undergoes reduced thermal and optical losses (Prakash et al., 2009) compared to other forms of receivers. It is for these reasons that we decided to use it. Wu et al. (2010b) and Shuai et al. (2008a) used a very open cavity that had large entrance apertures. This led to an appreciable amount of convection due to wind and therefore a reduction in the efficiencies of their receivers. This effect of forced convection due to wind can be minimised by reducing the cavity receiver's entrance aperture area (Shuai et al., 2008b; Wu et al., 2010a,b), and this effect was accounted for in the design of the receiver, as shown earlier in Section 4.1.6.

The minimum amount of material needed to achieve the desired output in this study was determined by calculating the area needed for copper tube using Equation 4.22 and finding the length needed depending on the diameter of the copper tube chosen. An initial ambient temperature of 25 ℃ was assumed, and the expected temperature difference between the hot and cold heat-transfer oil was required to be in the range of 20 to 25 ℃ and the calculated length of copper tube of 0.0095 m in diameter was found to be 40.44 m. The lengths of copper tube in the receiver parts (spiral and tapered helix) were then manufactured individually and silver soldered together to sum up to this minimum value. The three sections also were silver soldered together. Two sets of concentric stainless steel buckets were made as covers for the copper tubes. The copper tube was placed in the first stainless steel bucket and then the combination of the copper tube and the stainless steel bucket were placed in the second bigger stainless steel bucket and the space between the stainless steel buckets was stocked with ceramic wool, which was the insulating material used as shown in Figure 5-5.

Figure 5-5: Manufactured cavity receiver tube

The receiver was found to be very efficient, as most of the reflected rays of sunshine were captured by the receiver cavity, as seen in Figure 5-6.

Figure 5-6: Reflected rays on the receiver

The insulator used was a high-temperature ceramic wool, of which the thermal conductivity increased with temperature, from 0.07 W/m K at 200 ℃ to 0.22 W/mK at 600 ℃.

5.3 Dish and Receiver Support Stand

The dish had a square hinge at its back. As a result, a support hinge was constructed to hold the dish to the tracker stand, as shown in Figure 5-7. The frame was made of hollow mild steel, which was painted to prevent rusting. The disc at the end of the frame was used to attach the dish to the tracker stand using M21 bolts.

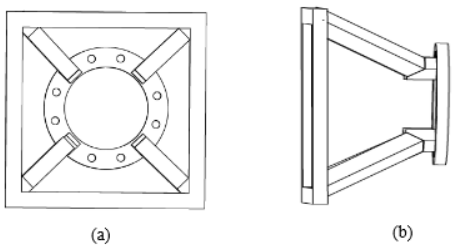

Figure 5-7: CAD drawing of the square support frame: Front view, (a); side view, (b)

A support rod was needed to fasten the receiver in a position facing the dish and fixed at the focus. A tripod type of support has been found to be most effective in dishes used for concentrating (Sen, 2004); therefore, three rods were made from a square steel bar to be joined with screws to the dish and the outer part of the larger stainless steel receiver bucket. This completed the solar energy collection subsystem. It was found to be firm and strong, as shown in Figure 5-8.

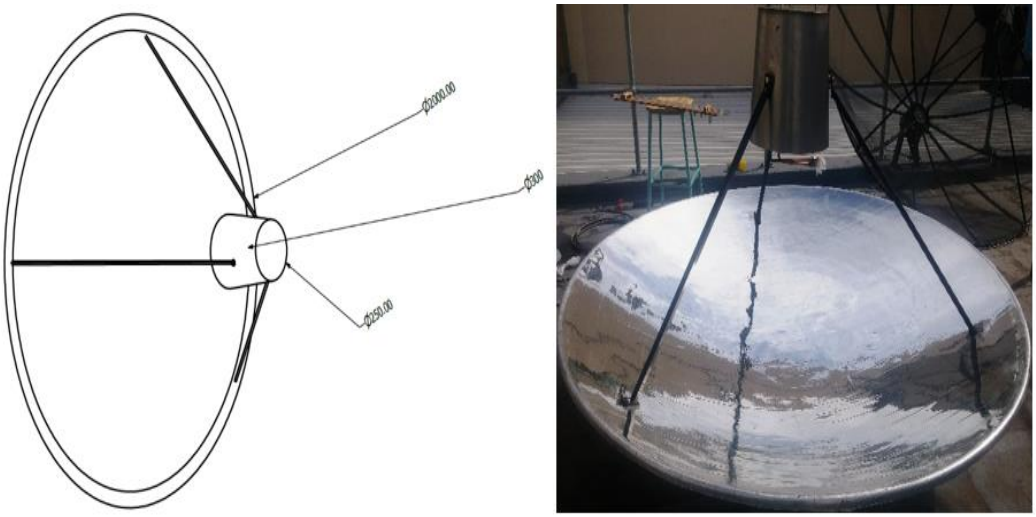

Figure 5-8: Receiver mounted on dish

5.4 Tracker Stand and Support

An accurate solar tracking system is a vital part of CSP technologies. The mode of operation of the tracking system used for this study was discussed and, in Chapter three, it was stated that the tracking system was set up on the tracking test stand of Prinsloo (2014). The initial stand was a pole for holding the two axes of the solar tracking system with no load and no braces, as shown in Figure 5-9. In order to support the weight of the collection subsystem to be mounted on it, support braces were made and welded to the base and sides (see Figure 5-9).

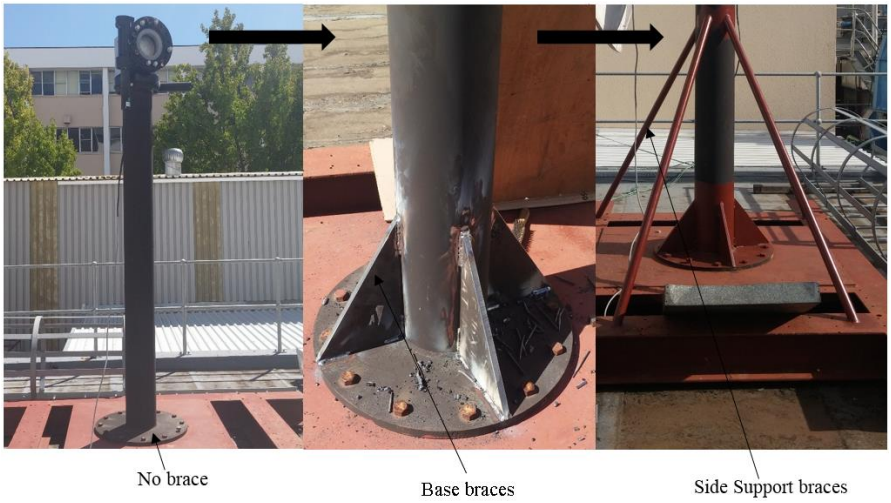

Figure 5-9: Tracker stand and support braces

A frame on which the dish could be mounted and that could also hold the dish on the tracker stand was constructed, as shown in Figure 5-10. Figure 5-10a shows the side attached to the tracker.

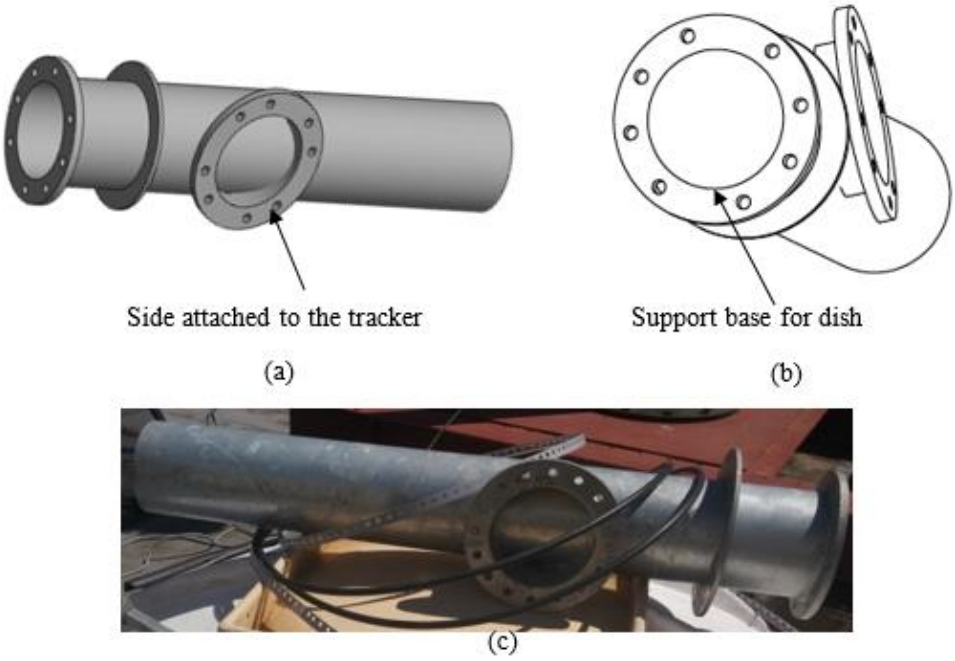

Figure 5-10: CAD drawing showing dish supports joints: side bolted to the tracker stand (a); the base on which the dish sits (b); manufactured frame (c)

This frame was then screwed to the tracker stand to allow the tracker rotation to be transmitted to the dish with no delay. This is shown in the CAD drawing in Figure 5-11a, where the direction of rotation is shown. The setup is shown in Figure 5-11b.

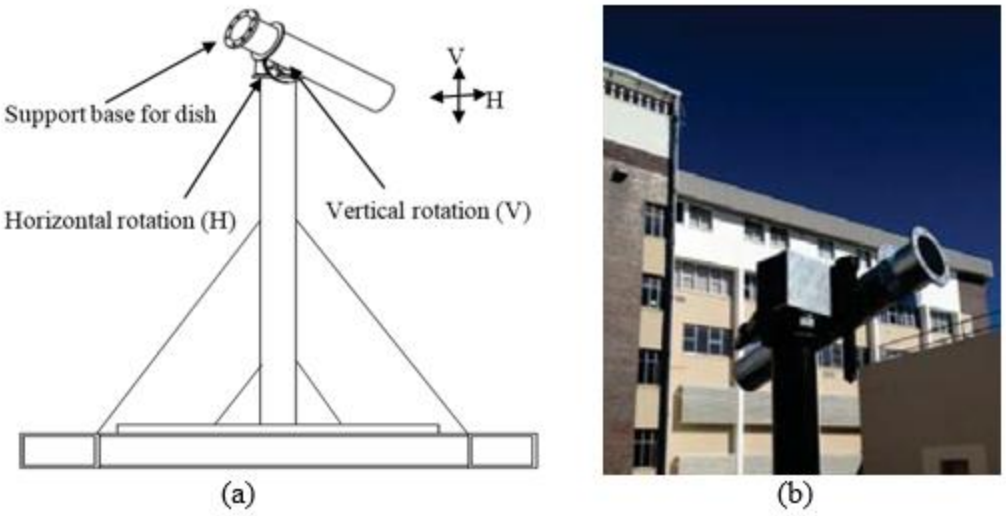

Figure 5-11: Tracker stand set-up CAD drawing showing vertical V and horizontal H rotation, CAD drawing (a), experimental set up (b)

The solar concentrating dish with the receiver was then mounted on the setup in Figure 5.11, and this is shown in Figure 5-12, with the dish facing away from the sun in a non-working position to prevent sunburn during the setting up in Figure 5-12a, while Figure 5-12b shows the setup in the active position of solar tracking.

(a) (b)

Figure 5-12: Heat collection system set-up showing: receiver, dish and tracker stand: non-working position (a); active tracking position (b)

5.5 Thermal Energy Storage and Cooking System

The various means by which heat energy is stored in solar cooking were discussed in Chapter two. It was pointed out that using latent heat storage has some major side effects, although it is efficient in terms of the time it retains heat. The side effects are due to the fact that the use of latent heat storage requires expertise, and it can be seasonal, whereas in most cases it does not melt in cloudy weather conditions or when there is not enough sunshine. Sensible heat, on the other hand, does not need melting, as the heat-transfer medium is in ready-made state and sensible heating as thermal storage has been found to achieve around 30 to 38 % thermal efficiency (Schwarzer & Vieira da Silva, 2008). The simplicity of sensible heat storage, its high thermal efficiency and its availability compared to special chemicals used in latent heat storage made us select it for our setup. Shell Oil S2 heat-transfer oil was selected as the heat-transfer fluid (HTF) for this experimental set up because of its low viscosity and its ability to work over a wide range of temperatures.

The HTF used in our setup also served as the storage medium. It was pumped from the storage section straight up into the cavity of the receiver, where it was heated by solar rays reflected from the parabolic dish. The hot hold then passed through the copper tube coiling and then flowed down straight to the lower part of the storage container, from where it rose up and returned through the top part, and the cycle was repeated. A semi-finite insulation method of wrapping up the tank with high-temperature insulating material was used in this design. The thickness of the insulation and the thermal resistance involved in using the semi-finite insulation were determined using Equations 4.53 and 4.54.

A cuboid-shaped tank was manufactured to be used as the storage tank. This tank was modified to serve a dual purpose as a storage tank and as the solar oven, as shown in Figure 5-13a to d. An inner depression was made in the top part of the tank to serve as hot plate

placed inside the hot oil, and a spiral copper tube was placed on the flat base of the depression on the cooker head with the aim of making it work on the principle of thermosiphoning. This coil was in a spiral form so it looked like an electric stove head, and it had enough surface area for the oil to transfer its heat through the copper tube to the pot. The cook head had two extensions/arms, both immersed in the hot oil, with one longer than the other (see Figure 5-13a). The hot oil in the tank was expected to be in the upper layer of the tank and it would rise into the tube through the shorter arm. The hot oil circulated in the spiral copper tube and then flowed back to the tank via the longer arm of the spiral cooking tube, and this makes a cycle. Cooking was performed by placing the pot or frying pan on the cooking head, as shown in the computer-aided drawing (CAD) in Figure 5-13b and the assembly in Figure 5-13d. Figure 5-13c shows the manufactured storage tank before the insulation was added to the system to reduce losses. The cover lid of the cooking section can be opened to place the cooking vessel or pot on the spiral cooking head and then covered again to make a closed system and reduce losses. When cooking takes place where the sun shines directly on the cooking section, the top is not insulated because of the direct heating from the top by the sunshine, as shown in Figure 5-14c, otherwise the top lid is insulated. The storage cooker lid can then be opened to remove cooked food, as shown in Figure 5-14a to d, where we show the baking of a brownie with the cooker

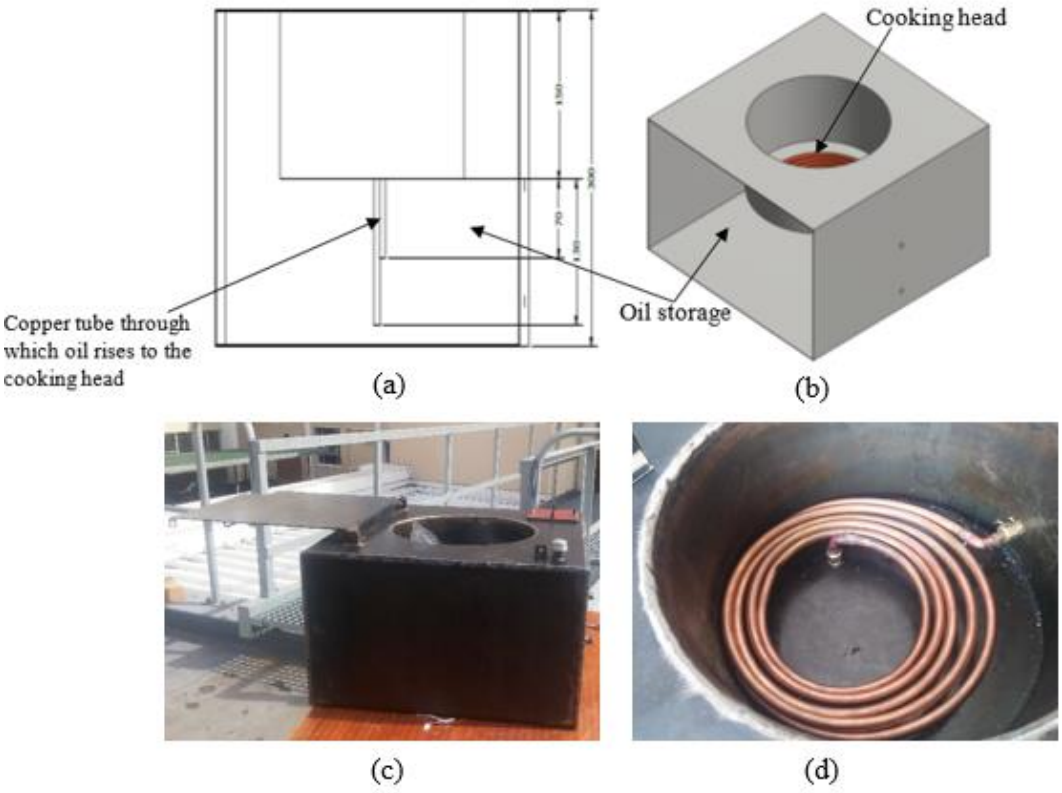

Figure 5-13: Thermal energy storage and cooker: dimensions (a); cut-away 3D CAD drawing (b); fabricated tank (c); cook top (d)

After the manufacturing, a trial experiment was done to test the effectiveness of the cooking section using the spiral copper tube head that looks like electric stove plate, as shown in Figure 5-14.

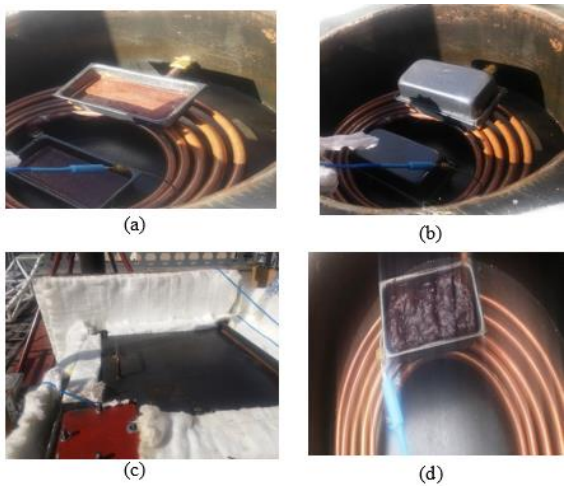

Figure 5-14: Baking brownie on the solar cooker head

In this first trial cooking, a cake tin was placed on the flat part of the cooker and another on the spiral cook top in order to ascertain the effectiveness of the cooking head. It was noticed that the tin on the flat part of the cooking section was done quickly, while the one on the spiral copper took hours and eventually did not get done. The reason was that the oil did not rise as desired in the cooking head thermosiphon, and a modification therefore had to be made.

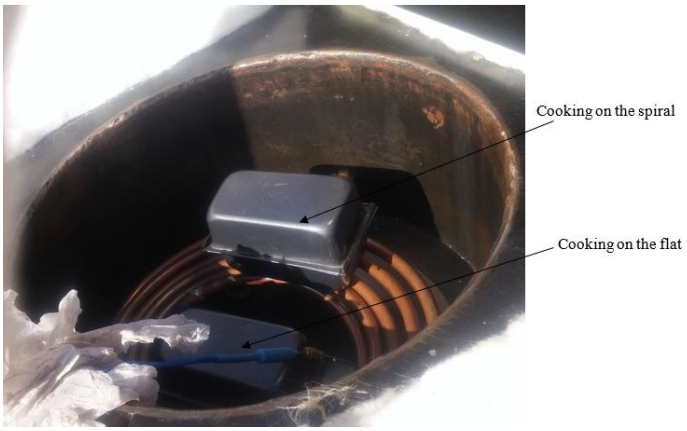

Figure 5-15: Trial cooking to test the effectiveness of the cooker head

The cooking section was then modified so that the rate at which the heated oil flowed through the coiled copper tubing head was increased. A new design was made in which the two arms were at 90 degrees to each other (rather than parallel, as shown in Figure 5-13a). The shorter arm of the thermosiphon was supposed to receive the hot oil was flattened, as shown in Figure 5-16a, and was connected in the cooking side in such a way that it went through the side of the depression in the storage tank, as shown in Figure 5-16c. This was to allow the hot oil to flow straight into the copper tubing through the side and circulate through the spiral while the cold/used oil flow back to the tank through the longer arm. The fabricated modified cook head is shown in Figure 5-16b.

Another cooking experiment was performed, but this time on heating water when the tank was fully charged and hot. It was discovered that the water on the modified cook top boiled at the same time as the one placed on the flat base of the oven, as shown in Figure 5-16d. This was desired.

The primary intention of the design was for the cooker section to work both as stove and oven, so that cooking can be done either directly on the flat plate or, as a stove, when a pot is placed on the spiral tube. The idea of indoor cooking was achieved when the whole cooking system containing the storage and the cooker were placed in the shade while the solar energy-collecting system was left outside.

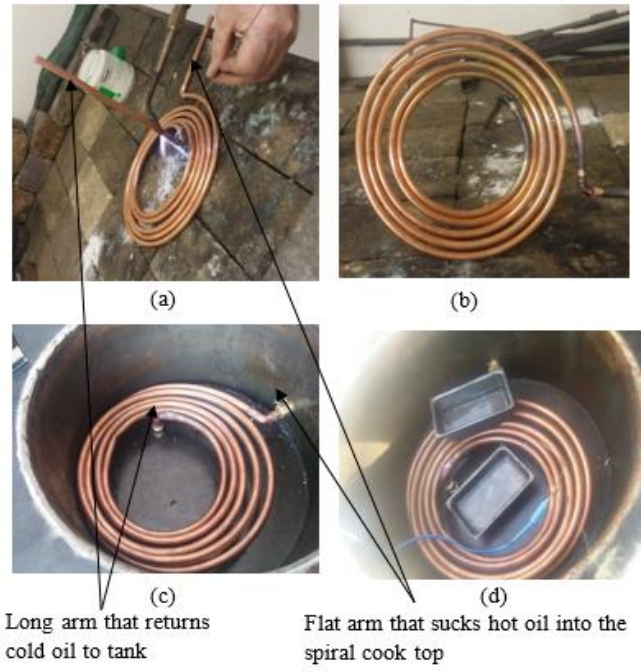

Figure 5-16: Modified cooker head; silver soldering of new cooker top (a); modified cook top after fabrication (b); how the modified cook top is fixed on the storage tank (c); water heating testing comparison (d)

5.6 Storage Insulation

Ceramic wool is a type of high-temperature insulating wool used because of its thermal and acoustic properties. It is light in weight, has high compactness, and is reported to have exceptional resilience (Morgan Thermal Ceramics, 2014). Ceramic wool is a type of insulation often preferred in applications with service temperatures ranging up to 1 200 °C. Its light weight is advantageous in terms of transportation and installation. It is chemically non-reactive and contains no impurities. When used as insulation material it does not promote mould growth, and it is non-corrosive to metal. Cooking when the sun has gone down was desired in the setup under consideration; therefore, there was a need to keep the temperature of the oil high from the hot day so that it was available for cooking at night and when there is no sunshine. In order to achieve this, ceramic wool was selected as the insulation material in our system, and the thickness of insulation required to achieve night cooking was determined using Equation 4.52. The body of the storage tank was covered and wrapped with the ceramic wool.

5.7 Pumping Systems

Another important part of this experimental setup was the pumping system. The challenge was transferring the HTF from the storage subsystem to the copper tubes in the cavity receivers on the tracker stand and back to the tank to continue the cycle. Also, it was important that the pump did not become deformed through the changes from room temperature to a very high temperature of more than 250 ℃. Various type of pumps are available for the desired function in this experiment, ranging from the very simple, positive-displacement pumps with a piston and diaphragm to complex rotatory ones. The criteria for the desired pump were that it must not be too expensive; it must be able to handle high temperatures; and it should be able to handle the desired low mass flow rate of around 0.01 kg/s. Positive-displacement pumps are preferred to the centrifugal type because of their ability to handle very low flow rates accurately. However, the positive-displacement pumps that met the requirements for this setup that were available in the market were very expensive, ranging from R45 000 to R70 000, depending on the manufacturer.

A constant flow rate was desired for the system, and to achieve this under various pressures the use of a positive-displacement pump is often encouraged. A popular type of simple positive-displacement pump is an automobile oil pump. It is a type of gear pump in which the movement of the gears creates a void. This void is filled with the fluid to be pumped, and the liquid is sucked in through the very same void caused by the gear separation at the entrance. The fluid is then discharged through the outlet on the other side. The automotive pump shown diagrammatically in Figure 5-17 was available and not too expensive; it could be modified to suit the demands of our system. This therefore was the kind of pump selected for this experiment

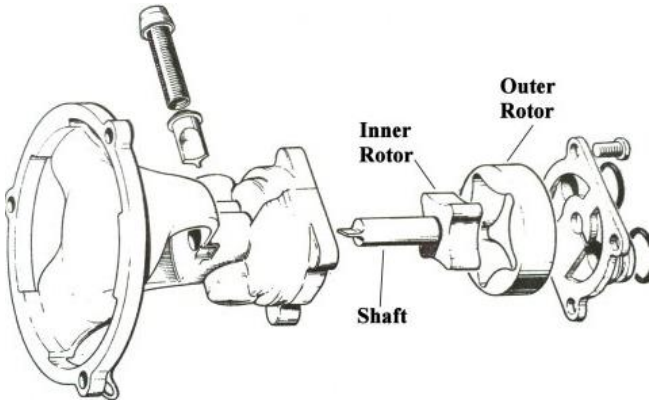

Figure 5-17: The gear type automotive oil pump (Holburn Eaton Oil Pumps, 2015)

A point to note is that any internal leakage in this type of positive-displacement pump will affect the outflow of the liquid and will distort its constant flow. Because the pump was not initially made for use under high temperatures, the gasket was changed to a high temperature Klingersil C-4430 gasket material in order to prevent leakage at the high temperatures are which the system would be working. Also, the gear type of automotive oil pumps are often bolted to the engine for stability, as shown in Figure 5-17. Since there was no engine case in this solar heating system, a flat L-shaped hinge was manufactured to provide a pseudo engine casing for the pump. Silicone gel was used to seal the joints, as shown in Figure 5-18b. The pump was then attached to the hinge, which provided both stability and protection for the pumping system. The normal working principle of the

automotive pump, which was the gear drives, was replaced with a timing V-belt pulley system (see Figure 5-18d).

With the gear system removed and with no auto engine, there was a need for a drive; this was achieved using an electric AC motor drive (3-phase, 12 V/360 W), as shown in Figure 5-18a. Due to the desired low flow rate, a variable speed drive, shown in Figure 5-18c, was attached to the three-phase motor and the speed of the electric motor could thus be regulated. The variable speed drive can be connected to a power supply of 12 volts, which can be electricity or power generated from photovoltaic PV.

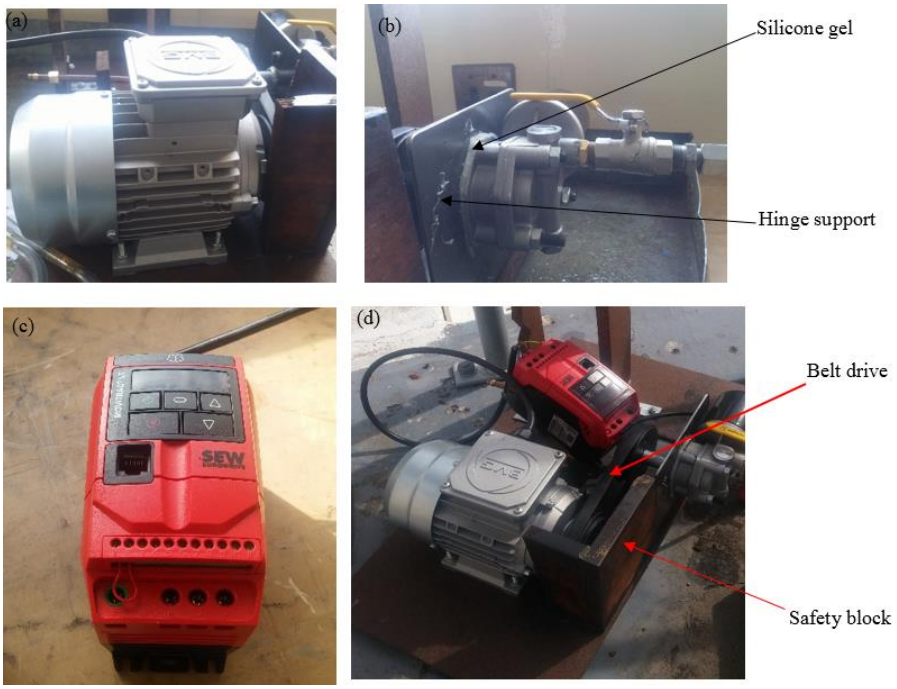

Figure 5-18: Pump and accessories; electric motor (a), pump system (b), variable speed drive (c), drive set up (d)

5.8 Chapter Summary

In this chapter the manufacturing and fabrications were highlighted. The reasons for selecting some of the materials and equipment used in the overall setup were discussed. A few new innovations were made. One was the spiral copper tube used to prevent forced convection in the receiver; another was the modification of the automobile pump and incorporating it into the system. Furthermore, the spiral cooker head was modified to allow hot oil to flow through it straight by reducing the height of the shorter arm, which reduced the pressure needed for the oil to flow through the spiral head. The setup then was ready for testing. Detailed analysis of the cost of production is shown in Table M-1 in Appendix M. The setup then was ready for testing. The next chapter will discuss the experiments performed and the results obtained from them.

6 Experimental Evaluation and Results

The idea of cooking with the sun may not be new to some. However, to those with no access to electricity or who cannot afford to buy expensive cooking gas, solar cooking is more than an art; it is a life saver and a divine blessing (Craig & Dobson, 2015). Although the experimental setup for this study looked good as it stood on the rooftop of the heat transfer laboratory of the mechanical engineering department at Stellenbosch University (SU), there was a need not to "count our chickens before they hatched". Several experiments had to be performed to prove that the set goals for the study had been achieved and to make the necessary recommendations, as these are the aim of any research work. In order to prevent the boredom and disjoint that may occur in writing up all experiments and discussing them, this chapter highlights the types of experiments performed individually, stating the goals, the experimental procedure, the results and the conclusion of each experiment in every section. All the experiments in this chapter were carried out at Stellenbosch University, latitude 33° 55' 41.10" S and longitude 18° 51' 58.80" E, at an elevation of 119 m above sea level.

6.1 No-load HTF Experiment

The setup in this study was tested in various ways to ascertain its cooking potential, as well as its heat-generation abilities. The behaviour of the heat-transfer fluid, the charging and discharging process as well as the general analysis of the system when it was not performing any cooking, were determined using a no-load heat-transfer experiment in which the HTF was just heated, with no cooking load added to the system.

6.1.1 Goals

The no-load solar cooking experiment was used to understand the manner in which and the time it takes the heat-transfer fluid in the system to be fully charged and discharged. This was to be used to predict the time it takes the system to cook various food items. This test prevented wastage of food items during the initial testing, as the temperatures that the HTF would rise to could be used to determine whether the overall system should be used for solar cooking or not. The no-load test also served as a means to determine the behaviour of the solar cooker during cooking, and the heating ability of the system under various climatic conditions.

6.1.2 Experimental procedure

The start-up procedure given in Appendix G was performed; the storage tank was filled with 50 litres of the heat-transfer fluid, leaving an expansion and pressure gap. The tank was not also filled because of the anticipated low DNI for the day. Two experiments were performed – one on 22 May 2015 and the other on 10 June 2015. The average DNI during the experiment on 22 May was 513.9 W/m^2 during peak hours, the data recording was done between 08:00 and 22:00, the whole body of the storage tank was well insulated, but the top cover of the tank was left uninsulated (open) during the day to check the effect of direct irradiation on the tank top. This would determine if the secondary DNI falling on the pot would add heat to the system or otherwise in order to recommend whether to wrap up the

cooking during day cooking or to expose it. In the second experiment, carried out on 10 June 2015, the whole tank was insulated, with no part exposed. The two experiments were performed outdoors and the results are discussed below.

6.1.3 Evaluation and summary of results

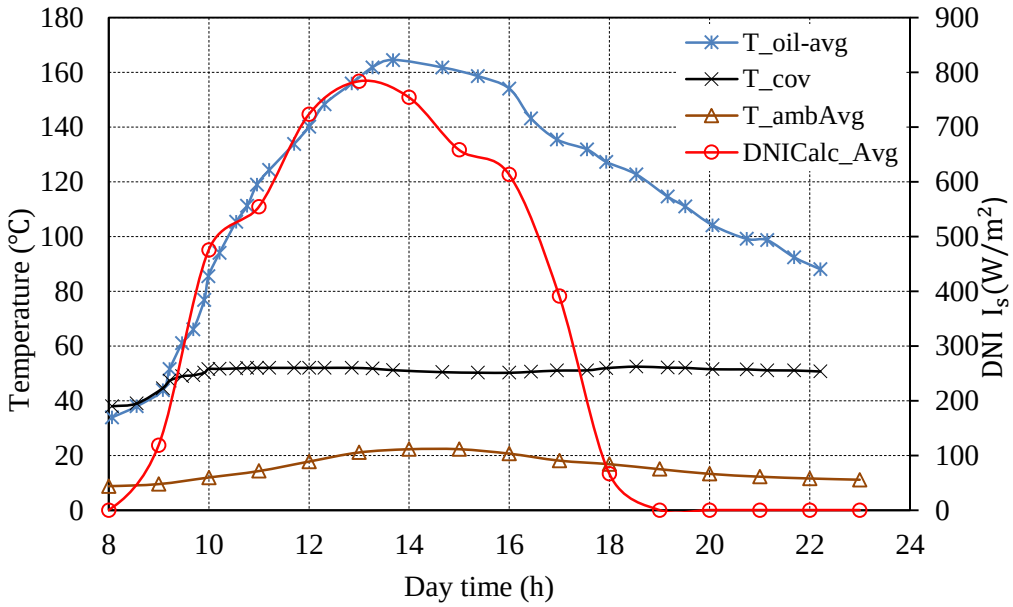

Figure 6-1: Storage oil temperature as a function of day time: no cover insulation

Figure 6-1 shows the available DNI during the first experiment, the average oil temperature, the ambient air temperature and the temperature of the exposed cover of the tank as a function of the time of the day from 08:00 to 23:00. The temperature of the storage tank cover, which was not insulated, rose up to 55 ℃. This temperature was really high compared to the ambient air temperature outside the tank, creating a high temperature difference, thus the average temperature of the heat-transfer oil inside the tank could not reach 200 ℃. The oil temperature attained its maximum temperature at around 13:30, which was four and a half hours after charging began. The system, however, retained a temperature of above 150 ℃ for four hours and above 100 °C for more than nine hours.

It was also noticed that the temperature of the tank top cover did not drop, even when the sun set. This means that more heat was lost through the top cover when it was exposed. It was then inferred that the effect of secondary irradiation (the DNI straight onto the tank cover) falling on the tank could be neglected in operation, as it was stationary and did not track the sun. The only time when the sun fell directly on the top was between 11:00 and 13:00, and this only caused its temperature to rise to a maximum of 57 ℃; at sunset, the temperature difference between the ambient air and the uninsulated cover stood at 35 ℃ average and it thus acted as a huge convective heat-loss medium. It was then suggested that another experiment be performed to compare the results when the cover was insulated. These results are shown in Figure 6-2.

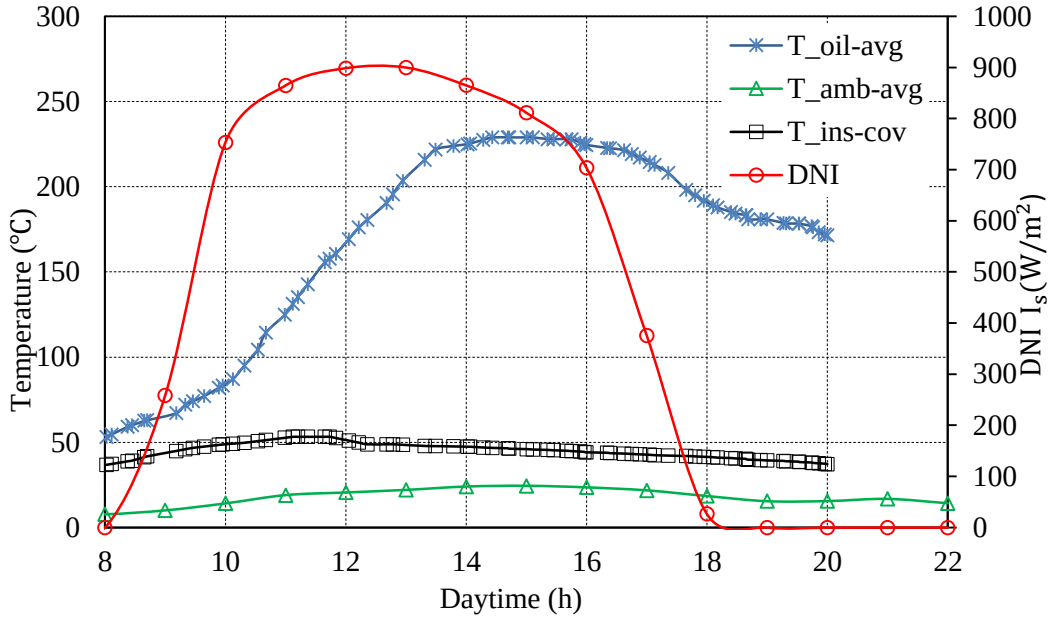

Figure 6-2: Storage oil temperature as a function of day time – insulated cover (8 June 2015)

In Figure 6.2, the same experimental setup as for Figure 6-1 was repeated, but the cover of the storage tank was completely insulated. The experiment was performed on 8 June 2015 and the average DNI during the experiment was 645.884 W/m^2. The heat-transfer oil during this experiment attained a maximum recorded temperature of 225 ℃ at around 13:30. The peak average temperature of around 210 ℃ was maintained for four hours. The system reached 150 ℃ a few minutes before 12:00. The average temperature of the ambient air was around 35 ℃ throughout the day. The insulated cover reached 50 ℃ and the temperature was noticed to drop as the sun set. The average temperature difference between the insulated cover temperature and the ambient temperature was 14 ℃ at sunset, compared to the 35 ℃ noticed in first experiment in Figure 6-1.

From these two experiments, it can be concluded that the average charging time for the heat-transfer oil is five hours on days with average insolation of 600 W/m^2. After the working conditions of the system had been established, there was a need to test its cooking ability, heat dissipation rate at load conditions and the heat loss coefficient, which are discussed in the next sections.

6.2 Water-boiling Experiment

The simplest experiment to perform on a solar cooker is the water-boiling experiment. All the cooking done in this experiment was in accordance with Funk's (2000) international standard for solar cooker testing. The following sections will discuss the different water-boiling experiments used to determine various solar cooker properties.

6.2.1 Goals

The experimental results from boiling water with solar cookers are often the basis on which the cookers' performance can be measured. Since almost all food items involve heating water, it is of the utmost importance that the behaviour of this solar cooker be checked during water boiling. This experiment was aimed at obtaining the parameters on which the system's cooking power and the efficiencies of the system could be calculated.

6.2.2 Experimental procedure

The experimental procedure in Appendix G was carried out. Water-boiling experiments were done from May through July 2015. The ones reported in this section took place from 12 to 19 June. Water boiling was performed using different volumes of water. The pot used was 200 mm in diameter and 100 mm high. Once the pot with water was put on the spiral cooker, the storage cooker top was covered and the insulator was placed in position to prevent heat loss through the top. The results of the various experiments are discussed in Section 6.2.3 below.

6.2.1 Evaluation of results

The first water-boiling experiment was performed on 12 June. The mass of water used was 4 kg. The cooking pot containing the water was placed in the cooking section by making its flat bottom sit on the modified spiral copper tube cooker. The average DNI per hour during the time in which the experiment which took (from 08:00 to 16:00) was $500.5\ \mathrm{W/m^2}$. The water reached boiling at about 12:30, four hours after it had been placed on the cooker. The oil temperature in the storage can be seen to rise fast (see Figure 6-3). This was because the heat-transfer oil was still warm, as it had been used the previous day. The initial temperature of the oil at the beginning of the experiment was 70 °C. The temperature of the spiral cook top, which is represented by the purple legend T_{ck-top}, can also be seen to increase directly proportional to the temperature at the top of the storage tank. The initial variation between the T_{ck-top} and the $T_{oil-avg}$ was caused by the initial resistance of the copper material used for the spiral head. After three hours, both of these temperatures reached equilibrium and the thermocouples in the top part of the storage tank and those on the spiral head were reading the same temperature. T_g is the temperature of the air between the water in the pot and the cover. It can be seen in Figure 6.3 that T_g rose to a temperature of about 65 ℃ just before boiling began, which means that the high temperature difference promoted convection. It therefore is recommended that a black cover be used on the pot when the cooking operation is performed so as to reduce the effect of the convection loss through the top.

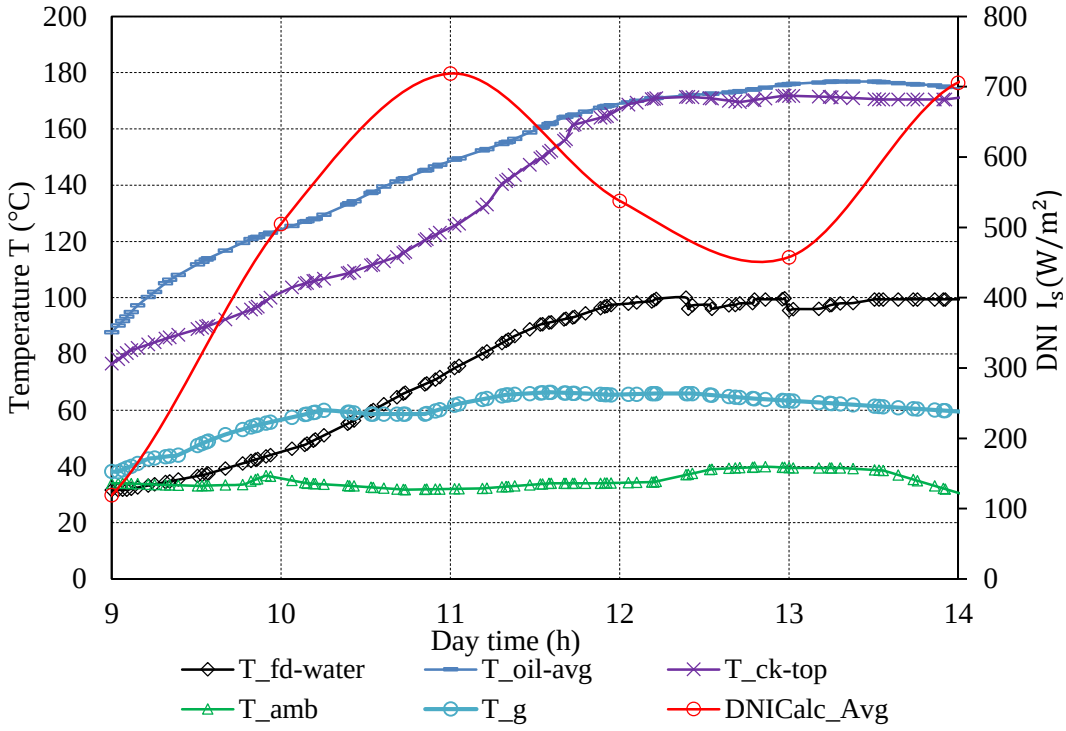

Figure 6-3: Water-boiling experiment, 12 June 2015

Water boiling is the basis for any performance evaluation of solar cookers. At this stage in this report, the cooking ability of the solar system has been established. However, further investigations were carried out using other water-boiling experiments to determine and discuss other performance criteria, as shown in the following sections.

6.3 Latent Cooking Power and Latent Efficiency

An experiment was performed to check the cooking power and efficiency of the system. The results of this water-boiling experiment, which was performed on 13 June, are displayed on Figure 6-4. This day had solar resources similar to those available on 12 June. The differences between these experiments were that the mass of water used here was 4 kg and the pot cover was taped externally with black insulator tape. The start-up temperature of the heat transfer oil was 76 ℃, as it was insulated through the night. The water boiled at 11 am and the sun set quickly on this day, although a higher supply of DNI was received in the morning compared to the 12th. At 10:00 the DNI had reached 600 W/m^2. It therefore can be said that the solar resources available affect daylight cooking directly, as the energy supply to the HTF is being used up simultaneously, therefore a higher DNI will automatically increase the cooking rate. The difference between the cooking head temperature, T_{ck}, and the average oil temperature $T_{oil-avg}$, can be seen to have reduced during the start-up, hence it can be inferred that there had been an appreciable reduction in losses due to convection in the cooking section.

The water was left to keep boiling for two hours in order to determine the average latent efficiency of the system. Power is the rate at which energy is used. It then can be said that

the latent cooking power of this parabolic solar cooking system, $\dot{Q}_{ck,power}$, was defined as the product of the latent heat of evaporation, h_{fg}, and the mass rate at which the water evaporated, $\dot{m}_{w,evap}$, as shown in Equation 6.1

$$P_{ck} = \dot{m}\, h_{fg} \tag{6.1}$$

Using the result from Equation 6.1 above, the latent efficiency of the system could be determined. Schwarzer and Vieira da Silva (2003) defined solar cooker latent efficiency as the ratio of the latent cooking power to the product of average solar radiation and the collector aperture area, as in Equation 6.2.

$$\eta_{latent} = \frac{P_{ck}}{A_a\, I_s} = \frac{\dot{m}\ h_{fg}}{A_a\, I_s} = \frac{m\ h_{fg}}{A_a\, I_s\, \Delta t} \tag{6.2}$$

Using the results displayed in Figure 6-4, the calculated average latent efficiency of the system was 34 %

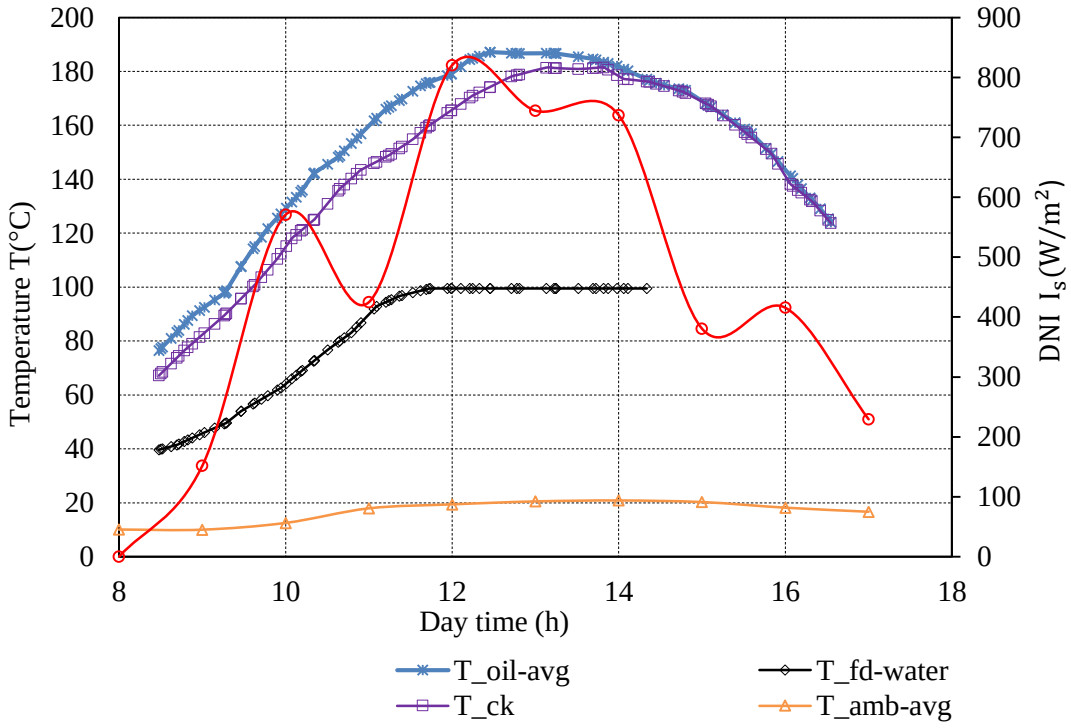

Figure 6-4: Water-boiling experiment, 13 June 2015

Having established the average latent efficiency of the system, further experiments were undertaken to determine the power generated by the system during cooking, and at various temperatures and solar irradiation. These are discussed in the next section.

6.4 Sensible Cooking Power

Sensible power is one of the performance analysis criteria for solar cookers; it is also known as the power rating or the effectiveness of the system and it shows how much power is needed by the system to boil a specific mass of water in a particular timeframe. Four separate water-boiling experiments were performed one after the other using the same setup

and mass of water (see Figure 6-5). The experiment was performed at 15:00 on Thursday, 18 June 2015, at the same location where all the previous experiment had been performed. The same experimental procedure was followed and 3 kg of water were boiled in an aluminium pot in each experiment. However, the system was allowed to charge fully before the solar cooking began. The red line shows the available DNI during the experiment, also displayed in blue in Figure 6-5, and is the rate at which the average oil temperature dropped during the whole water-boiling experiment. The first experiment started at 14:30 and the 3 kg of water reached boiling point in approximately 13 minutes; the result is shown in black. The pot was then emptied and 3 kg of tap water was put in it; this took 17 minutes to boil and its curve is represented in orange on the chart. Another 3 kg water was added after the boiled water from the second experiment was poured out. The water in the third experiment boiled in about 28 minutes (shown in purple), while the fourth experiment, shown in green, took 38 minutes to boil

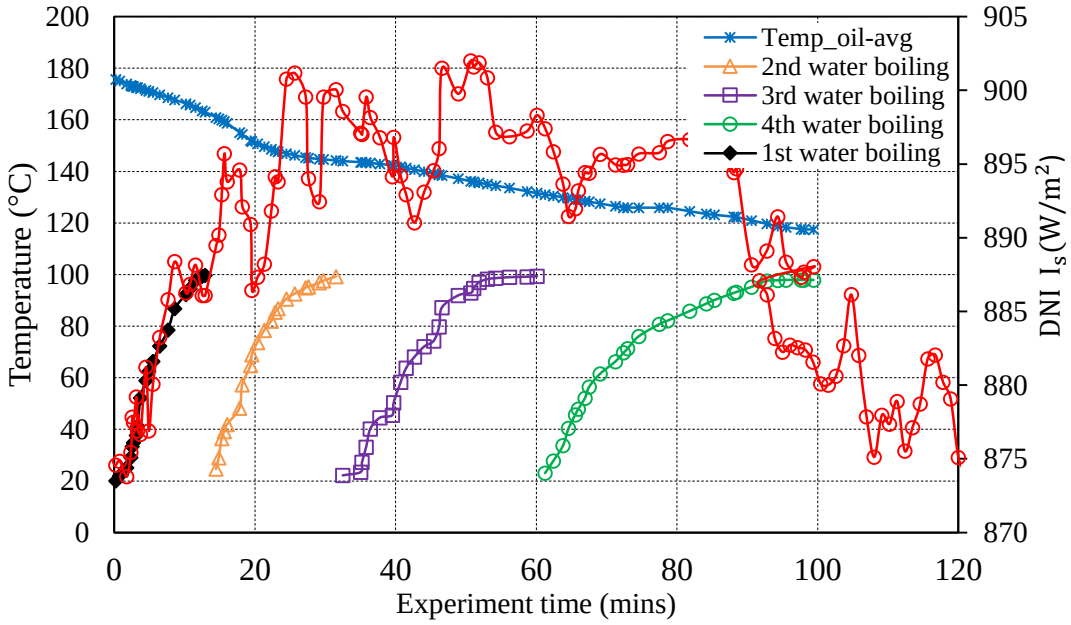

Figure 6-5: Water-boiling experiments with 3 ℓ of water; 18 June 2015

The mean temperature of the heat-transfer fluid is shown in blue. The various results from the analysis in Figure 6-5 can then be used to determine the sensible cooking power of the system. The equation for calculating sensible power can be defined in terms of the mass (m) of the water boiled, in kg, the temperature difference between the initial water temperature and the final water temperature, and the time it took in seconds, Δt, as shown in Equation 6.3

$$P_{ck} = \frac{mc\Delta T}{\Delta t} \tag{6.3}$$

Figure 6-6 shows the different sensible powers of the solar cooker in Watt. In the first water-boiling experiment, the cooker used 1 309 W to boil 3 kg of water in 13 minutes; to boil the same mass of water in 17 minutes required a power input of 915 W. In the third experiment, the water boiled in 28 minutes and the sensible cooking power was 585 W, and the final experiment, which took 38 minutes, used only 410 W

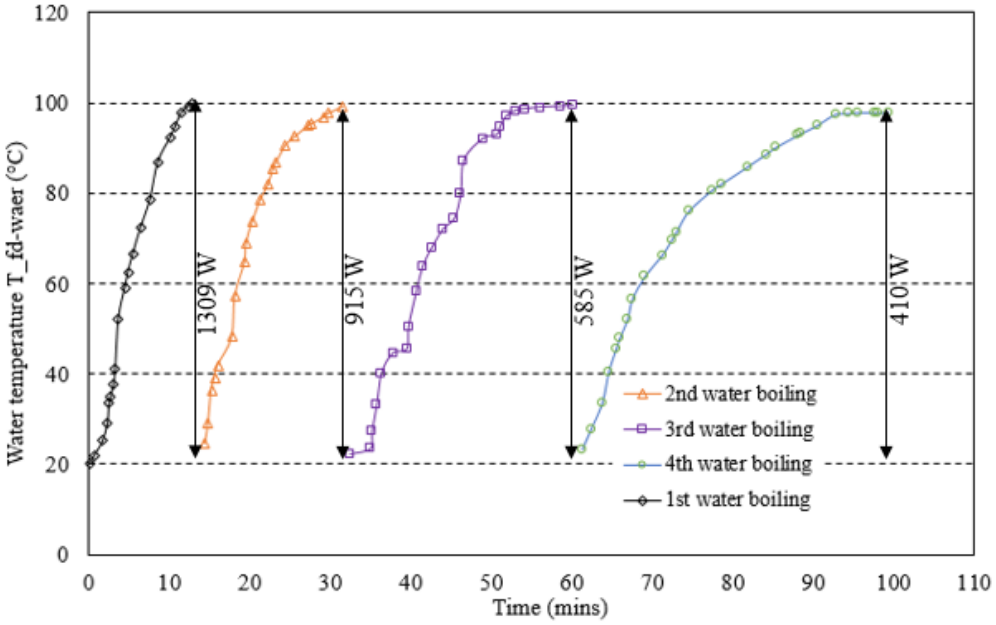

Figure 6-6: Water boiling and power rating of the system

The results from this experiment were then used to calculate the utilisation efficiency, the characteristic boiling time, the heat loss coefficient as well as the overall exergy analysis for the system, as discussed in Section 6.5 through 6.7.

6.5 Utilisation Efficiency and Characteristic Boiling Time

As was pointed out in Section 4.4 of this report, there are several criteria according to which the performance of a solar cooker can be determined. However, for the sake of comparison with other cookers under different insolation conditions and at different locations, El-Kassaby (1991) and Al-Soud et al. (2010) defined utilisation efficiency by η_u and t_c. The general mass (m_{fd}) of the food item to be cooked in Equation 4.83 can be replaced with the mass of water, m_w, to determine the utilisation efficiency, as shown in Equation 6.4.

$$\eta_u = \frac{m_w\, c\, \Delta T}{I_s\, A_a\, \Delta t} \tag{6.4}$$

Schwarzer and Vieira da Silva (2003) used continuous water boiling to determine the average utilisation efficiency as defined by El-Kassaby (1991). In this experiment the average overall utilisation efficiency was 0.39, which makes it more effective than most existing cookers.

In Section 4.4 it was also established that the characteristic boiling time can be determined using the results from Equation 6.4. The reference solar insolation, I_{ref}, was given as 900 W/m^2 by Khalifa et al. (1984).

$$t_c = t^b\, \frac{I_s}{I_{ref}} \tag{6.5}$$

where

$$t^b = \frac{\Delta t\, A_a}{m_w} \tag{6.6}$$

The average characteristic time for this solar cooking system for 3 kg of water is 3 min/kg. The results from this section can then be used to compare this cooker with other popular cookers in the literature.

6.6 Heat Loss Coefficient

The Funk (2000) standard for determining the heat loss coefficient of any solar cooker compares the cooker's cooking power with the temperature difference involved during water boiling. El-Sebaii and Ibrahim (2005) performed three water-boiling experiments and defined the heat loss coefficient as the slope of regression for a graph of cooking power as a function of temperature difference. This model was adopted here, as they also boiled 3 kg of water. Figure 6.7 was developed in accordance with the international standard by computing the cooker's power to a temperature difference of 50 ℃. The regression equation that was developed is presented as

$$P_{ck} = -3.6372\,\Delta T + 341.49 \tag{6.7}$$

In Figure 6-7, the coefficient of regression, R^2, was 0.985, which falls in the range of the test standards. The cooking power values on the y-axis, the (slope) heat loss coefficient in ℃/W and the adjusted temperature difference all satisfy the standard solar cooker test values (Funk, 2000).

On the basis of the results in this chapter, it is obvious that the parabolic solar cooker manufactured for this report satisfies the international standard procedure.

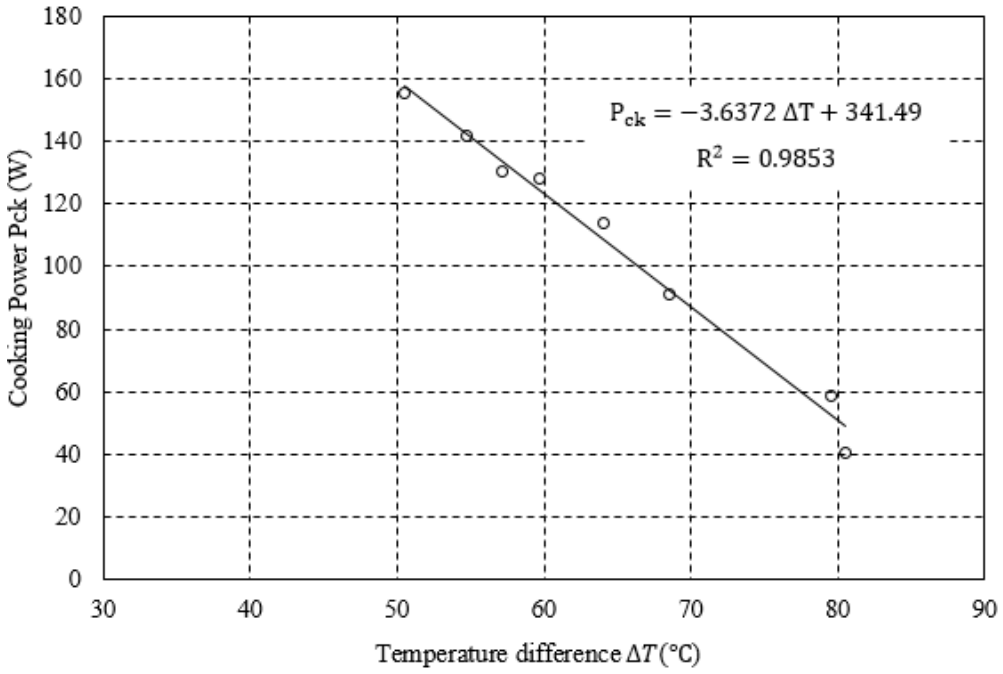

Figure 6-7: Cooking power as a function of temperature difference

6.7 Exergy Analysis

Having determined the various efficiencies of this system, the general criteria for the performance of solar cookers are exergy analysis and energy efficiency. The exergy analysis of any process is based on both the first and the second law of thermodynamics, while the efficiency is based only on the first law (Öztürk, 2004a). The exergy efficiency is defined as the ratio of the rate of output exergy transfer to that of input exergy transfer (Shukla, 2009). In this system, exergy is defined as the ratio of exergy gained by water to the input exergy from the solar radiation or, in simple terms, the "exergy out" of the cooking section to the "exergy in" through the collection section.

The generally accepted equation for determining the solar energy flux can be used to represent the amount of exergy that is entering the system, as shown in Equation 6.8

$$\psi_{in} = I_s \left(1 + \frac{1}{3} \left(\left(\frac{T_{amb}}{T_s} \right)^4 - \frac{4\,T_{amb}}{T_s} \right) \right) A_a \tag{6.8}$$

where I_s is the available solar irradiation, A_a is the collector aperture area and T_s is the temperature of the sun, which usually is taken as 6 000 K. The output exergy for boiling water was expressed in terms of the properties of water by Shukla (2009), as shown in Equation 6.9.

$$\psi_{out} = \frac{m_w\, c_{p,w} \left(\left(T_{wf} - T_{wi} \right) - T_{amb}\, In \left(\frac{T_{wf}}{T_{wi}} \right) \right)}{\Delta t} \tag{6.9}$$

The instantaneous exergy efficiency for this parabolic solar system can therefore be expressed as

$$\eta_{ex} = \frac{\psi_{out}}{\psi_{in}} \tag{6.10}$$

The calculated instantaneous exergy efficiency of this system ranges from 0.045 % to 0.052 %, which seems small compared to the energy efficiency calculated earlier. This is because it is a property and function of the state of the whole system, and energy takes the irreversible processes into account (Petela, 2003). The exergy input in the solar collection side is also known as the exergy of the heat source, while the exergy output in the solar cooking section is also known as the exergy of the heat sink for clarification. The low exergy efficiency in this system is not strange, because low efficiencies are common to all system using solar irradiation.

Table 6-1 below shows a comparison between the exergy efficiencies of similar systems in the literature and those obtained in this research

Table 6-1: Comparison of exergy efficiencies

Author	Cooker Type	Minimum exergy efficiency obtained	Maximum exergy efficiency obtained
Yettou et al. (2004)	Parabolic	0.07	1.52
Öztürk (2004b)		0.41	1.25
Petela (2005)	Parabolic	0.3	1.6
	Parabolic (single)	0.41	1.25
Shukla (2009)	Parabolic (arrays)	0.89	2.15
Current research	Parabolic	0.04	0.06

6.8 Other Cooking Experiments

Having satisfied all the performance and evaluation tests, the solar cooker was used to perform some other cooking experiments, such as heating of cooking oil and cake baking, to check the results against conventional cooking. On 25 May 2015, an experiment was performed on the solar cooker to heat up cooking oil. This was the first real cooking done besides the water heating in the water-boiling experiments. The temperature of the water in the previous experiments never rose above 99 ℃, which is understandable, as this is about the boiling temperature of water. In the oil experiment, a higher cooking temperature was expected. Sunflower cooking oil was put in a pot and heated on the stove. A temperature of 150 ℃ was achieved in the oil after about 120 minutes of heating, and this was because the cooking started long before the system was fully charged. Also, the day was very cloudy and the available DNI during the experiment kept fluctuating, as shown in Figure 6-8.

The oil was removed at this temperature and the experiment was stopped, as the oil was noticed to be drying up due to its fast evaporation.

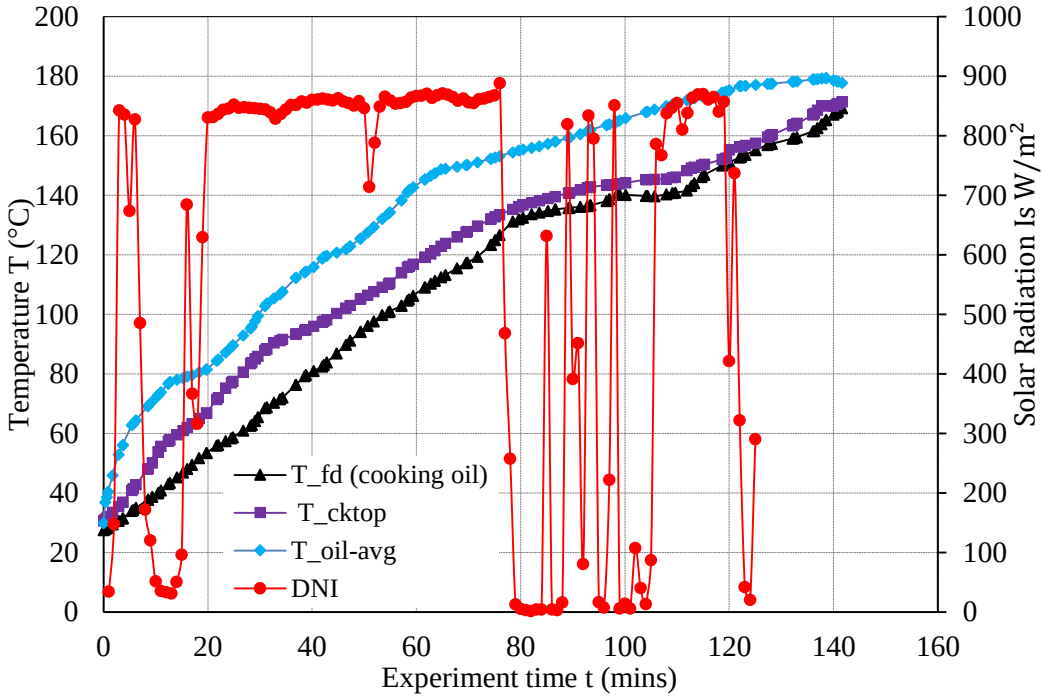

Figure 6-8: Experimental temperature as a function of time for the cooking oil experiment, 25 May 2015

Figure 6-9 shows the result of using the solar cooker for baking brownies. The brownies were baked after about 250 minutes and this was understandable, as the cake pans were put on the cooking section immediately the system started operation at around 08:30. Therefore, it took longer, as the initial oil temperature was around 25 ℃. The average irradiation during the experiment was about 750 W/m^2. If the cakes had been put in the oven when it was fully charged, the time for it to bake would have been reduced, just as in the case of water boiling in the previous experiments. Three thermocouples were put in the cake pans and their temperature readings were averaged to obtain the input food temperature.

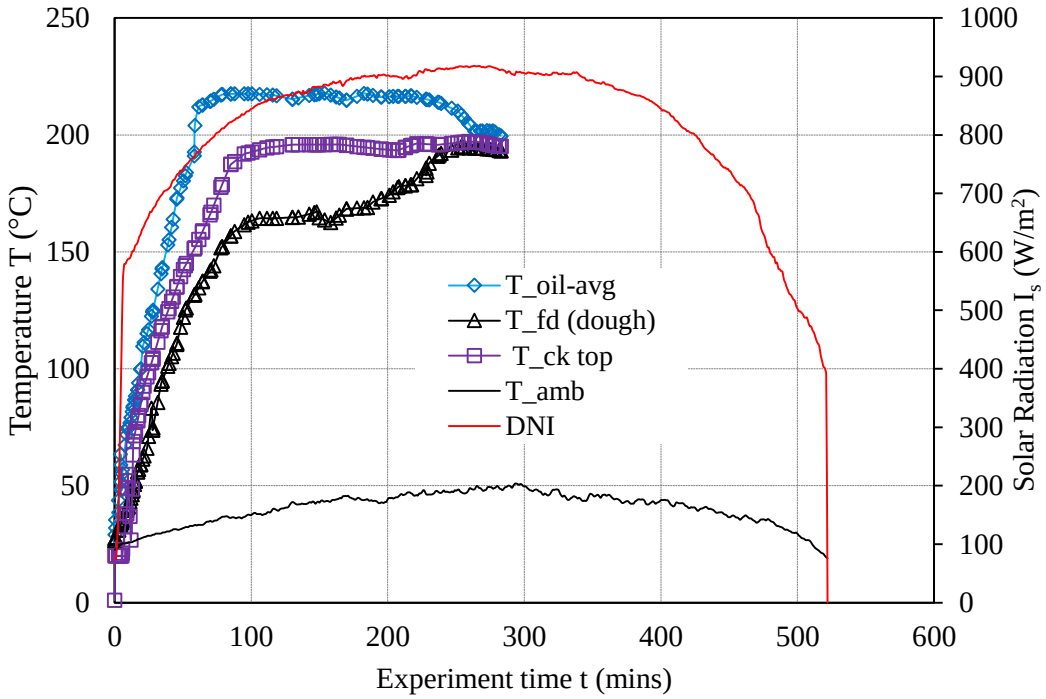

Figure 6-9: Experimental temperature as a function of experiment duration for the cake-baking experiment, 7 June 2015

6.9 Storage Capacity

An interesting result was achieved when the storage section of the experimental set up with this ceramic insulator material was theoretically compared with a system with no storage. A temperature profile as a function of time from Equation 3.52 to 3.54 was developed. The Shell S2 heat transfer fluid has a specific heat capacity of 2.7 kJ/kg K at 250 ℃. The values generated therefore from this result are shown in the graph in Figure 6-10 below. The theoretical analysis presented here was done with an assumption of no load condition in which the system performed no work (cooking) over 24 hours. The blue line legend represents the insulated system with ceramic wool while the red line legend represents a system with no insulation.

In Figure 6-10, the insulated tank will perform better as it held above the heat transfer oil at a temperature of 150 ℃ for over 12 hours under no loss (ideal) conditions, if it is charged with a temperature of around 260 ℃, the uninsulated system however would hold the same temperature for approximately 6 hours.

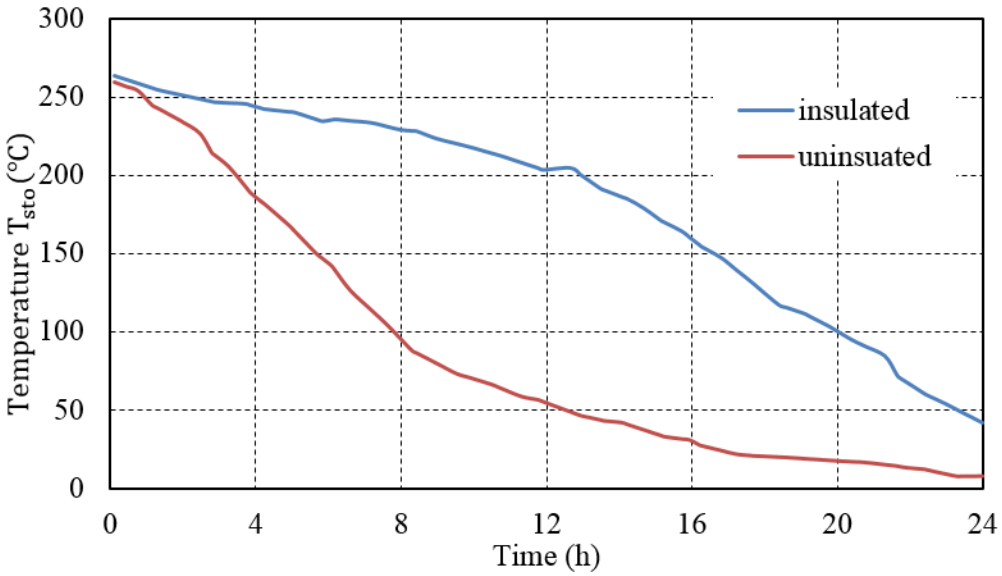

Figure 6-10: Theoretical comparison of insulated storage vs. uninsulated

6.10 Comparison with Existing System

Having reported the experiments which were performed using the manufactured system in this report, it would be necessary to compare the result with similar system in literature. The comparison is show in Table 6-2 below.

Table 6-2: Performance comparison between the current solar cooker and its equals

Author/manufacturer	Type		Mass (kg)	η_u	t_c(mins/kg)
Current research	Parabolic concentrator	Daylight	3	47.37	13.32
		Night		26.65	28.72
El-Sebah (1997)	Box with all side reflecting		3	31.00	
El-Sebaii & Ibrahim (2005)	Box type		4	26.70	
El-Kassaby (1991)	Parabolic concentrator		4	17.34	25.97
Khalifa et al. (1984)	Parabolic		4	12.15	43.20
	Solar oven		4	19.20	27.00

6.11 Chapter Summary

This chapter presented a comprehensive report on the experiments that were carried out using the manufactured parabolic solar cooker. The no-load testing and characteristics of the system were analysed. Several other experimental analyses of the system were also presented, ranging from water experiments done to calculate the efficiencies and other performance criteria, the heat coefficients, the second law analysis, which is exergy analysis as well as the theoretical analysis of the insulation used. The experiments in this report were carried out in winter which is often the major concern for most people interested in solar cooking. It was shown that, despite the low available irradiation, the system could still achieve a high temperature and could save heat, which is desirable. The solar cooker in the present research is more efficient than its equals in terms of both utilisation efficiency and the characteristic boiling time

The comparison on Table 6-1 shows the exergy efficiency of the system in this study was low as compared to the other similar system in literature which means that the quality of the energy transferred in the system was low. In contrast, Table 6-2 shows a higher useful energy efficiency for this system as compared to the other ones in literature. These results can however be suggested to be as a result of good solar resources available in South Africa, where this system was setup as compared to other countries on the table The necessary recommendations and suggestions for improvement are presented in the next chapter.

7 Conclusions and Recommendations

The international testing procedures for solar cookers, as set out by Funk (2000), were followed strictly in the experiments presented in this report, and a parabolic solar cooker that has the potential to contribute immensely to any community's development was presented. This chapter is divided into two parts – Section 7.1, which presents the conclusions and overall summary, and Section 7.2, which presents the recommendations as well as possible usages of the system.

7.1 Conclusions

Solar cookers are gradually gaining ground and a lot of research is being undertaken to ensure that they compete favourably with other conventional cookers. In this report, the concept of cooking with the sun was proven to be viable, and the ability of solar cookers to achieve high temperatures even with low solar resources was pointed out. Indoor cooking with solar energy was also achieved, and the complexities in parabolic solar cooker design were greatly reduced. The system achieved utilisation efficiency of up to 47% when used under direct sunlight, and around 27% average when used for late-hour cooking, as shown in Table 6-2 in the previous chapter.

The heat transfer and storage oil was found to be fully charged in five hours for 50 litres of HTF oil. This charging time was highly dependent on the solar irradiation available on the experimental test days. The parabolic solar cooker designed in this study was found to be more effective than many other solar cookers in existence. This was due to the reduced heat loss around its cavity receiver, which was achieved as a result of the optimised entrance aperture. The design also eliminated the need for the user to be exposed to direct sun radiation, because the heat generated in the solar collection subsystem was channelled into the storage tank, which can be placed at any convenient spot in a house or shed.

It was pointed out in Section 4.5 of this report that the parabolic concentrators often produce either excessive or insufficient heat flux, and that this challenge can be overcome by varying the geometric concentration ratio of the system. This invariably means varying the aperture areas of either the concentrators or the receiver, or even both. The experiments presented in this report were carried out in the southern hemisphere in winter and, during that period, the solar irradiation is low. In order to capture enough reflected rays, an extra 30 mm was added to the aperture diameter of the receiver, which was designed to capture the entire reflected image width, W_n, as calculated in Equation 4.20. The method of intensity modification used, namely increasing the diameter of the receiver, was a trade-off on heat loss. This is because, even though a larger aperture diameter allows more reflected rays to be captured, it also increases the possibilities of high heat losses. However, it was emphasised throughout the report that the entrance aperture area of the cavity receiver was packed with a flat spiral copper tube that had no pitch (gap), which ultimately reduced the heat losses due to convection. The size of the receiver was modified in this research because the concentrator was a television satellite dish that had an aperture diameter of 2 m. This was selected because it is a perfect parabola. This was in response to the observation in Section 2.2.2 that the manufacturing of standard parabolic cookers often requires expertise and precision fabrication. The television dish used was modified and the reflecting surface was covered with aluminium foil, which worked perfectly. The combined optical efficiency of the dish system based on the analysis in Section 4.1.7 was found to be 0.84, compared

to the 0.85 of Feuermann and Gordon (2001) and Kribus et al. (2006) and the 0.83 of Wu et al. (2010 a).

The latent efficiency of the system was found to be 34%, as highlighted in Section 6.3, but the exergy efficiency of the system, as shown in Section 6.7, was relatively low at an average of 0.05%. This was not unusual, as most systems that make use of solar irradiation often have low efficiencies and extremely low exergy efficiencies. There seems to be a very slim chance to raise the exergy efficiency of this system in terms of the geometry of solar collection or the overall experimental setup during the experiments. However, there would be a small improvement if the experiments were carried out in summer, because of a clearer sky and better constant solar irradiation. An improvement in the reflectivity of the parabolic dish by using better reflective material may also reduce the exergy loss. The exergy analysis offered a path to a possible optimisation of the system in future research, as it combined both thermodynamics and operational efficiency, which can be analysed stage by stage for system development. The result of the energy and exergy efficiencies in this setup was found to be dependent on three major factors, namely (i) the average ambient temperature, (ii) the available solar irradiation on the day and (iii) the mass of water that was boiled.

Solar cooking was achieved for six hours a day, with the ability to cook at night for up to two hours. Besides the desire to achieve both night-time and indoor cooking, the need for a low-cost setup was among the goals of this project, and that was achieved with the re-use of an old television dish that was refurbished as a solar collector/reflector. Also, the use of an automotive pump reduced the cost that would have been incurred by the purchase of a high-temperature positive-displacement pump. The modification done on the automotive pump by changing the gasket material and covering the joints with silicon gel eliminated the obvious spills that accompany working with oil as a heat-transfer fluid at high temperature.

Four sets of food were cooked when the system reported in the current study was fully charged. This was shown in the experiment discussed in Section 6.4, where the sensible cooking power reduced with an increase in cooking time. In this way, it can be concluded that the faster the cooking performed of the system, the higher the cooking power and the faster the rate of heat removal from the storage section, as shown in Figures 6-5 and 6-6. About 100 minutes after the experiment had begun, the average oil temperature dropped from 180 ℃ to 107 ℃ because there was no regulation of the flow rate of hot oil from the storage tank to the spiral cooking head, and no further heating of the oil was allowed, as the flow to the receiver cavity was stopped immediately after the experiment began.

The cooking power, latent efficiencies and heat loss coefficient equation for the system were analysed carefully. The results from these analyses show that the solar cooker is a viable system of international standard, as all the calculated values fell within the range of the international standard procedures for testing solar cookers and reporting performance. Other types of cooking heads can be designed to be used with this system to harness the heat in its storage tank.

7.2 Recommendations

The manufacturing cost of the parabolic solar cooker with all its parts was R9 000, despite the various innovative and improvisation ideas to reduce the cost. This was because the design cost was for a single system, and only one unit of some parts was needed. These individual units bought or fabricated would have been cheaper if they was obtained in bulk,

therefore the manufacturing of this solar cooker on large scale will automatically reduce the production cost (due to mass production), and its marketability will then be viable. For future research, there is a need to design a system that can be used to vary the flow of hot oil into the spiral head of the cooking section so that the heat flow to the cook top can be regulated, as in any conventional cooker. In order to encourage the durability of the oil pump without leakage, a system setup in which a high-temperature oil pump is immersed in the storage setup should be considered. One of the lessons learnt in the course of this research is that, when working with oil at a high temperature, one must be prepared for unnecessary leaks, as the oil becomes very light and can sneak through the smallest of joints.

A comprehensive exergy analysis of the system should also be performed, as this can be stratified and done at various points in the system and can be used to know exactly where the energy quality is lost. The overall exergy efficiency loss point then can determined and necessary improvements can be made.

The cooking section of this parabolic cooker presently works both as a solar oven and a stove, but this can be modified, based on the needs of the user, to perform functions such as water pasteurisation, industrial bread making, industrial agricultural food processing that requires high temperatures, cooking meals for either individuals or families, institutional/community cooking, meat/fish roasting and general cooking. These modifications can be used for development in African communities as listed below:

- Water pasteurisation

Globally, waterborne diseases are the second highest cause of deaths in children under the age of five, ranked just behind deaths from acute respiratory infections (Gleick, 2002). Safe water is far from being accessible to dwellers in rural African communities, while the quality of water in cities is fast deteriorating. Heating contaminated water to 65 ℃ kills all germs or infectious organisms, as well as contaminating bodies (Aliber, 2003). Therefore the cooking section can be developed to act as a solar water heater for communities or family in need of water pasteurisation.

- Industrial development

Most baking and pastry-making processes are accomplished under 210 ℃ (Mondal & Datta, 2008). With these cooking system used directly as an oven, these industries can be set up in rural areas and will automatically provide employment for the teeming populace of the villages while reducing overdependence on supplies from the cities.

- Educational development

In South Africa, for example, the National School Nutrition programme enhances school learning through the provision of healthy food. The food is prepared using electricity or coal where there is no access to the grid (Spaull, 2013). Using this parabolic cooking system will reduce the costs incurred by purchasing cooking fuel/coal or the load on the national grid. It will also preserve the natural taste of the food. The costs incurred during food cooking, which would have been averted by using the solar cooker over time, therefore could be used for educational development.

- Cooking breakthrough

When used as a home unit, the system can also serve women in rural areas, saving them the time used in gathering firewood for cooking. It will save unnecessary stress and injuries to health that could result from cooking with firewood (Otte, 2013). The system can be

used for cooking community festive feasts. Institutions like hospitals, refugee camps, prisons and the military could also use the solar cooking system for various specific purposes

References

Agyenim, F., Hewitt, N., Eames, P., & Smyth, M. (2010). A review of materials, heat transfer and phase change problem formulation for latent heat thermal energy storage systems (LHTESS). *Renewable and Sustainable Energy Reviews*, *14*(2), 615–628. doi:http://dx.doi.org/10.1016/j.rser.2009.10.015

Ahmad, B. (2001). Users and disusers of box solar cookers in urban India—: Implications for solar cooking projects. *Solar Energy*, *69*, 209–215. http://dx.doi.org/10.1016/S0038-092X(01)00037-8

Aliber, M. (2003). Chronic poverty in South Africa: Incidence, causes and policies. *World Development*, *31*(3), 473–490. http://dx.doi.org/10.1016/S0305-750X(02)00219-X

Al-Soud, M. S., Abdallah, E., Akayleh, A., Abdallah, S., & Hrayshat, E. S. (2010). A parabolic solar cooker with automatic two axes sun tracking system. *Applied Energy*, *87*(2), 463–470. doi:DOI 10.1016/j.apenergy.2009.08.035

Amer, E. H. (2003). Theoretical and experimental assessment of a double exposure solar cooker. *Energy Conversion and Management*, *44*(16), 2651–2663. doi:10.1016/S0196-8904(03)00022-0

Arenas, J. M. (2007). Design, development and testing of a portable parabolic solar kitchen. *Renewable Energy*, *32*(2), 257–266. doi:10.1016/j.renene.2006.01.013

Barrios, S., Bertinelli, L., & Strobl, E. (2006). Climatic change and rural–urban migration: The case of sub-Saharan Africa. *Journal of Urban Economics*, *60*(3), 357–371. http://dx.doi.org/10.1016/j.jue.2006.04.005

Basantani, M. (2008). World's largest 38500-meal solar kitchen in India.. Retrieved June 15, 2014, from http://inhabitat.com/world's-largest-solar-kitchen-in-india-can-cook-upto-38500-meals-per-day/

Biermann, E., Grupp, M., & Palmer, R. (1999). Solar cooker acceptance in South Africa: Results of a comparative field-test. *Solar Energy*, *66*(6), 401–407. http://dx.doi.org/10.1016/S0038-092X(99)00039-0

Bryceson, D. F. (1996). Deagrarianization and rural employment in sub-Saharan Africa: A sectoral perspective. *World Development*, *24*(1), 97–111. http://dx.doi.org/10.1016/0305-750X(95)00119-W

Çengel, Y. A., & Cimbala J, M. (2006). *Fluid mechanics fundamentals and applications* (2nd ed.). New York: McGraw- Hill.

Chapra, S. C., & Canale, R. P. (2003). *Numerical methods for engineers*. New York: Mcgraw-hill.

Christie, S., & Gandar, M. (1994). Commercial and Social Forestry Draft Position Paper. (L. and A.P.C.P. in N. R. Management, Ed.). LAPC, Johannesburg.

Cochetel, S. (2012). *Identifying the barriers to the deployment of solar cookers in the energy-poor households of sub-Saharan Africa*. *Renewable Energy*. Honours dissertation. University of Exeter. Retrieved June 15, 2014 from http://citeseerx.ist.psu.edu/viewdoc/download?doi=10.1.1.463.1892&rep=rep1&type=pdf

Craig, O. O., & Dobson, R. T. (2015). Stand-alone parabolic solar cookers and rural industrialisation in Southern Africa. In *Southern African Solar Energy Conference (SASEC) 2015* (pp. 278–282). Skukuza, South Africa. Retrieved from http://hdl.handle.net/2263/49491

Cuce, E., & Cuce, P. M. (2013). A comprehensive review on solar cookers. *Applied Energy*, *102*, 1399–1421. doi:10.1016/j.apenergy.2012.09.002

Department of Environmental Affairs. (2012). Statistics South Africa, General Household Survey (Statistical release P0318). Retrieved January 27, 2015, from http://soer.deat.gov.za/1325.html

Diabaté, L., Blanc, P., & Wald, L. (2004). Solar radiation climate in Africa. *Solar Energy*, *76*(6), 733–744. http://dx.doi.org/10.1016/j.solener.2004.01.002

Duffie, J. A., & Beckman, W. A. (2013). *Solar engineering of thermal processes* . doi:10.1002/9781118671603.fmatter

El-Kassaby, M. M. (1991). New solar cooker of parabolic square dish: Design and simulation. *Renewable Energy*, *1*(1), 59–65. http://dx.doi.org/10.1016/0960-1481(91)90104-W

El-Sebah, A. (1997). Thermal performance of a box-type solar cooker with outer-inner reflectors. *Energy*, *22*(10), 969–978. doi:10.1016/S0360-5442(97)00027-3

El-Sebaii, A. A., & Ibrahim, A. (2005). Experimental testing of a box-type solar cooker using the standard procedure of cooking power. *Renewable Energy*, *30*(12), 1861–1871. doi:10.1016/j.renene.2005.01.007

Esen, M. (2004). Thermal performance of a solar cooker integrated vacuum-tube collector with heat pipes containing different refrigerants. *Solar Energy*, *76*(6), 751–757. doi:10.1016/j.solener.2003.12.009

Eskom. (2014). What is load shedding? Retrieved July 20, 2015, from http://loadshedding.eskom.co.za/loadshedding/description

Espinar, B., Ramírez, L., Drews, A., Beyer, H. G., Zarzalejo, L. F., Polo, J., & Martín, L. (2009). Analysis of different comparison parameters applied to solar radiation data from satellite and German radiometric stations. *Solar Energy*, *83*(1), 118–125. doi:10.1016/j.solener.2008.07.009

Incorpea, F., Dewitt, D., Bergman, T. L., & Adrienne, S. L. (2007). *Fundementals of heat and mass transfer* (6th ed.). New York. John Wiley & Sons, Inc.

Feuermann, D., & Gordon, J. M. (2001). High-concentration photovoltaic designs based on miniature parabolic dishes. *Solar Energy*, *70*(5), 423–430. doi:10.1016/S0038-092X(00)00155-9

Figliola, R. S., & Beasley, D. E. (2009). Theory and design for mechanical measurements. *Measurement Science and Technology*, *7*(7). doi:10.1088/0957-0233/7/7/016

Funk, P. A. (2000). Evaluating the international standard procedure for testing solar cookers and reporting performance. *Solar Energy*, *68*(1), 1–7. doi:10.1016/S0038-092X(99)00059-6

Gleick, P. H. (2002). Dirty Water : Estimated Deaths from Water-Related Diseases 2000-2020. *Pacific Institute Research Report*, 1–12.

Goldstein, R. J., Ibele, W. E., Patankar, S. V, Simon, T. W., Kuehn, T. H., Strykowski, P. J., Mittal, R. (2010). Heat transfer—A review of 2005 literature. *International Journal of Heat and Mass Transfer*, *53*(21–22), 4397–4447. doi:http://dx.doi.org/10.1016/j.ijheatmasstransfer.2010.05.005

Grundy, W. N. (1995). Solar Cookers and Social Classes in Southern Africa. *Techné: Journal of Technology Studies*, *Vol. V*, *Wi*(Gray Norton, ed.), 3–7.

Gueymard, C. A. (2012). Clear-sky irradiance predictions for solar resource mapping and large-scale applications: Improved validation methodology and detailed performance analysis of 18 broadband radiative models. *Solar Energy*, *86*(8), 2145–2169. doi:10.1016/j.solener.2011.11.011

Halacy, B., & Halacy, C. (1992). Cooking With the Sun. (J. Howel, Ed.). Lafayete, CA.

Haridas, A. (2013). Construction of a Parabolic Reflecting Solar Cooker. *International Journal of Applied Engineering Research*, *8*(18), 2075–2080. Retrieved December 4, 2014, from http://www.ripublication.com/ijaer.htm

Harris, J. A., & Lenz, T. G. (1985). Thermal performance of solar concentrator/cavity receiver systems. *Solar Energy*, *34*(2), 135–142. doi:10.1016/0038-092X(85)90170-7

Helal, O., Chaouachi, B., & Gabsi, S. (2011). Design and thermal performance of an ICS solar water heater based on three parabolic sections. *Solar Energy*, *85*(10), 2421–2432. doi:10.1016/j.solener.2011.06.021

Higgins, J. (2013). What type of food do people eat in Africa? ehow.com. Retrieved September 8, 2014, from http://www.ehow.com/facts_5575439_type-do-people-eat-africa.html

Holburn Eaton Oil Pumps. (2015). Automotive Oil Pump Refurbishing. *Gryphon Design and Manufacturing*. Retrieved February 10, 2015, from http://gryphondesign.co.uk/oilpumpHE.html

IFAD. (2009). Rural poverty in Africa. International Fund for Agricultural Development. Retrieved June 10, 2014, from http://www.ifad.org/operations/gmaps/pf/index.htm

Kalogirou, S. A. (2009). *Solar Energy Engineering Processes and Systems*. Academic Press Elsevier.

Kaushika, N. ., & Reddy, K. . (2000). Performance of a low cost solar paraboloidal dish steam generating system. *Energy Conversion and Management*, *41*(7), 713–726. doi:10.1016/S0196-8904(99)00133-8

Khalifa, A., Akyurta, M. M., & Taha, M. M. (1986). On Prediction Of Solar Cooker Performance And Cooking In Pyrex Pots. *Solar & Wind Technology*, *3*(1), 13–19.

Khalifa, A. M. A., Taha, M. M. A., & Akyurt, M. (1984). An energy thrifty solar cooler—The mina oven. *Solar & Wind Technology*, *1*(2), 81–91. doi:10.1016/0741-983X(84)90010-9

Kimambo, C. Z. M. (2007). Development and performance testing of solar cookers. *Journal of Energy in Southern*, *18*(3).

Knudson, B. (2004). State of the Art of Solar Cooking. *A Global Survey of Practices & Promotion Programs. SCI, Sacramento*.

Kousksou, T., Bruel, P., Cherreau, G., Leoussoff, V., & El Rhafiki, T. (2011). PCM storage for solar DHW: From an unfulfilled promise to a real benefit. *Solar Energy*, *85*(9), 2033–2040. doi:http://dx.doi.org/10.1016/j.solener.2011.05.012

Kribus, A., Kaftori, D., Mittelman, G., Hirshfeld, A., Flitsanov, Y., & Dayan, A. (2006). A miniature concentrating photovoltaic and thermal system. *Energy Conversion and Management*, *47*(20), 3582–3590. doi:10.1016/j.enconman.2006.01.013

Kuehn, T. H., & Goldstein, R. J. (1976). Correlating equations for natural convection heat transfer between horizontal circular cylinders. *International Journal of Heat and Mass Transfer*, *19*(10), 1127–1134. doi:10.1016/0017-9310(76)90145-9

Kumar, S., & Reddy, K. (2007). Numerical investigation of natural convection heat loss in modified cavity receiver for fuzzy focal solar dish concentrator. *Solar Energy*, *81*, 846–855. doi:10.1016/j.solener.2006.11.008

Lecuona, A., Nogueira, J.-I., Ventas, R., Rodríguez-Hidalgo, M.-C., & Legrand, M. (2013). Solar cooker of the portable parabolic type incorporating heat storage based on PCM. *Applied Energy*, *111*(0), 1136–1146. doi:http://dx.doi.org/10.1016/j.apenergy.2013.01.083

Mathioulakis, E., & Belessiotis, V. (2002). A new heat-pipe type solar domestic hot water system. *Solar Energy*, *72*(1), 13–20. doi:10.1016/S0038-092X(01)00088-3

Melchior, T., Perkins, C., Weimer, A. W., & Steinfeld, A. (2008). A cavity-receiver containing a tubular absorber for high-temperature thermochemical processing using concentrated solar energy. *International Journal of Thermal Sciences*, *47*, 1496–1503. doi:10.1016/j.ijthermalsci.2007.12.003

Mills, A. F., & Ganesan, V. (2009). *Heat Transfer* (2nd ed.). Prentice Hall.

Misselhorn, A. A. (2005). What drives food insecurity in southern Africa? a meta-analysis of household economy studies. *Global Environmental Change*, *15*(1), 33–43. doi:http://dx.doi.org/10.1016/j.gloenvcha.2004.11.003

Mondal, A., & Datta, A. K. (2008). Bread baking – A review. *Journal of Food Engineering*, *86*(4), 465–474. doi:http://dx.doi.org/10.1016/j.jfoodeng.2007.11.014

Morgan Thermal Ceramics. (2014). *Asia Pacific Product Data Brochure Morgan Thermal Ceramics solutions*.

Muthusivagami, R. M., Velraj, R., & Sethumadhavan, R. (2010). Solar cookers with and without thermal storage—A review. *Renewable and Sustainable Energy Reviews*, *14*(2), 691–701. doi:http://dx.doi.org/10.1016/j.rser.2008.08.018

Nahar, N. M. (2003). Performance and testing of a hot box storage solar cooker. *Energy Conversion and Management*, *44*(8), 1323–1331. doi:http://dx.doi.org/10.1016/S0196-8904(02)00113-9

NMISA (2012). National Metereology Institute of South Africa. Measurement Units and Measurement Standards Act, 2006. Retrieved April 4, 2015, from http://www.nmisa.org/Technical/EM/Pages/Temperature and Humidty.aspx

NREL GIS. (2015). Solar Maps. *National Renewable Energy Laboratory: Dynamics Maps, GIS and Analysis Tools Data*. Retrieved March 17, 2015, from http://www.nrel.gov/gis/solar.html

NUFUNetwork, P. (2013). *Small scale concentrating solar energy system with heat storage*. The Norwegian Program for Development, Research and Higher Education.

Otte, P. P. (2013). Solar cookers in developing countries—What is their key to success? *Energy Policy*, *63*(0), 375–381. doi:http://dx.doi.org/10.1016/j.enpol.2013.08.075

Öztürk, H. H. (2004). Experimental determination of energy and exergy efficiency of the solar parabolic-cooker. *Solar Energy*, *77*(1), 67–71. doi:10.1016/j.solener.2004.03.006

Öztürk, H. H. (2004). Second Law Analysis for Solar Cookers. *International Journal of Green Energy*, *1*(2), 227–239. doi:10.1081/GE-120038754

Panwar, N. L., Kaushik, S. C., & Kothari, S. (2012). State of the art of solar cooking: An overview. *Renewable and Sustainable Energy Reviews*, *16*(6), 3776–3785. doi:http://dx.doi.org/10.1016/j.rser.2012.03.026

Petela, R. (2003). Exergy of undiluted thermal radiation. *Solar Energy*, *74*(6), 469–488.

Petela, R. (2005). Exergy analysis of the solar cylindrical-parabolic cooker. *Solar Energy*, *79*(3), 221–233. doi:http://dx.doi.org/10.1016/j.solener.2004.12.001

Pih, P., & Kalogirou, S. A. (1997). Design and Construction of a One-axis Sun-tracking System, *57*(6), 465–469.

Prakash, M., Kedare, S. B., & Nayak, J. K. (2009). Investigations on heat losses from a solar cavity receiver. *Solar Energy*, *83*(2), 157–170. doi:http://dx.doi.org/10.1016/j.solener.2008.07.011

Prinsloo, G. J. (2014). *Automatic positioner and control system for a motorized parabolic solar reflector*. Master's thesis. Stellenbosch University. Retrieved March 26, 2015, from https://scholar.sun.ac.za/handle/10019.1/96137

Radabaugh, J. (2011). Heaven's Flame. *Solar Cooker History*. Retrieved June 10, 2014, from http://solarcooking.org/history.html

Ramadan, R. I. (1988). A model of an improved low cost - indoor - solar- cooker in Tanta. *Solar & Wind technology* Vol. 5. No. 4. pp. 387 393, 1988

Reddy, K. & Ranjan, M. (2003). Solar resource estimation using artificial neural networks and comparison with other correlation models. *Energy Conversion and Management*, *44*(15), 2519–2530. doi:10.1016/S0196-8904(03)00009-8

Reddy, K. S. & Sendhil Kumar, N. (2009). Convection and surface radiation heat losses from modified cavity receiver of solar parabolic dish collector with two-stage concentration. *Heat and Mass Transfer/Waerme- Und Stoffuebertragung*, *45*(3), 363–373. doi:10.1007/s00231-008-0440-2

Rogers, D. S., Duraiappah, A. K., Antons, D. C., Munoz, P., Bai, X., Fragkias, M., & Gutscher, H. (2012). A vision for human well-being: transition to social sustainability. *Current Opinion in Environmental Sustainability*, *4*(1), 61–73. doi:http://dx.doi.org/10.1016/j.cosust.2012.01.013

Roth, P., Georgiev, a., & Boudinov, H. (2005). Cheap two axis sun following device. *Energy Conversion and Management*, *46*, 1179–1192. doi:10.1016/j.enconman.2004.06.015

Schwarzer, K., & da Silva, M. E. V. (2008). Characterisation and design methods of solar cookers. *Solar Energy*, *82*(2), 157–163. doi:http://dx.doi.org/10.1016/j.solener.2006.06.021

Schwarzer, K., & Vieira da Silva, M. E. (2003). Solar cooking system with or without heat storage for families and institutions. *Solar Energy*, *75*(1), 35–41. doi:http://dx.doi.org/10.1016/S0038-092X(03)00197-X

Sen, Z. (2004). Solar energy in progress and future research trends. *Progress in Energy and Combustion Science*, *30*(4), 367–416. doi:http://dx.doi.org/10.1016/j.pecs.2004.02.004

Sharma, S., Buddhi, D., Sawhney, R., & Sharma, A. (2000). Design, development and performance evaluation of a latent heat storage unit for evening cooking in a solar cooker. *Energy Conversion and Management*, *41*(14), 1497–1508. doi:10.1016/S0196-8904(99)00193-4

Sharma, S., Iwata, T., Kitano, H., & Sagara, K. (2005). Thermal performance of a solar cooker based on an evacuated tube solar collector with a PCM storage unit. *Solar Energy*, *78*(3), 416–426. doi:10.1016/j.solener.2004.08.001

Shilston, M. J., & Probert, S. D. (1979). Thermal insulation provided by plain, horizontal annular cavities containing atmospheric pressure air. *Applied Energy*, *5*(1), 61–80. doi:10.1016/0306-2619(79)90006-0

Shuai, Y., Xia, X.-L., & Tan, H.-P. (2008a). Radiation performance of dish solar concentrator/cavity receiver systems. *Solar Energy*, *82*(1), 13–21. doi:http://dx.doi.org/10.1016/j.solener.2007.06.005

Shuai, Y., Zhang, H. C., & Tan, H. P. (2008b). Radiation symmetry test and uncertainty analysis of Monte Carlo method based on radiative exchange factor. *Journal of Quantitative Spectroscopy and Radiative Transfer*, *109*, 1281–1296. http://dx.doi.org:10.1016/j.jqsrt.2007.10.001

Shukla, S. K. (2009). Comparison of energy and exergy efficiency of community and domestic type parabolic solar cookers. *International Journal of Green Energy*, *6*(5), 437–449. http://dx.doi.org:10.1080/15435070903227912

Solar-Cooker-International. (2001). Basics of Solar Cooker Design. *Interntional, Solar Cookers*. Retrieved July 12, 2014, from http://www.solarcookers.org/network/

Solar-GIS. (2011). Poster maps (wall maps) for solar energy. Retrieved February 15, 2014, from http://solargis.info/doc/postermaps

Spaull, N. (2013). Poverty & privilege: Primary school inequality in South Africa. *International Journal of Educational Development*, *33*(5), 436–447. http://dx.doi.org/10.1016/j.ijedudev.2012.09.009

Stine, W. & Geyer, M. (2001). Power From The Sun. Retrieved February 15, 2014, from Power from the sun.net. http://www.powerfromthesun.net/book.html

Telkes, M. (1959). Solar cooking ovens. *Solar Energy*, *3*(1), 1–11. http://dx.doi.org/10.1016/0038-092X(59)90053-2

University of Oregon Solar Radiation Monitoring Laboratory. (2007). Sun path chart program. Universirty of Oregon.

Von Braun, J. (2010). Food insecurity, hunger and malnutrition: necessary policy and technology changes. *New Biotechnology*, *27*(5), 449–452. http://dx.doi.org/10.1016/j.nbt.2010.08.006

Wentzel, M., & Pouris, A. (2007). The development impact of solar cookers: A review of solar cooking impact research in South Africa. *Energy Policy*, *35*(3), 1909–1919. doi:DOI 10.1016/j.enpol.2006.06.002

Wu, S.-Y., Xiao, L., Cao, Y., & Li, Y.-R. (2010a). A parabolic dish/AMTEC solar thermal power system and its performance evaluation. *Applied Energy*, *87*(2), 452–462. doi:http://dx.doi.org/10.1016/j.apenergy.2009.08.041

Wu, S.-Y., Xiao, L., Cao, Y., & Li, Y.-R. (2010b). Convection heat loss from cavity receiver in parabolic dish solar thermal power system: A review. *Solar Energy*, *84*(8), 1342–1355. doi:10.1016/j.solener.2010.04.008

Yao, Y., Hu, Y., Gao, S., Yang, G., & Du, J. (2014). A multipurpose dual-axis solar tracker with two tracking strategies. *Renewable Energy*, *72*(0), 88–98. doi:http://dx.doi.org/10.1016/j.renene.2014.07.002

Yettou, F., Azoui, B., Malek, A., Gama, A., & Panwar, N. L. (2014). Solar cooker realizations in actual use: An overview. *Renewable and Sustainable Energy Reviews*, *37*(0), 288–306. doi:http://dx.doi.org/10.1016/j.rser.2014.05.018

Yogo, K., & Ishikawa, M. (2000). Recent progress in environmental catalytic technology. *Catalysis Surveys from Japan*, *4*(1), 83–90. doi:Doi 10.1023/A:1019088121877

Zawilska, E., & Brooks, M. J. (2011). An assessment of the solar resource for Durban, South Africa. *Renew*

Appendices

A. Orifice Flow Meter

The general principle of the orifice flow meter is an attempt to obstruct the flow of fluid in any convenient manner using a desired mechanical device. Often, an orifice can be used to determine the flow rate of a fluid. In our system, in order to measure the heat-transfer fluid flow rate, an orifice was built, as shown in Figure A.1, to obstruct the initial flow direction. The density of the oil at various temperatures of the heat-transfer fluid (Shell oil S2) can be read from the manufacturer's technical data sheet.

Figure A-1: Orifice flow meter

For a given pressure drop across the orifice plate, one can determine the flow rate and the average flow rate, as presented in the orifice analysis in Figure A-2 below.

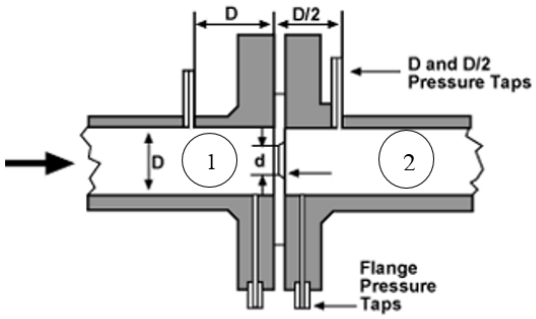

Figure A-2: Orifice flow meter (Çengel & Cimbala, 2006)

The assumptions made are that the flow is steady and incompressible. From Figure A-2 (Çengel & Cimbala, 2006) it can be stated that the principle of orifice flow meters is based on the Bernoulli equation,

$$\frac{P_1}{\rho g} + \frac{V_1^2}{2g} + z_1 = \frac{P_2}{\rho g} + \frac{V_2^2}{2g} + z_2 \qquad [m] \qquad (A.1)$$

as well as on the mass balance equation for incompressible flow:

$$\dot{V} = A_1 V_1 = A_2 V_2 \qquad [m^3/s] \qquad (A.2)$$

Therefore

$$V_1 = \frac{A_2}{A_1} V_2 = \beta^2 V_2 \qquad [m^2/s] \qquad (A.3)$$

β is the diameter ratio, D and d, being outer and inner diameters

$$\beta = \frac{d}{D} \qquad (A.4)$$

$$A = \frac{\pi d^2}{4} \qquad (A.5)$$

and the pressure is the same, since only oil is used, therefore

$$P = \rho g h \qquad (A.6)$$

From the above sets of equations, the flow rate relation for obstruction meters will be

$$\dot{V} = A_0 C_d \sqrt{\frac{2}{\rho\left[1 - \left(\frac{A_0}{A_1}\right)^2\right]}} \qquad (m^3/s) \qquad (A.7)$$

$C_d$is the discharge coefficient for this type of obstruction flow meter, which can be calculated using Çengel and Cimbala J's (2006) equation for determining the discharge coefficient, stated as

$$C_d = \begin{cases} 0.5959 + 0.0312\beta^{2.1} - 0.184\beta^8 + \dfrac{91.71\beta^{2.5}}{Re^{0.75}} & if\ 10^4 < Re < 10^7 \\ 0.61 & if\ Re > 30000 \end{cases} \qquad (A.8)$$

The Reynold's number can then be calculated:

$$Re = \frac{\rho V_{avg} D}{\mu} \qquad (A.9)$$

The average velocity in the heat-transfer hose can also be determined using the ratio of the flow rate to the cross-sectional area of the flexible pipe used to transfer the heat:

$$V = \frac{\dot{V}}{A_p} \qquad (A.10)$$

B. Thermocouple Calibration

A major aspect of this experiment was heat-transfer analysis. Thus, temperature had to be measured at various points in the experimental setup. Thermocouples as shown in Figure B.1 were thus attached to various points in the experiment

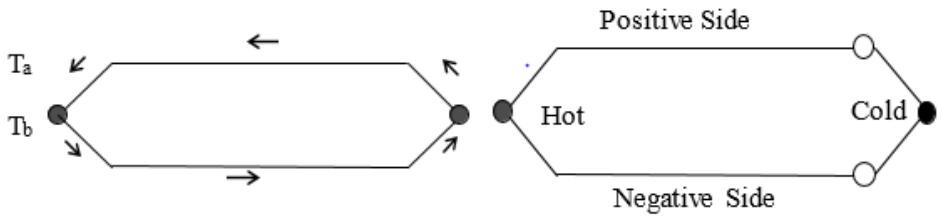

Figure B-1: Schematic diagram of thermocouple system

B.1 Theories

Thermocouples are sensors used to measure temperatures. They are made up of two wires of separate metals joined together (soldered or welded) to form a junction at one end. These junctions are different, considering that one serves as a reference and the other as the one to be measured. Whenever there is variation in the temperature at the joint, voltage is created (Figliola & Beasley, 2009). This voltage can then be converted to temperature using the thermocouple reference tables or a data logger. A data logger is a machine that converts the voltage (millivolts) to temperature with the aid of impulses sent by external thermocouples attached to it. This machine can then be connected to a computer system to generate the resultant temperatures in Excel format. The data logger machine was used in our experiment.

Two types of thermocouples were used in this experiment: (i) the T type (made of copper as positive leg and constantan as negative leg), which was used to measure temperature where the expected maximum temperature was below 150 ℃, and (ii) the K type (made of chromel as positive side and alumel (nickel -5 %, aluminium and silicon)), which was used when the expected temperature at a point was expected to be higher than 150 ℃.

B.2 Thermocouple Calibration

The T-type was calibrated with reference to a platinum-resistant thermometer, while the K-type was calibrated with reference to the calibrator temperature display. The first step taken in this calibration was to install the Agilent Bench Link software on the laptop computer to be used for the experiment. This Agilent links the computer to the thermocouples through the data logger. To achieve good accuracy in measurement, three thermocouples were used to measure temperature at most of the positions in the setup. The results from these three thermocouples, shown in Table B-1 below, were averaged to get the most accurate value

Table B-1: Data from thermocouples during calibration

Reference T_{ref} (°C)	T_1 (°C)	T_2 (°C)	T_3 (°C)
25	24.60	25.01	24.90
50	49.43	49.848	49.58
75	74. 95	74.90	74.89
100	99.89	99.95	99.24
125	125.02	125.08	125.18
150	149.28	149.19	149.87

The measured temperature for each of the thermocouples was then plotted against the reference temperature, as shown in Figures B2 to B4, in order to generate the linear trend line equations B.1 to B.4.

$$T_{1,corr} = 1.0001T_{1,meas} - 0.3123 \quad \text{(B. 1)}$$

$$T_{2,corr} = 0.9962T_{2,meas} + 0.1614 \quad \text{(B. 2)}$$

$$T_{3,corr} = 1.0011T_{3,meas} - 0.3214 \quad \text{(B. 3)}$$

$$T_{out} = \frac{T_{1,meas} + T_{2,meas} + T_{3,meas}}{3} \quad \text{(B. 4)}$$

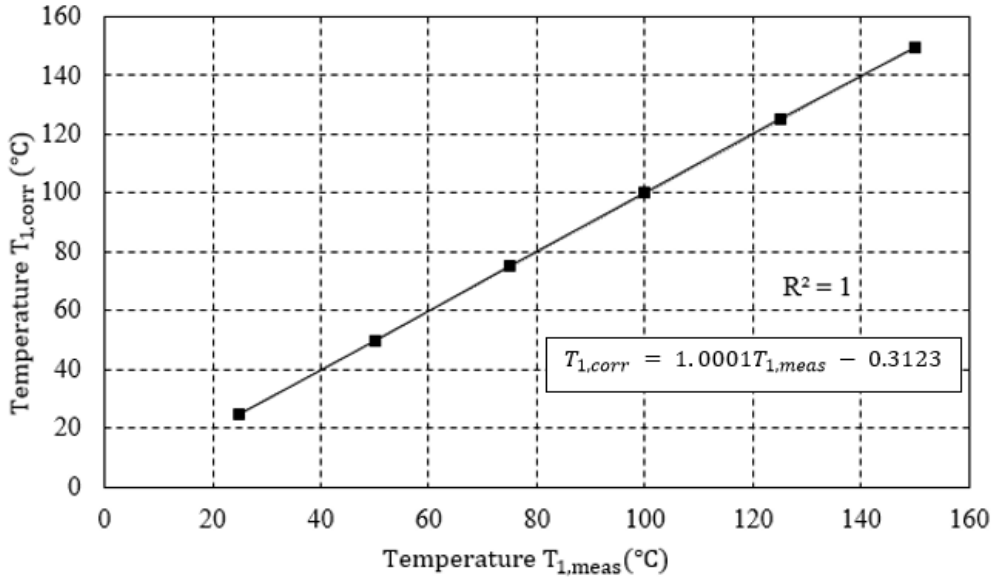

Figure B-2: Thermocouple 1

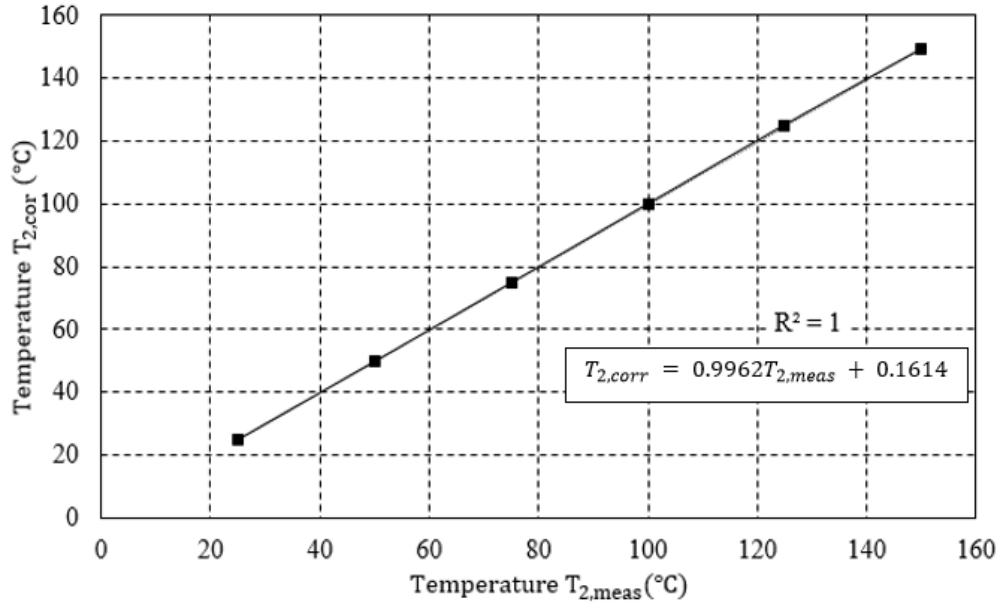

Figure B-3: Thermocouple 2

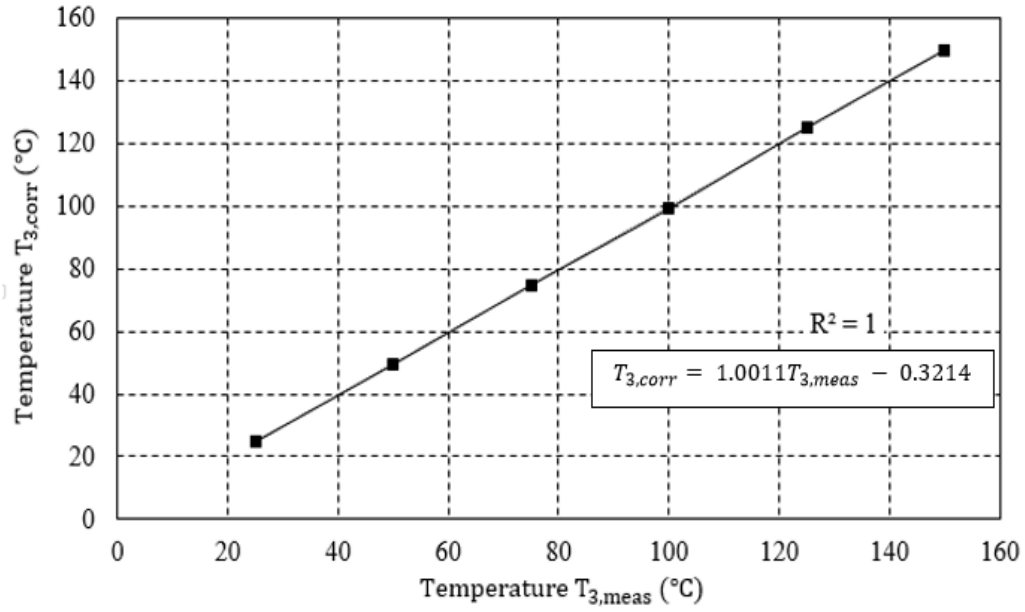

Figure B-4: Thermocouple 3

The K-type thermocouple calibration was done with an immersion depth of 150 mm, and the unit under test (UUT) was calibrated according to standards for laboratory calibration determined by national measuring standards for temperature, as shown in Tables B.2 to B.4 below.

Table B-2: Summary of the results K-type calibration

Actual Temp	UUT reading (Ohms)	UUT reading (℃)	Correction (℃)	Uncertainty U (℃)
50.02	119.42	+0.076	-0.037	±0.70
99.99	138.54	+100.09	-0.100	±0.70
179.82	168.47	+179.98	-0.154	±0.70
300.00	212.13	+300.23	-0.225	±0.70

Table B-3: Laboratory standards and equipment used for measurement

Standard of equipment	Serial number	Certificate number
ASL F250 digital thermometer	1344029856	TH\DG-6460
Pt 100 prob	PT100.1-20	TH\DG-6460
Calibrator	RAPO 1G	

Table B-4: Procedure utilised

Code	Meaning
1016	Determination of uncertainties
2001	Ice point
2003	Calibration of RTD/PT100

The photograph taken during the calibration is shown below in Figure B-5

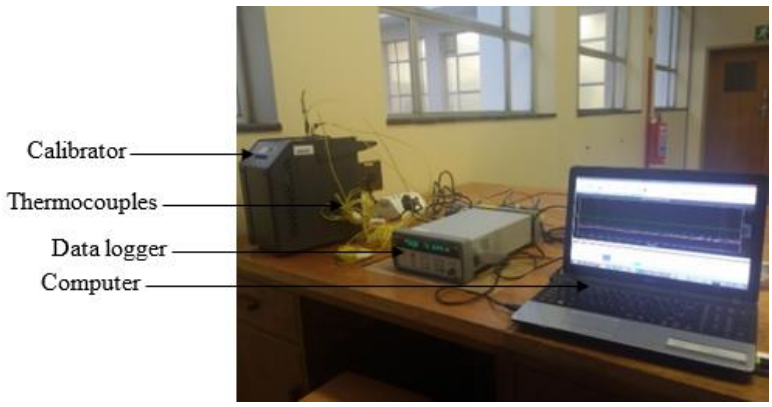

Figure B-5: Calibration setup

Type T thermocouple calibration equipment details:

Calibrator: Fluke Field metrology setup

Model number: 9142

Serial number: B2921

Calibration range: $-20\ ℃$ to $150\ ℃$

Reference temperature source: Isotech platinum resistance thermometer

Model number: 9351472

Serial number: 191069

Calibration certificate number: SANAS, RAP15738

Laptop: Acer Aspire

Model number: E1-571-53234G1TMaks

Serial number: NXM09EM136325183A83400

SNID: 32509924034

RAM: 4 GB DDR3 memory

Manufacturing date: 21/06/2013

C. Sample Calculations and Validation

C.1 Sample Calculations

Calculate the (i) sensible cooking power, (ii) utilisation efficiency and (iii) characteristic boiling time for a parabolic solar cooker to cook water of mass 3 kg at 21.9 ℃ to boiling (99.7 ℃) in a record time of 12.9 minutes if the average solar insolation available in the period was 880 W/m^2. If the same boiling water is left to boil for two hours with no appreciable rise in temperature, calculate (iv) the latent solar cooker efficiency of the setup. Take the specific heat of water to be 4 186 J/kg K, the h_{fg} to be 2 257 kJ/kg K and the standard reference insolation to be $I_{ref} = 900\ W/m^2$. Also determine the exergy efficiency of the system if it took 12 minutes to boil to a temperature of 97.7 ℃ ; take the collector aperture to be 3.142 m^2 , the temperature of the sun to be 6 000 K.

Solutions:

Using Equation 6.3 in this report, determine the sensible cooking power P_{ck}

$$P_{ck} = \frac{mc\Delta T}{\Delta t}$$

and m = 3 kg, c = 4 186 kJ/kg K, and Δt = (12.9 *60)

$$P_{ck} = \frac{3 * 4186 * (99.7 - 20.1)}{(12.9 * 60)} = 1309\ W$$

Equation 6.4 can be used to get the utilisation efficiency, η_u, of the system

$$\eta_u = \frac{m_w\ c\ \Delta T}{I_s\ A_a\ \Delta t}$$

$$\eta_u = \frac{3 * 4186 * (99.7 - 20.1)}{3.142 * 880 * (12.9 * 60)} = 0.46$$

Characteristic boiling time, t_c, can be calculated from Equations 6.5 and 6.6 of this report:

$$t^b = \frac{\Delta t\ A_a}{m_w}$$

$$t_c = t^b\ \frac{I_s}{I_{ref}}$$

$$t_c = \frac{12.09 * 3.142}{4} * \frac{880}{900} = 8.4\ \text{mins/kg}$$

Latent cooking power can be determined from Equation 6.1, as

$$\eta_{latent} = \frac{\dot{Q}_{ck,power}}{A_a\ I_s} = \frac{\dot{m}\ h_{fg}}{A_a\ I_s} = \frac{m\ h_{fg}}{A_a\ I_s\ \Delta t}$$

$$\eta_{latent} = \frac{3 * 2257 * 1000}{3.142 * 880 * 2 * 60 * 60} = \quad 0.34$$

To calculate the exergy efficiency, Equations 6.5 to 6.7 of this report would be used. The first step is to determine the rate of exergy input to the system from the sun, using the equations below and working out the temperatures in kelvin:

$$\psi_{in} = I_s \left(1 + \frac{1}{3}\left(\left(\frac{T_{amb}}{T_s}\right)^4 - \frac{4\,T_{amb}}{T_s}\right)\right) A_a$$

$$\psi_{in} = 880 * \left(1 + \frac{1}{3}\left(\left(\frac{298}{6000}\right)^4 - \frac{4 * 298}{6000}\right)\right) * 3.142$$

Now the rate of exergy output through the cooking section can also be determined, as

$$\psi_{out} = \frac{m_w\, c_{p,w}\left(\left(T_{wf} - T_{wi}\right) - T_{amb}\, In\left(\frac{T_{wf}}{T_{wi}}\right)\right)}{\Delta t}$$

$$\psi_{out} = \frac{3 * 4186 * \left((370.76 - 293) - 298 * ln\left(\frac{370.76}{293}\right)\right)}{720}$$

From the expressions above, the exergy efficiency of the system can be determined using

$$\eta_{ex} = \frac{\psi_{out}}{\psi_{in}} = 0.05$$

C.2 Comparing Theoretical and Experimental Values

Aims and Objectives: To ascertain the correctness of the theoretical model and the efficiency of the cooker, and compare the measured data with the values obtained from the theoretical model using water boiling as the easiest experiment.

Procedure: The temperatures from the experiment were recorded with thermocouples as shown in Appendix B. The necessary thermocouple correction equations shown in Section B.2 were applied, after which the output temperature was recorded. The mass of water = 0.5 kg and the date of the experiment was 11 June. Average day DNI was 451.63 W/m^2 and 659.95 W/m^2 during the experiment. The experiment took place between 13:30 and 14:30.

The theoretical equations in Equations 4.76 to 4.79 are then solved numerically, and the results calculated and compared to the experimental values, as shown in Table C-1 below.

Table C-1: Comparing the experimental results with the theoretical values

	Mass = 0.5 kg, I_s=659.95 W/m^2				
Time	Experiment	Theory			
(mins)	T_{fd} (℃)	T_{fd} (℃)	T_{pot} (℃)	T_g (℃)	T_{cov}(℃)
0	40	40	40	40	40
10	54.65	59.90	65.79	56.7	46.64
15	67.65	76.19	81.30	67.17	49.07
30	81.85	85.01	86.28	68.54	52.65
40	97.15	106.44	107.99	84.27	56.00
53	97.75	122.99	125.38	92.15	59.01

The results from the table are plotted for comparison in Figure C-1 below, and Figure C-2 shows the deviation between the experimental and theoretical values.

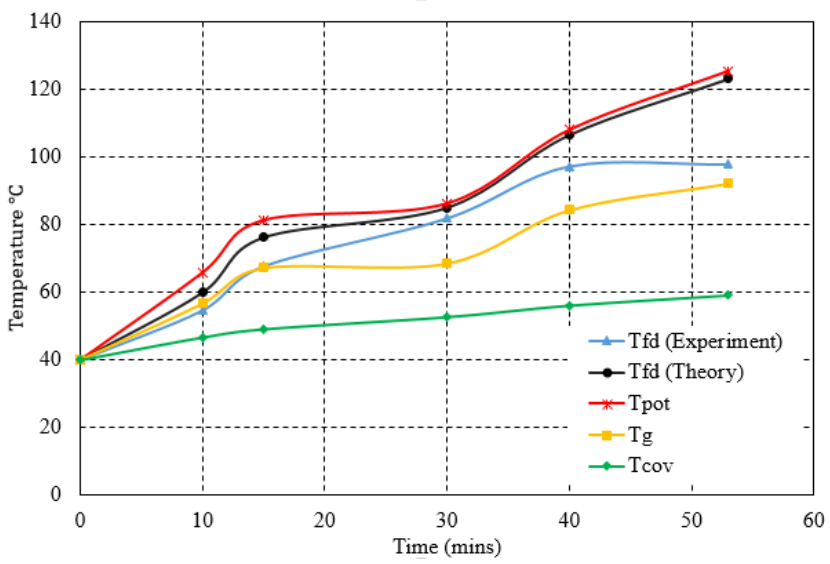

Figure C-1 : Comparison between theoretical and measured temperatures

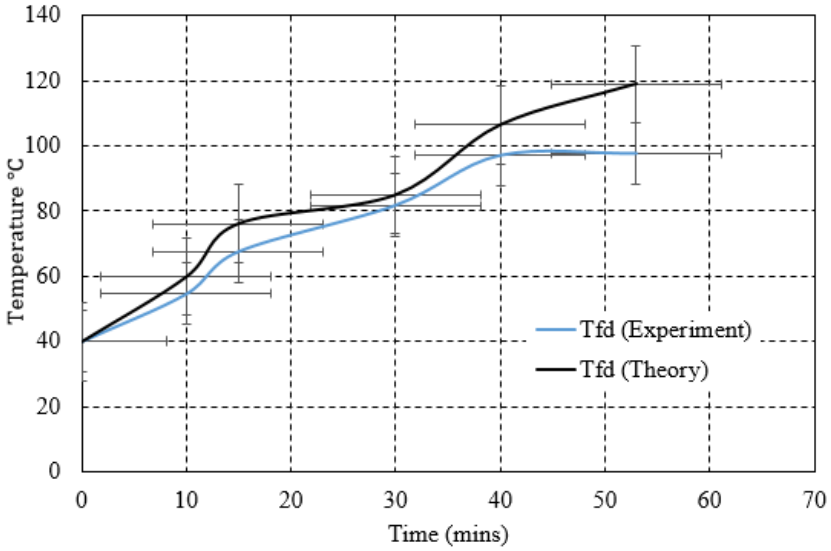

Figure C-2: Experimental and theoretical temperatures of the water with error bars

C.3 Measured Data from the Experiment

Table C-2: Results from boiling 3 kg of water boiling in sets

	time(mins)	Water boiling temp °C	DNI/ (mins)	Calculations	
	0.19	20.04	874.57		
	0.78	22.00	874.84	I_ref	900
	1.76	25.14	873.78	m (kg)	3
	2.34	29.06	875.45	c	4186
	2.54	33.39	877.83	Aprt_area	3.14
	2.73	34.83	877.49		
	3.13	37.70	879.19		
	3.32	41.24	876.89	t^b	13.32
	3.71	52.24	876.65		
	4.50	58.92	881.23	Average DNI	880.79
	4.89	62.45	876.90		
	5.47	66.38	880.07	I_s* A	2767.44
	6.45	72.26	883.25		
	7.63	78.5426	885.80	Quseful (cooking power Pck)	1311.09
1st water boiling	8.61	86.79	888.38		
	10.17	92.28	886.25	n (efficiency)	0.47

	10.76	94.63	886.857		
	11.54	97.77	888.15	t_c	13.04
	12.52	99.33	886.09		
	12.91	99.72	886.09		
	14.48	24.65	889.47		
	14.87	28.97	890.18		
	15.26	36.437	892.94		
	15.65	39.18	895.71		
	16.04	41.93	893.80		
	17.80	48.20	894.60	t^b	17.83
	18.19	57.24	892.09		
	19.37	64.69	890.92	Average DNI	893.76
	19.56	69.02	886.43		
2nd water					
boiling	20.35	73.73	887.33	I_s* A	2808.19
	21.33	78.44	888.21		
				Quseful (cooking power	
	22.30	81.96	891.83	Pck)	916.33
	22.89	85.49	894.13		
	23.28	86.77	893.78	n (efficiency)	0.326
	24.46	90.59	900.76		
	25.63	92.55	901.17	t_c	17.708
	27.20	94.89	899.56		
	29.15	96.85	892.46		
	29.74	97.63	899.55		
	31.50	99.18	900.05		
	32.48	22.13	898.56		
	35.02	23.40	897.11		
	35.22	27.23	896.99		
	35.81	33.12	899.55		
	36.39	40.18	898.16		
	37.76	44.49	896.79		
	39.53	45.47	894.15		
	39.72	50.37	896.82		
	40.70	58.23	894.19		
	41.48	63.73	892.93	t^b	28.89
	42.66	68.04	891.02		
3rd water					
boiling	44.03	72.03	893.09	Average DNI	897.38
	45.40	74.31	894.57		

	46.18	79.81	896.06	I_s* A	2819.57
	46.57	87.26	901.51		
				Quseful	
				(cooking power	
	48.92	91.96	899.76	Pck)	585.71
	50.68	92.87	901.99		
	51.07	94.70	901.59	n (efficiency)	0.21
	51.85	97.05	901.87		
	53.03	98.22	900.85	t_c	28.82
	56.16	98.97	896.86		
	58.70	99.17	897.24		
	60.07	99.34	898.31		
	61.25	23.09	897.41		
	62.42	27.80	895.84		
	63.79	33.69	893.63		
	64.57	40.37	891.45		
	65.55	45.69	891.97		
	65.94	47.82	893.19		
	66.92	52.14	894.43		
	67.51	56.46	894.38		
	69.08	61.55	895.67		
	71.23	66.25	894.95	t^b	39.97
	72.40	69.64	894.93		
	72.99	71.35	894.98	Average DNI	893.33
	74.55	76.05	895.69		
	77.49	80.74	895.77	I_s* A	2806.83
4th water					
boiling	78.66	82.13	896.54		
				Quseful	
				(cooking power	
	81.80	85.8199	896.66	Pck)	410.07
	84.14	88.68	896.12		
	85.32	90.12	896.96	n (efficiency)	0.15
	88.06	92.84	894.44		
	88.45	93.20	894.69	t_c	39.67
	90.60	95.18	888.17		
	92.75	97.52	889.12		
	95.49	97.89	888.35		
	97.65	97.88	887.34		
	98.04	97.88	887.67		
	99.41	97.86	888.04		

D. Numerical Solver Codes

For an equation in which y is a function of t, and where t is an independent variable, as shown in

$$\frac{dy}{dt} = f(t) \tag{D.1}$$

Fourth order Runge-Kutta method is one of the popular ways for numerically solving this type of Ordinary differential equation (ODE). Some authors refer to it as classical fourth-order RK methods. The general form of the Equation is written below

$$y_{i+1} = y_i + \left(\frac{1}{6}K_1 + \frac{2}{6}K_2 + \frac{2}{6}K_3 + \frac{1}{6}K_4\right) h \tag{D.2}$$

and the values of Ks in the equation above are as follows:

$$K_1 = f(t_i, y_i) \tag{D.3a}$$

$$K_2 = f\left(t_i + \frac{1}{2}h, y_i + \frac{1}{2}K_1 h\right) \tag{D.3b}$$

$$K_3 = f\left(t_i + \frac{1}{2}h, y_i + \frac{1}{2}K_2 h\right) \tag{D.3c}$$

$$K_3 = f(t_i + h, y_i + K_3 h) \tag{D.3d}$$

In the experiments in the setup in this report, temperature was a function of time, so T, which stood for the temperature values, replaced the y in the equation sets above, and an M-file script was written as follows:

```
function [t,T] = odeRK4 (ODE,ti,tf,h,TIni)
 % odeRK4: Solve the system ODEs using fourth-order Runge-
kutta method
 % input variables:
 % ODE Name for function that calculates dT/dt
 % TIni = inittial values of the temperature
 % h = step size
 % ti = first value of time
 % tf = last value of time
 % Output variables:
 % t = vector of time variable
 % T = vector of solutions to the temperature variables
```

```
t(1) = ti; T(1)= TIni; % input the initial values of the
variables
n = (tf-ti)/h;          %determine the number of steps
for i = 1:n
    t(i+1) = t(i) + h;   %calculate the next value of time
which is
                              %the independent variable
    K1 = ODE(t(i), T(i)); %calculate the values of K1 using
Equations
    thalf = t(i) + h/2;
    TK1 = T(i) + K1*h/2;
    K2 = ODE(thalf,TK1);  % calculate the values of K2 using
Equations
    TK2 = T(i) + K2*h/2;
    K3 = ODE(thalf,TK2);  calculate the values of K3 using
Equations
    TK3 = T(i) + K3*h;
    K4 = ODE(t(i+1),TK3);  % calculate the values of K4 using
Equations
    T(i+1) = T(i) +(K1+2*K2+2*K3+K4)*h/6;
end
```

E. Heat Transfer Fluid Technical Data Sheet

Shell Heat Transfer Oil S2: High performance heat transfer fluid

Table E-1: Typical physical characteristics

Density at 15 °C	kg/m^3	ISO 12185	866
Flash point PMCC	°C	ISO 2719	210
Flash point COC	°C	ISO 2592	220
Fire point COC	°C	ISO 2592	255
Pour point	°C	ISO 3016	-12
Kinematic viscosity		ISO 3104	
at 0 °C	mm^2/s		151
at 40 °C	mm^2/s		25
at 100 °C	mm^2/s		4.7
at 200 °C	mm^2/s		1.1
Initial boiling point	°C	ASTM D 2887	355
Auto-ignition temperature	°C	DIN 51794	360
Neutralisation value	mgKOH/g	ASTM D974	< 0.05
Ash (oxide)	%m/m	ISO 6245	< 0.01
Carbon residue (Conradson)	%m/m	ISO 10370	0.02
Copper corrosion (3 h/100 °C)		ISO 2160	class 1

Typical Design Data

Temperature	°C	0	20	40	100	150	200	250	300	340
Density	kg/m^3	876	863	850	811	778	746	713	681	655
Specific heat capacity	kJ/kg K	1.809	1.882	1`.954	2.173	2.355	2.538	2.72	2.902	3.048
Thermal conductivity	W/m K	0.136	0.134	0.133	0.128	0. 125	0.121	0.118	0.114	0.111
Prandtl no.		3375	919	375	69	32	20	14	11	9

Shell Lubricants August 2010

F. Safety Report

Summary

The system is a stand-alone CSP parabolic cooker. It involves setting up a cooking system that will use up to 210 °C temperature generated from the reflected rays of the sun from a cavity receiver for cooking processes such as water boiling and baking bread and pancakes. The setup consists of a parabolic dish with a heat-receiving element to be mounted on the tracker stand on the roof, and flexible pipes/hose that will channel the heat to the storage tank. The storage system uses Shell HTF S2 as the heat-transfer fluid and it is linked to the cooking area.

Tasks that were involved include:

- Design and setting up of concentrating parabolic dish
- Dish modifications
- Attachment of a heat receiver in the focus of the dish
- Mounting of the parabolic dish on the tracker stand
- Setting up a storage tank to containing heat-transfer fluid
- Connecting the systems with high-temperature pipes
- Setting up the pumping system and bypass arena
- Setting up an electrical source to power the pump and control system
- Performing various types of cooking
- Taking measurements: Temperatures (tank, collector, ambient)

The entire operation was performed with strict adherence to the safety rules and precautions of the Solar Thermal Energy Research Group, Stellenbosch University. None of the experiments was carried out in isolation, as someone was always available to help. Some of the safety signs that were used to prevent unsafe acts are shown in Figure F-1

Figure F-1: Safety signs

The details of the likely hazards in this kind of experimental analysis are displayed in Table F-1

Table F-1: Safety analysis

Risk	Design impact	Operating instructions
Elevated dish with potential to fall	Ensure a sturdy construction for frame and a good dish support	Fasten dish on the tracker stand and inspect that the dish is firmly secured before starting daily tasks
Elevated system with potential wind disruption	Ensure a sturdy construction for frame schedule and work during calm wind conditions	Ensure that parabolic collector is properly fitted
Hot oil spills from storage tank, collector or pipework	Establish 'no' zones	Inspect for leaks daily Indicate hot oil operation Use of oil spill tray/ spill-catching tray to prevent slips and oil leakage on the ground
Exposure to sun	-	Wear sun screen protection. Wear hat
Electrical shock	Insulated wires	Ensure wires are insulated before start of daily tasks Ensure wires are kept neat and out of way
Falling objects from roof	Set up experiment away from roof edge	Ensure no tools or equipment are placed on roof edge

OO CRAIG RT DOBSON

In conclusion, ensure safety first; only work when the PPE is right and when the set-up is in a safe condition.

G. Setup Procedures

G.1 Start-up

- Remove the protective cover from the reflecting surface of the concentrating dish and check for dirt or dust
- Open the cover of the receiver cavity
- Check the temperature of the storage tank
- Check for leakages around the pump and all connecting sections
- Check if all the thermocouples are in good condition
- Switch on the data logger and the CPU for the tracking system
- Connect the data logger to the computer systems
- Check the initial readings of the systems
- Open all the valves and start up the tracking unit
- Start the variable speed drive linked to the power source and the pump

G.2 Operating Conditions and Cooking

- Start the data logger temperature scanning
- Check if the reflected sun disc is well sucked into the cavity receiver
- Check for the temperature difference between the temperatures in and out of the storage section
- Wait till the temperature difference is constant to confirm fully charged system
- Prepare whatever food is to be cooked
- Open the cooking section and place the pot or baking pans inside
- Close the cover of the cooker and fasten the insulator to it
- Open the cooker to check for the cooking status of the food

G.3 Shut Down and Stow Positioning

- When the sun has set or there is an emergency, it is necessary to stop operations
- Stop the variable speed drive linked to the pump
- Close all the valves
- Turn the dish to back the sun and the reflecting aperture to face the ground
- Wait for an hour and cover the solar collection receiver setup
- Leave the thermocouple data logger on to take night readings
- Cover the storage section if the cooking is done outside

H. Receiver manufacturing stages in photos

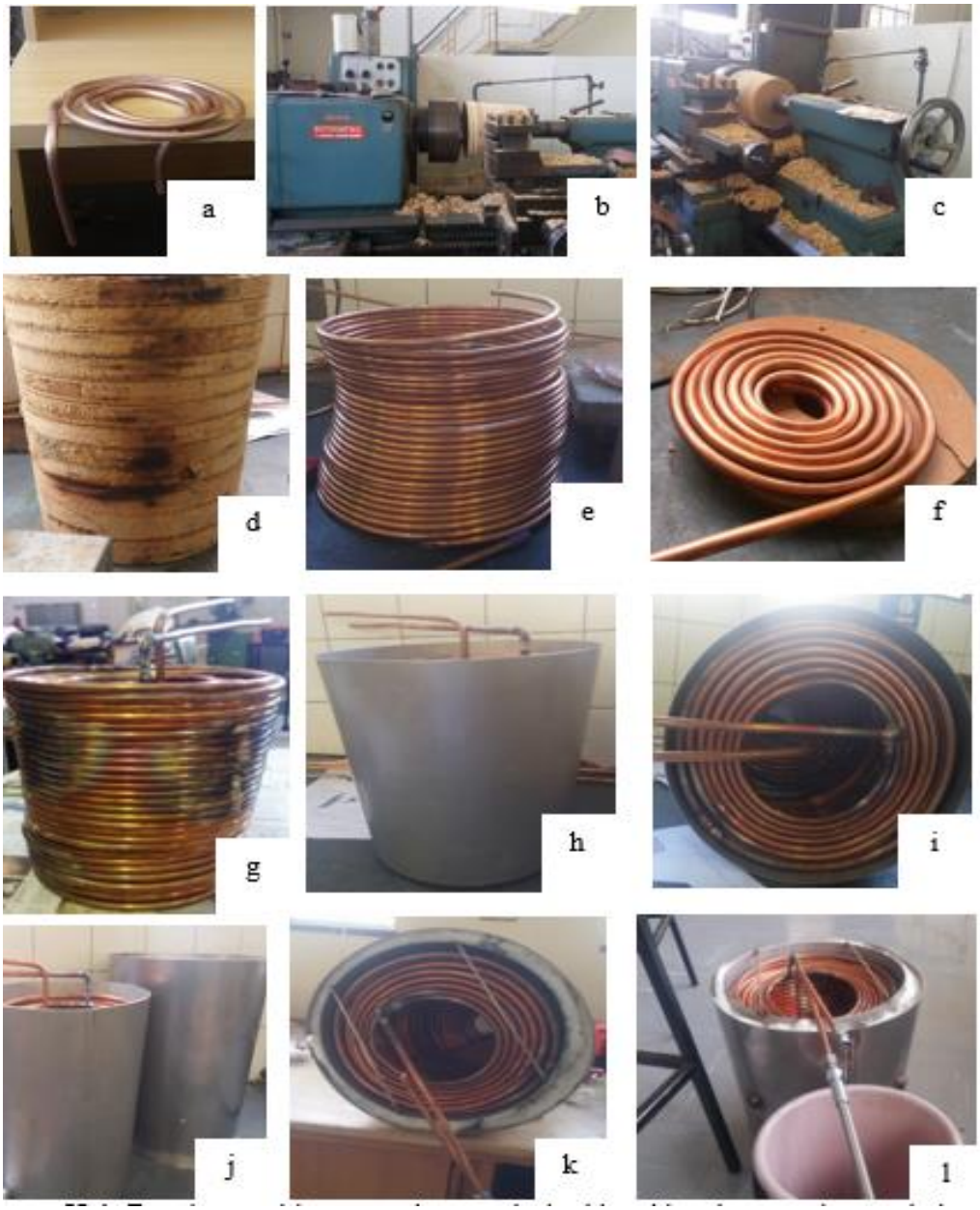

Figure H-1: Receiver fabricaingg procedure, undesired hand bend a, template on lathe machining on b, c, template d, frustum shape body e, spiral front to prevent forced convention f, complete receiver coil set up g, coil in stainless container h, i, second stainless to hold the insulator j, complete receiver with insulator k, test for leakage l

I. Experiment Site

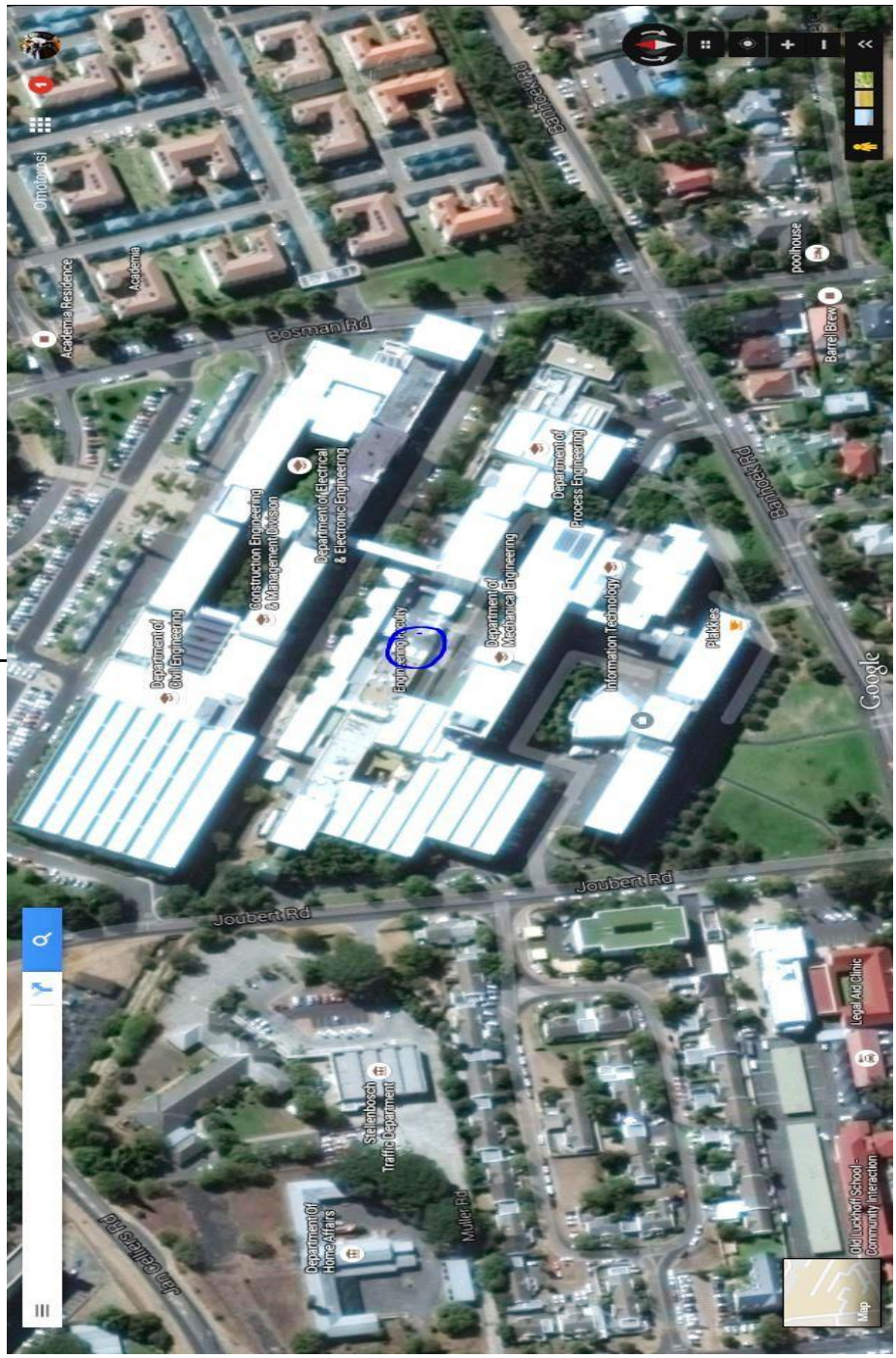

Figure I-1: Heat transfer lab roof top mechanical engineering building, SU latitude 33 ° 55 ’ 41.10 ” S and longitude 18 ° 51 ' 58.80 " E with elevation of 119 m above sea level (Google maps, 2015)

J. Oil Expansivity Table

The lowest and highest possible expansion by the heat-transfer oil was calculated using simple volume expansivity equations in relation to the possible minimum and maximum temperature differences in the experimental setup. The result is presented in the table below. The highest possible expansion would be 16.5 % using the HTF properties in Appendix E

Table J-1: Maximum possible expansivity of the HTF

Initial Volume	Final Volume	Maximum Expansion
0	0	0
5	5.83	0.83
10	11.65	1.65
15	17.48	2.48
20	23.30	3.30
25	29.13	4.13
30	34.95	4.95
35	40.78	5.78
40	46.60	6.60
45	52.43	7.43
50	58.25	8.25
55	64.08	9.08
60	69.90	9.90
65	75.73	10.73
70	81.55	11.55
75	87.38	12.38
80	93.20	13.20
85	99.03	14.03
90	104.85	14.85
95	110.68	15.68
100	116.50	16.50

The values in the table above can be used to determine the expansion limit of the heat-transfer oil used, depending on the assumed theoretical temperature to be worked with. In this setup, the range was between 20 ℃ and 295 ℃. The working fluid was found to fall within this range throughout the testing. It is recommended that the storage tank should not be filled to maximum capacity with the HTF; some space should be left, depending on the maximum expansivity of the HTF.

K.Other Experimental Pictures

The various setup positions of the parabolic solar cooker, the baking and tasting pictures, as well as pictures of some other fabrication processes, are displayed in Figure K-1 below.

Figure K-1: Other pictures from the set up

L. Receiver CAD Drawings

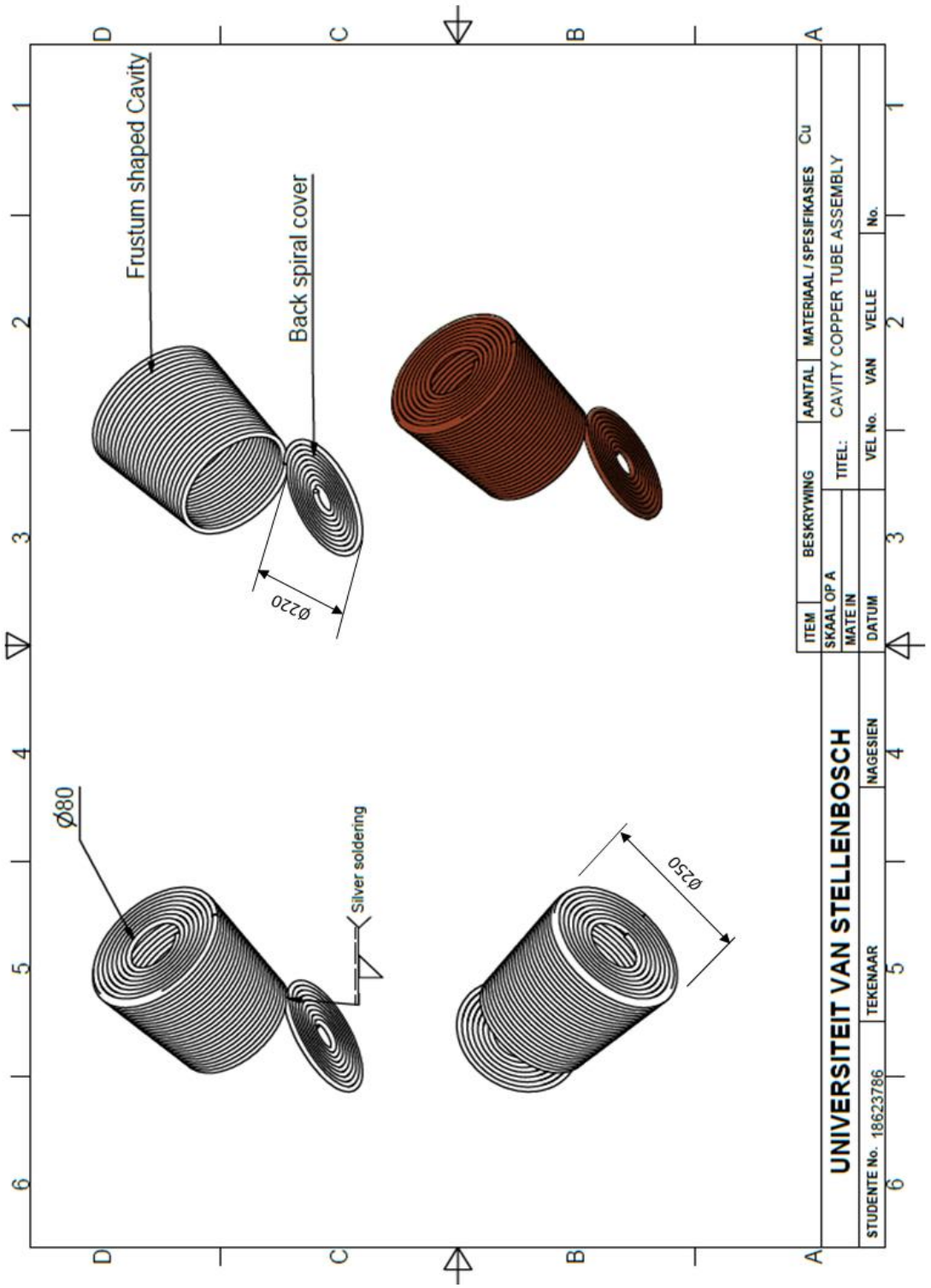

Figure L-1: CAD drawings of the copper tube cavity receiver

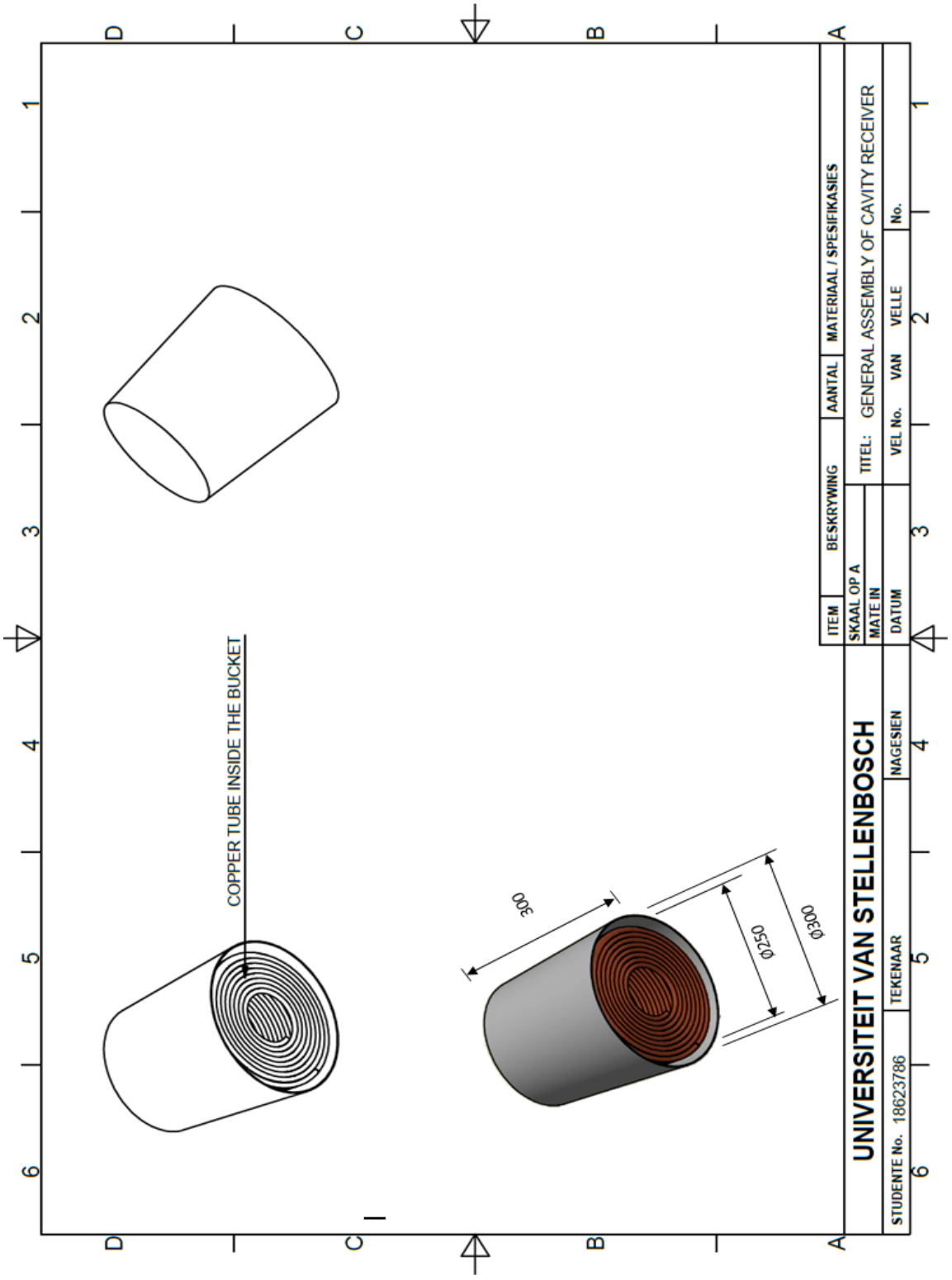

Figure L-2: CAD drawing of complete cavity receiver setup

M. Cost of Production

The system manufactured in this study cost approximately 9 000 rands, Table M-1 below shows the detailed cost of all the purchased, ordered and manufactured parts.

Table M-1: Cost of production

Item/ Parts	Suppliers	Descriptions	Unit cost (ZAR)	Quantity	Total (Rands)
Shell oil S2		Shell oil S2 20 litres per unit	1799.69	3	5399.07
Copper tube and fittings	Stellenbosch Refrigeration and air conditioning cc	(9.53 mm) 3/8" Copper tube coil	242.2	2	485
		(9.53 mm) 3/8" Brase count	30	2	60
		(9.53 mm) 3/8" Elbows	6.1	5	30.5
		(9.53 mm) 3/8" Couplings	4	5	20
Pipe fittings	Hydroscand Cape Town	0110122007 BSP STR MALE	23.98	6	143.87
		0110122007 STRAIGHT	25.69		102.78
		(15.88 mm) 5/8" METRIC FEMALE 10-06	28.9	4	115.6
		3/8" Teflon collar (9.525 mm)	15.69	8	125.48
		brass GE 10L 3/8 (9.525 mm)	43	2	86
Dish support		Support base for dish			214.22
Receiver bucket	Fabrinox	Bucket body		2	800.46
		Bottom plate		2	85.7
Support braces					655.28
Miscellaneous		Other materials with no official orders			676
Total cost					R 8999.96

N. Publications from this research

The study presented in this report has been supported by some publications, which are listed below

N.1 Papers prepared for submission to Solar Energy journal

Craig, OO, Dobson, RT, (2015), "A novel parabolic solar cooker for African conditions"

N.2 Peer reviewed papers at international conferences

Craig, O. O., & Dobson, R. T. (2015). Parabolic solar cooking: Cooking with spiral copper tubes or cooking with heat pipes", International Solar Energy Society, ISES Solar world Congress 2015, South Korea

Craig, O, O., & Dobson, R. T. (2015). Parabolic solar cookers: Cooking with heat pipes vs direct spiral copper tubes. Solar Paces 2015, Cape Town October 2015 (to be published in American Institute of Physics Conference Proceedings)

Craig, O. O., & Dobson, R. T. (2015). Stand-alone parabolic solar cookers and rural industrialisation in Southern Africa. In *Southern African Solar Energy Conference (SASEC)2015* Skukuza, South Africa, pp. 278–282. http://hdl.handle.net/2263/49491

Craig, O. O., & Dobson, R. T. (2014) Stand-alone parabolic solar cooker for African conditions. Mechanical, Manufacturing and Materials Engineering Conference, South African Institute of Mechanical Engineering, Western Cape Branch, Stellenbosch. 6 November 2014 (abstract published).